Experimental Extension of the Texture Method for Structure Solution of Polycrystalline Materials

A dissertation submitted to

ETH Zurich

for the degree

Doctor of Sciences

presented by

Lars Alexander Massüger
Dipl. Werkstoff-Ing. ETH

Born 11. August 1975

citizen of Täuffelen (BE)

accepted on the recommendation of

Prof. Dr. W. Steurer, examiner
Dr. Lynne B. McCusker, co-examiner
Dr. Christian Baerlocher, co-examiner
Dr. Luca Lutterotti, co-examiner

2007

to Prisca and Curdin

Abstract

Before any crystalline material, whether extracted from natural sources or synthesized in a laboratory, can be further processed, it's physical properties have to be explored. An essential part of this process is the determination of its crystal structure. Whenever single crystals of sufficient size (ca. 50 x 50 x 50 μm^3) and quality are available, single crystal studies are the method of choice. Otherwise powder diffraction is usually the only alternative. Unfortunately, reflections with similar lattice spacings overlap in powder data, and this results in an inexact estimation of their integrated intensities. This increases the likelihood that structure determination will fail. Several approaches have been developed over the years to overcome these limitations. One of them is the improvement of the powder diffraction experiment itself, and that is the topic of this project.

In 1999, Wessels *et al.* demonstrated the practical viability of the 'texture method' for resolving reflections that overlap in a powder diffraction pattern. More information about the relative intensities of overlapping reflections could be obtained by collecting synchrotron data on a textured polycrystalline sample as a function of sample orientation. In contrast to other related approaches, a full texture analysis was used to establish how the crystallites were oriented in the sample. This information was then used to extract a single set of single-crystal-like reflection intensities via a joint refinement procedure using all diffraction patterns (between 5 and 1296) simultaneously.

The main drawbacks of this first implementation of the method, which used a reflection geometry, were: (1) three days of synchrotron beamtime were required, (2) severe intensity corrections had to be applied to the data collected at high sample tilt angles, and (3) a large homogeneous sample (ca. 2.5 cm) had to be prepared. By collecting data in transmission mode using an 2-dimensional imaging plate detector, these disadvantages could be overcome (Prokić, 2004). The beamtime could be reduced to ca. 6 h per sample; no tilt correction was necessary, and only a very small sample was required. However, these advantages were gained at the expense of data resolution in both d-spacing (2θ range) as well as in peak width (FWHM). These drawbacks were addressed in this project.

First, an attempt was made to improve the resolution of the transmission geometry setup, by shifting the area detector diagonally so that only a single (non-redundant) quadrant of the original data was collected. In a second series of experiments, the setup was adapted to accommodate the one-dimensional Si-microstrip detector that had just been installed on the powder diffractometer on the Materials Science Beamline at the SLS (Schmitt *et al.*, 2004). This setup allowed the resolution of the data to be improved both in 2θ (from 0-35º to 0-60º) and in peakwidth (from ca 0.06 $^o\theta$ to ca 0.03 $^o\theta$) with an acceptable increase in the amount of beamtime required (ca. 12 h per sample).

The data analysis software *Expol* was adapted accordingly. New techniques for preparing textured samples were developed and standardized, so that the sample prepared is not dependent on the person preparing it. The data collection procedure itself was further optimized. For the latter, it was reasoned that once the orientation distribution function (ODF) has been determined for

a specific sample, the sample orientations that yield the best resolution of the overlapping reflections can be identified using a cluster analysis algorithm. Data collection was then concentrated on these specific orientations (5 - 12 of the 1296 possible orientations) to yield fewer patterns (without significant loss of information) and better counting statistics. This, in turn, facilitates the final intensity extraction step, which uses all of these patterns simultaneously.

The method was applied to zeolites with known structures: (1) synthetic offretite to evaluate different sample preparation techniques and to test the data analysis procedure, and (2) a single-crystal like agglomerate of the high-silica zeolite IM-12 to explore the limitations of the method.

The method was also applied to samples of unknown structures. The structure of the layer silicate DLM-2, $|$ $((CH_3)_3N)_8(H_2O)_{20}|$ $[Si_24O_56]$ was solved using the powder charge flipping algorithm included in the program *Superflip* (Palatinus & Chapuis, 2006) and intensities extracted from diffraction patterns collected on a textured sample. For the zeolite catalyst IM-5, some partial structural models were obtained, but none were sufficient for structure solution. The structures of two other materials, silver behenate and a novel niobium silicate, remain elusive.

A major problem was the poor quality of the diffraction data, obtained from the prototype Si-microstrip detector, because the count-rate was low and many counting channels defective. Fortunately, the next generation of the detector which is presently being commissioned, will provide a much higher counting rate and almost no defective counting channels. The amount of amorphous matrix material in the samples also reduced the quality of the data. Therefore, new methods that use only a very limited amount or no matrix material at all need to be developed. Further improvement in the final intensity extraction step, could be gained by refining the initial orientation distribution function together with the reflection intensities.

Zusammenfassung

Vor der Anwendung oder Weiterverarbeitung von natürlich vorkommenden oder künstlich hergestellten kristallinen Materialien werden normalerweise die physikalischen Eigenschaften bestimmt. Ein wesentlicher Teil des Charakterisierungsprozesses ist die Bestimmung der Kristallstruktur. Wenn immer möglich werden dazu Röntgendiffraktionsexperimente an Einkristallen benutzt. Sind die Kristalle aber kleiner als ca. 50 x 50 x 50 μm^3 ist Pulverdiffraktion meistens die einzige Alternative. Unglücklicherweise ist die Qualität von Pulverdaten schlechter, da sich die Peakpositionen von Reflexen mit ähnlichen Netzebenenabständen überlappen. Als Folge davon können ihre Intensitäten nicht korrekt aus den Daten extrahiert werden, was die Wahrscheinlichkeit der erfolgreichen Strukturbestimmung mit direkten Methoden verringert. Um dieses Problem zu lösen wurden verschiedene Methoden entwickelt. Eine davon ist die Verbesserung des Pulverdiffraktionsexperiments, welche das Thema der vorliegenden Arbeit ist.

Wessels *et. al* zeigten im Jahre 1999, dass die 'Texturmethode' zur Auflösung überlappender Reflexpositionen in Röntgenpulverdaten in der Praxis anwendbar ist. Die Intensitäten von sich überlappenden Reflexen konnten exakter bestimmt werden, wenn Pulverdiffraktionsdaten als Funktion der Probenorientierungen einer texturierten polykristallinen Probe an einem Synchrotron gemessen werden. Im Vergleich zu verwandten Methoden wird aber eine quantitative Texturanalyse zur Bestimmung der Orientierung der Kristallite in der Probe benutzt. Auf deren Grundlage kann ein Satz von Intensitäten aus allen Diffraktogrammen (zwischen 5 und 1296) gleichzeitig extrahiert werden, welcher nahezu dem eines Einkristallexperiments entspricht.

Die ersten Umsetzung der Methode basierend auf Messungen in Reflektionsgeometrie, brachte folgende Nachteile mit sich: (1) eine Messdauer von drei Tagen an der Synchrotronstrahlungsquelle, (2) starke Korrektur der bei grossen Kippwinkel gemessenen Intensitäten und (3) die Herstellung einer relativ grossen (2.5 cm) homogenen Probe. Die zuvor aufgezählten Nachteile konnten durch Übertragen der Messanordnung in eine Transmissionsgeometrie und Aufnahme der Daten mittels einer Bildspeicherplatte (imaging plate) überwunden werden (Prokić, 2004). Die benötigte Messzeit reduzierte sich dadurch auf 6 h pro Probe Leider ging dies auf Kosten der Auflösung der Daten in 2θ und der Breite der Reflexe (FWHM).

In der vorliegenden Arbeit wurde versucht, die Auflösung der Transmissionsanordnung durch eine diagonale Verschiebung des Flächendetektors zu verbessern, in dem nur noch ein Quadrant der Originaldaten aufgezeichnet wird. Des Weiteren wurde die experimentelle Messanordnung an den eindimensionalen Si-Microstrip Detektor (Schmitt *et al.*, 2004) angepasst, welcher zur Zeit an der Synchrotron Lichtquelle Schweiz entwickelt wird. Diese Messanordnung ermöglicht es eine Verbesserung der Auflösung der Daten in 2θ (von 0-35º auf 0-60º) und in der Peakbreite (von 0.06º2θ auf 0.03º2θ) zu erreichen. Der Preis dafür ist eine Verlängerung der Messzeit, von 6 auf 12 h pro Probe. Das Program *Expol* zur Auswertung der Daten wurde entsprechend angepasst. Neue Techniken zur Präparation von texturierten Pulverproben wurden entwickelt und standartisiert, damit die Proben nicht durch die präparierende

Person beeinflusst werden können. Die eigentliche Messprozedur wurde wie folgt optimiert. In einer ersten schnellen Messung wird die Orientierungsverteilungsfunktion (ODF) für eine spezifische Probe bestimmt. Mit Hilfe einer Klusteranalyse können aus der ODF diejenigen Probenorientierungen bestimmt werden, welche die beste Auflösung zur Trennung der überlappenden Reflexe ermöglichen. In einer zweiten Messung werden dann nur noch Daten mit besserer Statistik an diesen Orientierungen (zwischen 5 - 12 aus allen Orientierungen) gemessen. Dies vereinfacht den letzten Schritt, nämlich die gleichzeitige Extraktion der Intensitäten aus allen Diffraktogrammen.

Die Methode wurde zuerst auf Texturproben, hergestellt aus Zeolithen mit bekannter Struktur, angewendet: (1) synthetisch hergestelltem Offretith, um verschiedene Probenpräparationstechniken und die Datenanalyse zu testen und (2) eine Probe aus dem Zeolith IM-12, welcher während der Synthese grössere, stark vorzugsorientierte Agglomerate bildeten.

Schlussendlich wurden Texturproben aus Substanzen mit unbekannter Struktur hergestellt und mit der optimierten Methode untersucht. Die Struktur des Schichtsilikats DLM-2, $\mid ((CH_3)_3N)_8(H_2O)_{20} \mid [Si_{24}O_{56}]$, konnte gelöst werden mit dem für Pulverdaten erweiterten Charge-Flipping Algorithmus und Intensitäten extrahiert aus Diffraktogrammen, welche an einer texturierten Probe des Materials gemessen wurden. Für den Zeolithkatalysator IM-5 wurden mit derselben Kombination aus Charge-Flipping und mit aus Texturdaten extrahierten Intensitäten Strukturmodelle erhalten. Keines konnte jedoch soweit vervollständigt werden, dass damit die Struktur hätte gelöst werden können. Die Struktur eines neuen Niobsilikates, konnte trotz Anwendung der Texturmethode noch nicht gelöst werden.

Das Hauptproblem war die schlechte Qualität der Daten, welche vorallem auf die begrenzte Zählrate und die defekten Kanäle des Prototypdetektors zurück zuführen ist. Glücklicherweise wird die neue Detektorgeneration, welche momentan getestet wird, eine viel höhere Zählrate ermöglichen und keine defekten Kanäle mehr haben.

Die Probenpräparation sollte weiter optimiert werden damit nur noch sehr wenig oder gar kein Matrixmaterial mehr benötigt wird, was die Qualität der gewonnen Daten weiter verbessern wird. Auch sollten die Unsicherheiten in der Texturbestimmung weiter reduziert werden können, durch eine zusätzliche Verfeinerung der anfangs bestimmten Orientierungsverteilungsfunktion zusammen mit den Intensitäten im letzten Extraktionsschritt aus allen Daten.

Contents

Contents

1 Introduction

Many technologically and industrially important materials are synthesized and employed only in polycrystalline form and cannot be grown as single crystals. As a result, the crystals are not suitable for the application of single-crystal methods. These materials are treated in the form of powders (assemblies of millions of small single crystals). Unfortunately, the quality of the powder diffraction data is generally lower than that of single crystal data. Reflections with similar lattice spacings overlap, and this results in an inexact estimation of their integrated intensities, and this increases the likelihood that the structure determination process will fail. Several approaches have been developed over the years to overcome these limitations. For example: incorporating chemical information available from other studies on the material in the structure determination process, development of new structure solution algorithms or improvement of the powder diffraction experiment itself. The latter is the topic of this project.

1.1 Structure Determination from Single Crystal Data

X-rays are short-wavelength (0.1 - 2.0 Å) electromagnetic waves that are scattered strongly by the electron density of the atoms arranged within a crystalline material. In conventional diffraction experiments for structure determination, monochromatic X-rays with wavelengths ranging from 0.5 Å to 1.8 Å are used. Single crystals are preferred for such investigations, because they exhibit a single continuous lattice throughout the entire sample volume and this results in a discrete diffraction intensity for each set of lattice planes.

In a conventional single-crystal diffraction experiment, reflection intensities I_{hkl}, which are a function of the lattice planes *hkl* and their corresponding scattering angle 2θ, are measured. The scattering angle 2θ depends only on the dimensions and the shape of the unit cell, whereas the reflection intensities are a function of the atom types and their arrangement within the unit cell. The intensity of a reflection *hkl* is proportional to the square of the structure factor F_{hkl} (equation 1.1)

$$I_{hkl} \propto F_{hkl}^2 \tag{1.1}$$

and the structure factor can be calculated from the types and positions of the atoms in the unit cell (equation 1.2):

$$F_{hkl} = \sum_{i=1}^{N} f_i \, e^{-2\pi i \,(hx_i+ky_i+lz_i)} \, e^{-B_i sin^2/\lambda^2} \tag{1.2}$$

In equation 1.2, f_i is the atomic scattering factor of the *i*th atom, which has the coordinates (x_i, y_i, z_i), B_i is the Debye-Waller factor and λ is the wavelength.

Equation 1.2 can also be written in the form

$$F_{hkl} = \mid F_{hkl} \mid e^{i\phi_{hkl}} \qquad (1.3)$$

where $|F_{hkl}|$ is the amplitude and ϕ_{hkl} is the phase of the reflection. From the structure factor amplitudes and phases, the electron density within the unit cell can be calculated directly by the inverse Fourier Transform (equation 1.4):

$$\rho(x, y, z) = \frac{1}{V} \sum_{all \; hkl} F_{hkl} \; e^{i\phi_{hkl}} \qquad (1.4)$$

Unfortunately, the phase angles are lost in a conventional diffraction experiment, so the crystal structure cannot be reconstructed directly. This central obstacle to structure determination is known as the 'phase problem'. Various algorithms to address this problem have been devised (e.g. direct methods, Patterson methods, maximum entropy, charge flipping).

For the reconstruction of the electron density, both the structure factor amplitudes and their corresponding phases are needed. While the measurement of the structure factor amplitudes in neutron or X-ray diffraction experiments is straightforward, the phase angles have to be determined. In direct methods, phases are estimated on the basis of reflection relationships (e.g. triplets and quartets) and the measured intensities. Some of the common direct methods packages are *SHELX* (Sheldrick, 1997), *XTAL* (Hall *et al.*, 1995) and *SIR2004* (Burla *et al.*, 2004).

An alternative is the Patterson method, which exploits the Patterson autocorrelation function (Patterson, 1934). From the Patterson function, calculated directly from the extracted intensities $\mid F^2 \mid$, detailed information about the magnitudes and the directions of the interatomic vectors between all pairs of atoms in the crystal structure can be obtained. The Patterson method is most effective in determining structures with a few heavy atoms, because their interatomic vectors are easily seen and can be used to determine the positions of the heavy atoms. Because the heavy atoms dominate the scattering, the phases calculated from this partial structure are close enough to the correct ones to allow the missing atoms to be located.

Another method for phase determination is the maximum entropy approach. This approach partitions the intensities of groups of overlapping reflections and allows information of these peaks to be included in the phase determination process. The different trial phase sets are ranked and refined according to a criteria combining entropy and likelihood (Bricogne & Gilmore, 1990). This method works best if initiated at low resolution (about 1.5 Å).

The charge flipping algorithm (CF) was first introduced by Oszlányi and Sütő in 2004 (Oszlányi & Sütő, 2004). The main advantage of the CF algorithm is it's striking simplicity (flowchart in figure 1.1). Besides the unit cell dimensions and experimental structure factor amplitudes down to a resolution of about 1.0 Å, no additional information (e.g. number and kind of atoms in the cell, the space group, etc.) is needed. An electron density map is generated by assigning random phases to the structure factors and applying an inverse Fourier transform. The calculated density is sampled on a N_1xN_2xN_3 pixel grid. Then all pixels with density values below a certain small and positive
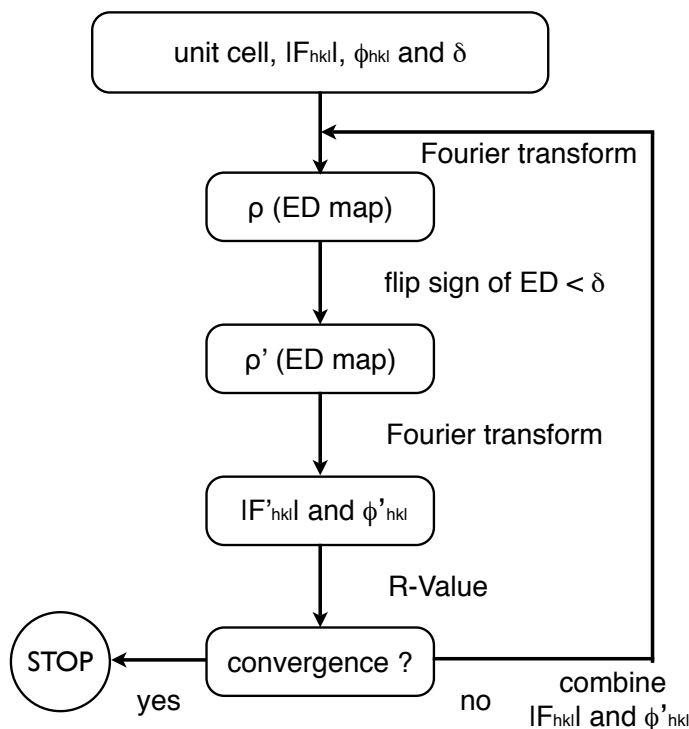
Figure 1.1: Flowchart of the charge-flipping algorithm

threshold value δ, are mutliplied by -1 (i.e. their sign is 'flipped'). The rest of the electron density remains unchanged. From this density map, a new set of structure factors is calculated, the phases of these structure factors are combined with the measured amplitudes and a new ED map is calculated and the cycle repeated. An R-value comparing the calculated structure factor amplitudes with the measured ones serves as an indicator of the convergence of the procedure. The algorithm was extended to superspace for the solution of modulated structures by Palatinus (Palatinus, 2004) and was implemented in the program *Superflip* (Palatinus & Chapuis, 2006).

1.2 Structure Determination from Powder Diffraction Data

In powder diffraction experiments, the 3 dimensional information accessible in a single-crystal experiment is lost, because it is projected onto a single dimension, the d-spacing or scattering angle 2θ (see figure 1.2). This projection to a single dimension causes accidental and systematic overlap of reflection positions in the measured data. As a result, a further problem is added to the phase problem: the intensities of overlapping reflections are ambiguous. Nevertheless, different approaches for dealing with overlapping reflections have been developed over the years.

In figure 1.3, the conventional procedure for solving a crystal structure from powder diffraction data is shown. Usually, data are collected on powder sample with randomly oriented crystallites, either in Bragg-Brentano (reflection)
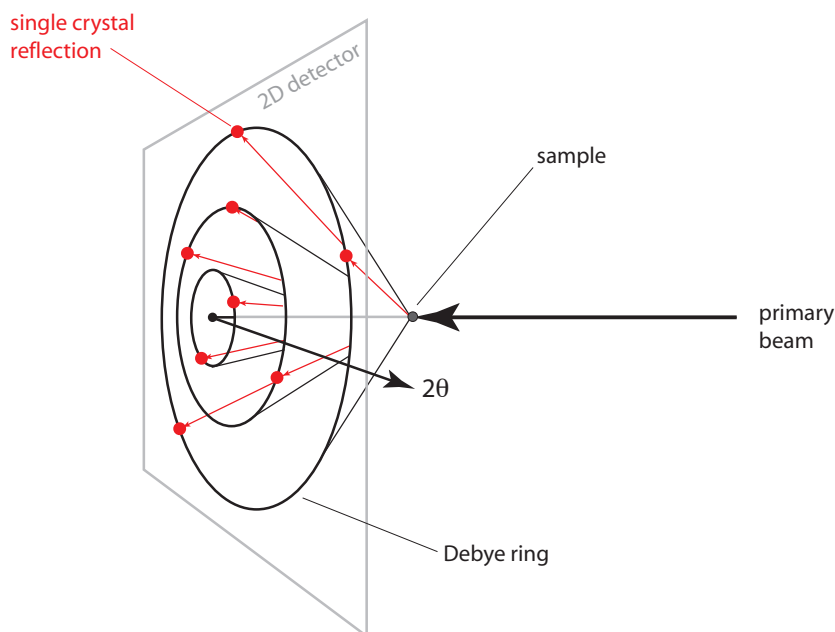
Figure 1.2: 3-dimensional information accessible for a single crystal in an X-ray diffraction experiment, superimposed on the collapsed information from a powder sample

geometry for strongly absorbing materials or in transmission geometry for lighter element samples. At this stage, care must be taken that the samples do not exhibit any preferred orientation effects, otherwise the measured intensities won't be representative of the material.

After data collection, the pattern is indexed. That is, the cell parameters and space group are determined from the positions of the peaks in the powder pattern using one of the available computer programs (e.g. N-TREOR (Altomare *et al.*, 2000), DICVOL04 (Louër & Boultif, 2006), TOPAS (Coelho, 2003)).

The most probable space groups are determined from systematic absences, but because reflections overlap, uncertainties often remain. Using the unit cell information from the indexing step, the integrated intensity of each reflection is then extracted from the diffraction pattern. Difficulties arise, of course, where reflections overlap. Several strategies for distributing the intensity of a peak over the contributing reflections have been developed (see next section), but the most common approach is to divide it equally (equipartitioning).

The structure is then solved by applying a method appropriate to the chemical composition of the material. If necessary, the structure is completed using difference Fourier analysis and finally the structure is refined using the Rietveld method (Rietveld, 1969).

```
           ┌─────────────────────┐
           │   Polycrystalline   │
           │       sample        │
           └─────────────────────┘
                     │
                     ▼
           ┌─────────────────────┐
           │   Data collection   │
           └─────────────────────┘
                     │
                     ▼
       ┌───────────────────────────────┐
       │ Indexing: unit cell, space group │
       └───────────────────────────────┘
                     │
                     ▼
         ┌─────────────────────────┐
         │   Intensity extraction  │
         └─────────────────────────┘
                     │
                     ▼
         ┌─────────────────────────┐
         │     Structure solution  │
         └─────────────────────────┘
                     │
                     ▼
     ┌──────────────────────────────────────┐
     │  Structure completion and refinement  │
     └──────────────────────────────────────┘
```
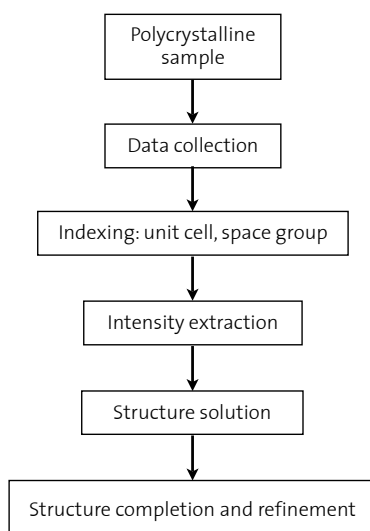
Figure 1.3: Flowchart of the conventional procedure for solving a crystal structure from powder data

1.2.1 Using Single Crystal Methods

Before conventional (single-crystal) methods of structure solution can be used, integrated reflection intensities have to be extracted from the powder diffraction pattern. The simplest way of dealing with overlapping reflections, is to equipartition the intensity over all the contributing reflections. Of course intensities extracted in this way are of low quality. A few more sophisticated methods of partitioning overlapping reflections have also been devised: e.g. Fast Iterative Patterson Squaring (FIPS) (Estermann & Gramlich, 1993), direct methods for powder diffraction e.g. EXPO (Altomare *et al.*, 1999), XLENS (Rius, 2004) and maximum entropy MICE (Gilmore *et al.*, 1990).

1.2.2 Chemical Information

Another way to compensate, in part, for the loss of information, is to use chemical information to supplement the powder diffraction data. Several such approaches have been developed over the years.

For both molecular structures and zeolites, simulated annealing (Monte Carlo) approaches, generating chemically sensible models and matching their calculated powder patterns against the experimental data, have been devised (e.g. Deem & Newsam (1989), FOX (Favre-Nicolin & Cerny, 2002), TOPAS (Coelho, 2003), DASH (David *et al.*, 2006),).

The *Focus* method (Grosse-Kunstleve, 1996), flowchart shown in figure 1.4, combines automated Fourier recycling, using integrated intensities extracted from a powder diffraction pattern (starting with random phases), with a framework search specific to zeolite structures (3-dimensional 4-connected frameworks). This approach showed clearly that the use of chemical and geometrical knowledge can compensate in part for the loss of information due to reflection overlap. Recently, it has been demonstrated that by using phases
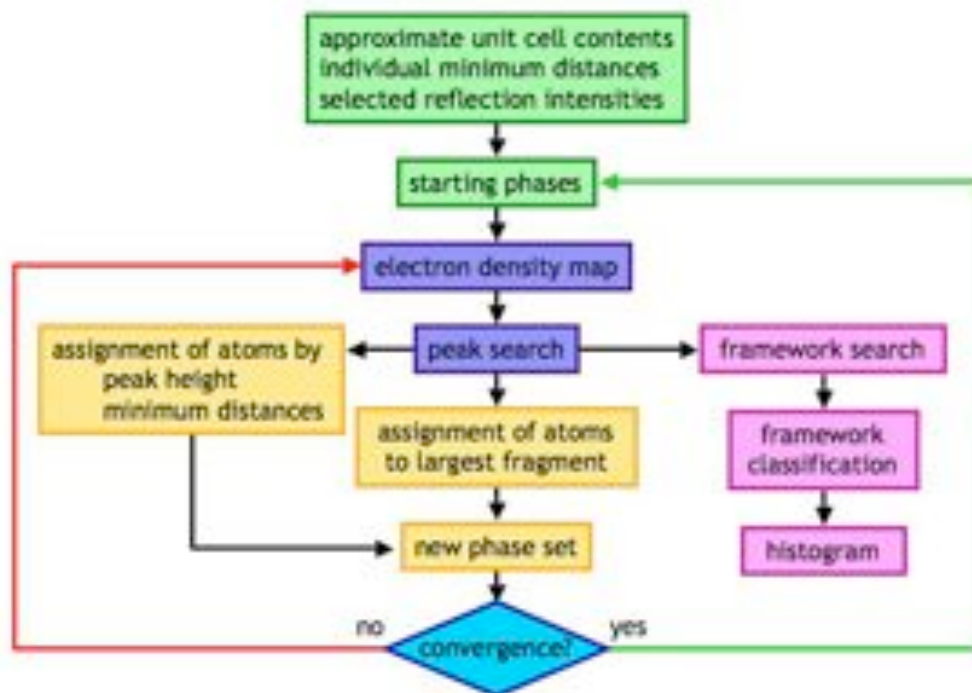
Figure 1.4: FOCUS algorithm flowchart from (McCusker *et al.*, 2001)

calculated from high resolution transmission electron microscopy images as starting phases for some reflections instead of random ones, the power of the algorithm is significantly enhanced. With this approach, (Gramm *et al.*, 2006) were able to solve the structure of the high-silica zeolite TNU-9 with 24 Si-atoms in the asymmetric unit.

Genetic algorithms, maintain a population of possible solutions for a molecular structure and perform a selection process, based on the chemical sensibility and the agreement to experimental data of each trial structure. The torsion angles are to be determined from user supplied information, which is the connectivity of the atoms, the bond lengths and angles. The population evolves by use of genetic operators that recombine and vary the initial structures or generate new structures from the fittest models by mutation. The population grows until one or a few structures reach the global minimum. This method was first applied by two research groups: (Kariuki *et al.*, 1996) and (Shankland *et al.*, 1997a).

1.2.3 Charge Flipping with Histogram Matching

The charge-flipping algorithm, which was found to be very powerful for solving structures from single-crystal data, has been adapted to the powder diffraction case: (Wu *et al.*, 2006) and (Baerlocher *et al.*, 2007a). Baerlocher *et al.* extended the iterative procedure to include an additional cycle, during which the histogram of the calculated electron density is compared with a reference histogram (of a related material) and the electron density is periodically modified to match the reference. A Fourier transform of this modified map

produces modified structure factor amplitudes, and these are used to repartition the amplitudes of the structure factors in each overlap group. These new structure factors are then used as input for the next iteration. This modified procedure proved to be very robust and successful in solving structures of organic as well as of inorganic polycrystalline materials. Recently, to access even more complex structures, the powder charge flipping algorithm with histogram matching was modified to work with phases calculated from high resolution transmission electron microscopy images. With this new procedure the structure of the zeolite catalyst IM-5 was solved (Baerlocher *et al.*, 2007b).

1.2.4 Experimental Approaches

Another approach to the problem of reflection overlap is to collect several datasets on the same sample under different conditions. For example, if a material contracts or expands anisotropically without undergoing a phase transition in a certain temperature range, the relative positions of the reflections will change as a function of temperature, but their relative intensities will not. By taking advantage of the different overlap patterns, more single-crystal-like reflection intensities can be extracted. This anisotropic thermal expansion approach was used by Zachariasen as early as 1963 to solve the structure of β-Pu (Zachariasen & Ellinger, 1963). More recently, (Shankland *et al.*, 1997b) and (Brunelli *et al.*, 2003) exploited the method to solve the structure of larger molecular crystals. Of course, this method is restricted to materials that display anisotropic thermal expansion.

A different experimental approach is the texture method, in which data are collected on powder samples in which the crystallites are preferentially orientated. By collecting data at different sample orientations, information about how the crystallites in the sample are oriented can be gained and the contribution of each reflection in an overlap group for each orientation determined. This in turn allows the relative intensities of overlapping reflections to be estimated more reliably.

1.3 Objective of the Project

The viability of the texture method to resolve overlapping reflections in powder diffraction data experimentally, was demonstrated by Wessels *et al.* (1999). These initial experiments were performed in reflection mode and required 3 days of synchrotron beamtime for a single sample. Furthermore, severe corrections for the data collected at high sample tilt angles were necessary and a large homogeneous sample was required ($\sim$ 2 cm diameter circular plate). To address these problems, the method was adapted to a transmission geometry with a 2-dimensional imaging plate detector. Data collection time could be reduced to about 6 hours, no tilt corrections were necessary and only a small (0.2 - 0.3 mm diameter) spherical sample was needed. Unfortunately, these advantages could only be gained at the cost of resolution both in 2θ (ca. 30º vs 60º) and in peakwidth (FWHM) (ca 0.06 º2θ vs 0.02º).

The objective of this project was to address these problems by adapting the

method to the 1-dimensional Silicon microstrip detector (Schmitt *et al.*, 2004) that had just been installed on the powder diffractometer on the Material Science Beamline (Patterson *et al.*, 2004) at the Swiss Light Source (SLS). This detector covered an angular range of 60º in 2θ and had an intrinsic resolution of 0.004º. Initial tests indicated that spherical samples with a diameter of about 0.3 mm would yield FWHM's in the range of 0.03º 2θ and that reasonable counting statistics could be achieved in about 10 seconds counting time. However, because the detector is only 1-dimensional, the sample had to be mounted on a Eulerian cradle in order to access all the orientations needed, and a suitable data collection strategy had to be devised.

2 The Texture Method

In 1997, Hedel and co-workers (Hedel *et al.*, 1997) described a two step procedure for deconvoluting overlapping reflections using powder diffraction data collected on a textured sample at different sample orientations. In model calculations, they showed that by using a full texture analysis to determined how the crystallites are oriented in the sample a single-crystal-like dataset can be extracted. Two years later, the practical viability of the method was demonstrated by Wessels *et al.* (1999). A conventional reflection setup was used to collect the diffraction data. More recently, the method has been adapted to transmission geometry (Prokić, 2004). The data collection strategies and analysis for both, have been described by Baerlocher *et al.* (2004). A summary of the basic concepts of the method and its practical implementation, is given in the following sections.

2.1 Concept

Because the reflection intensities extracted from powder diffraction data are of lower quality than those measured on a single crystal, the phasing procedure is less straightforward. The probability for direct methods to fail is increased, if additional ambiguities arise from the overlap of reflections. Synchrotron radiation can help, because it's high intensity and highly parallel X-ray beam allows the peak width and thereby the degree of overlap to be reduced. However, overlap is not eliminated.

The concept behind the texture method is that overlapping reflections can be separated experimentally, by preparing a sample with a preferred orientation of the crystallites. The idea is illustrated in figure 2.1 for a 2-dimensional case. On the left, the diffraction pattern for a powder sample, in which the crystallites are randomly ordered, is shown. In the 3-dimensional case, the circles become concentric spheres. The scattering angle is measured from the origin outwards. Because the intensity distribution on the rings is homogeneous for an ideal powder sample, it does not matter in which direction the pattern is measured (i.e. how the sample is oriented in the X-ray beam). On the right, the same situation is shown, but for a powder sample exhibiting preferred orientation. Now the reflections are concentrated in certain regions on the rings. In the 3 dimensional case, they are concentrated in certain regions of the concentric spheres. In both cases, the single-crystal diffraction pattern has been superimposed. The four arrows indicate a set of reflections that overlap in the conventional powder diffraction pattern. As can be seen on the right, these reflections can be separated in reciprocal space if the crystallites are oriented. More information regarding their relative intensities can be accessed by collecting patterns at different sample orientations (rotation angle ψ, tilt angle δ).

From the variations in the intensities of non-overlapping reflections as a
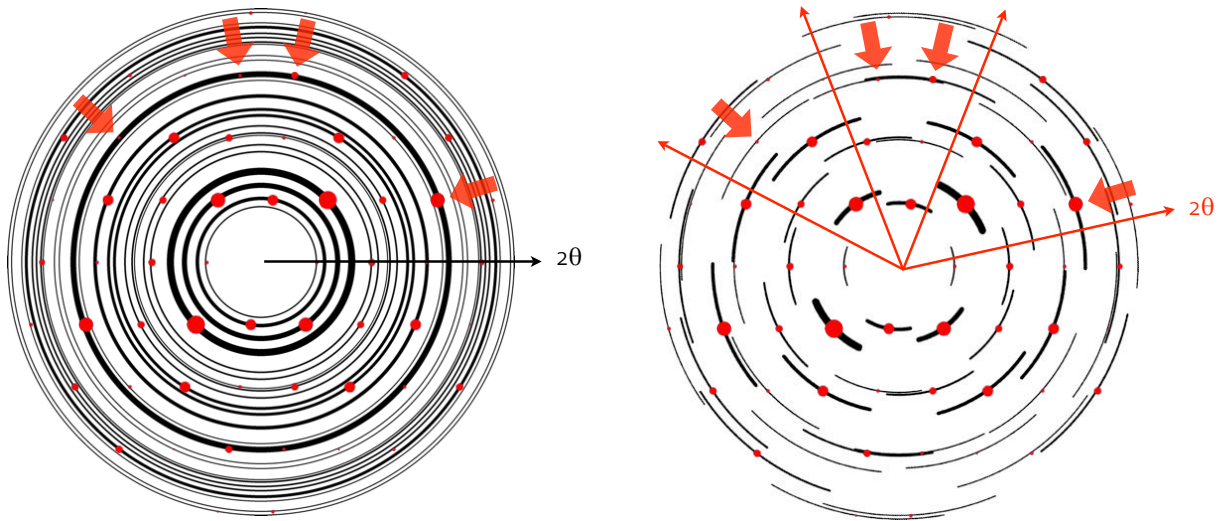

Figure 2.1: Two dimensional cuts through reciprocal space for monochromatic x-ray radiation and a random powder sample (left) and a textured powder sample (right), superimposed on both is the corresponding single crystal, accidental overlap is indicated by the arrows in both.

function of sample orientation, the orientations of the crystallites in the sample can be deduced. In practice, a full texture analysis is performed and a so-called orientation distribution function (ODF) is calculated. On the basis of the ODF, the factors $P_{hkl}(\psi,\delta)$ for all reflections can be calculated. That is, the orientations at which a specific reflection *hkl* will be strong and those at which it will be weak are known. Finally, this P_{hkl} information is combined with the diffraction data *(y)* measured at different sample orientations (ψ,δ) in a set of equations 2.1 to extract a single set of single-crystal like intensities I_{hkl}.

$$y(2\theta, \psi, \delta) = \sum_{hkl} I_{hkl} \; P_{hkl}(\psi, \delta) \; G(2\theta - 2\theta_{hkl}) \tag{2.1}$$

Where G is the standard Rietveld peakshape function.

2.2 Reflection Geometry

Wessels (1999) developed an experimental setup on the Swiss Norwegian Beamlines (SNBL) at the ESRF in Grenoble, for collecting data on textured samples in reflection mode. For this experiment, a 25 mm x 0.35 mm disk-like specimen of a homogeneously textured sample is required. To characterize the preferred orientation present in the sample, conventional pole figure measurements are performed. The intensity changes for a single reflection are plotted onto a pole grid (figure 2.2), where each point represents a different sample orientation. The 5º x 5º pole grid in ϕ and χ is used for these pole figure measurements. Standard texture software packages (e.g. BEARTEX (Wenk *et al.*,

1998), MAUD (Lutterotti *et al.*, 1997)) are used to calculate the orientation distribution function from a set of measured pole figures. The number of pole figures needed depends on the crystal symmetry, the unit cell and the method used for the ODF computation.
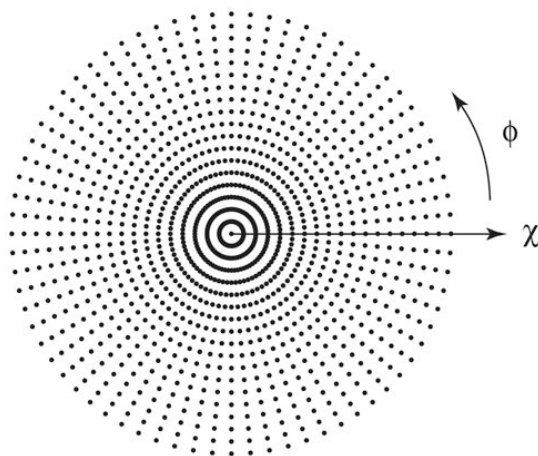

Figure 2.2: Pole grid for a conventional reflection geometry data collection

To tilt and rotate the sample in a controlled manner, two additional circles (the tilt χ and the rotation ϕ) were installed on the powder diffractometer on beamline BM01B at SNBL. Data are collected on samples mounted perpendicular to the ϕ-axis (shown in figure 2.3).
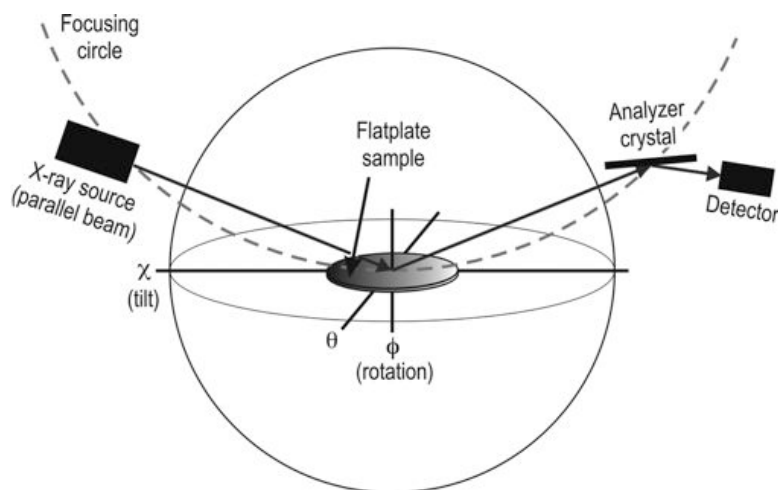
Figure 2.3: Schematics of the reflection geometry setup, with the rotation axis ϕ and the tilt axis χ

In conventional Bragg-Brentano geometry, tilting the sample in χ leads to a violation of the parafocussing condition and severe peak broadening of the diffraction peaks is the consequence. This effect was eliminated by taking advantage of the high intensity and parallel nature of the synchrotron beam,

and using a pre-detector analyzer crystal, which acts as a very narrow receiving slit.

Because the footprint of the beam on the sample changes dramatically as a function of the sample tilt χ and the scattering angle 2θ, the measured intensities have to be corrected. The irradiated sample volume is not the same for all sample orientations. To derive the necessary empirical correction curves, data had to be collected on an untextured sample of a material of known structure and a similar absorption before the main measurements.

Once the calibration measurements had been done, pole figures were collected on non-overlapping reflections for the determination of the ODF. The detector was placed at the 2θ position appropriate for the reflection and then the sample was rotated in ϕ from 0º to 360º in 5º steps. The sample was then tilted in χ and the rotation repeated. Generally, the sample was tilted from 0º to a maximum 80º in 5º steps (total of 72 x 16 + 1 = 1153 orientations). The ODF was calculated using the texture packages *Unvoll* (Dahms & Bunge, 1989) and *Beartex* (Wenk *et al.*, 1998). From the measured pole figure data, 5 to 10 orientations with the highest intensity contrast were chosen for collecting full diffraction patterns in θ - 2θ mode. The whole procedure, including the collection of the intensity correction curves as a function of tilt and 2θ angles, required about 3 days of synchrotron beamtime. Several structures have been solved using the above setup. The most impressive was that of the high-silica zeolite UTD-1F, with 117 atoms in the asymmetric unit by Wessels *et al.* (1999).

2.3 Transmission Geometry

To overcome some of the problems encountered with the reflection setup, Prokič (2004) adapted the experiment to a transmission geometry on SNBL station A. In transmission mode, a small (approximately spherical) sample with a diameter of about 0.2 - 0.3 mm is fully bathed in the beam for all sample orientations, so absorption effects can be neglected, no corrections to the data are necessary and only a small sample is required. Furthermore, a 2-dimensional *Mar345* imaging plate detector was used to collect the data, so a full series of tilt angles for each rotation were collected at once. Consequently, the whole procedure requires only 3 - 6 hours of synchrotron beamtime. The samples were prepared, as for the reflection mode experiment, but a small (0.2 - 0.3 mm) sample was cut from the larger one for data collection. The final sample was mounted on the tip of a glass capillary for the measurement. As shown in figure 2.4, the setup allows full diffraction patterns to be collected at all orientations.

The pole grid for the intensity measurements could be extended, because now all orientations were accessible: the rotation angle ψ is measured from 0º - 180º/ 0º - 360º and the tilt angle δ from 0º - 180º/ 0º - 90º, both in 5º steps (a total of 1296 unique orientations). But the price paid for the reduction in data collection time was a poorer resolution of the data in peakwidth (FWHM) as well as in 2θ ($d_{min.}$). In the final data collection procedure datasets were collected at a sample-to-detector distance of 240 mm and 400 mm and

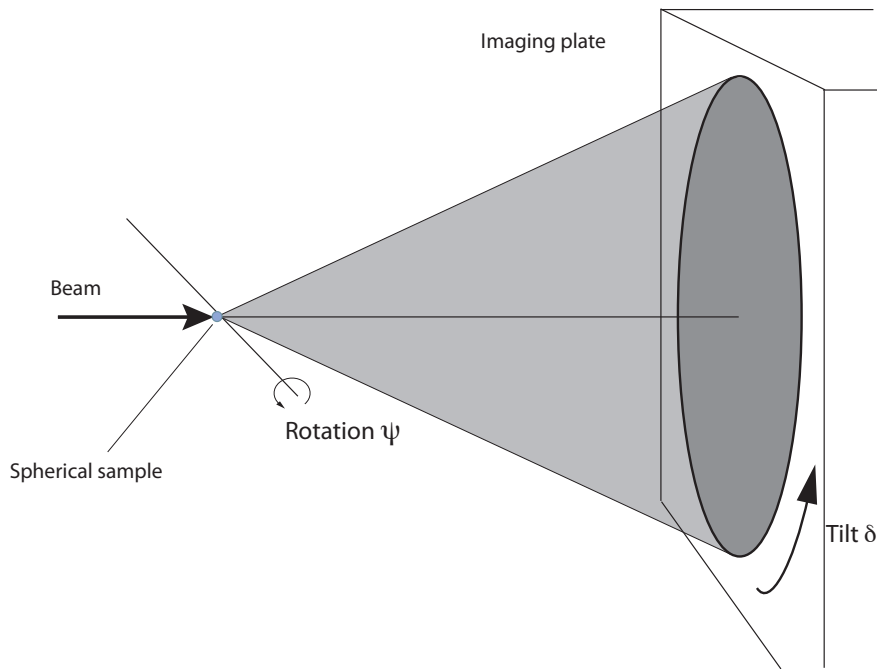Figure 2.4: The transmission setup with an image plate detector, allowing full patterns to be collected at the rotation angle ψ and the tilt δ

these were combined to increase the resolution in $d_{min.}$ from 2.0 Å (400 mm) to about 1.3 Å (240 mm) at a wavelength of 0.8 Å (figure 2.5). However, there is a concomitant increase in peakwidth from about 0.06°θ at 400 mm to 0.09°θ at 240 mm. The 2 datasets were combined to yield data with the high $d_{min.}$-resolution needed for structure determination with sharp FWHM's to increase the quality of the extracted integrated intensities at lower angles. From data collected at 240 and 400 mm on a textured sample of the calcium silicate CAS-1, a set of structure factors was extracted and could be used to solve the structure using direct methods (Jorda *et al.*, 2005). The same procedure applied to a textured sample of the aluminophosphate AlPO-M, however, did not succeed. By including high-resolution powder diffraction data collected on an untextured capillary sample in the intensity extraction procedure (i.e. both texture and high-resolution data), more reliable structure factors were obtained and the structure could be solved (Baerlocher *et al.*, 2004).

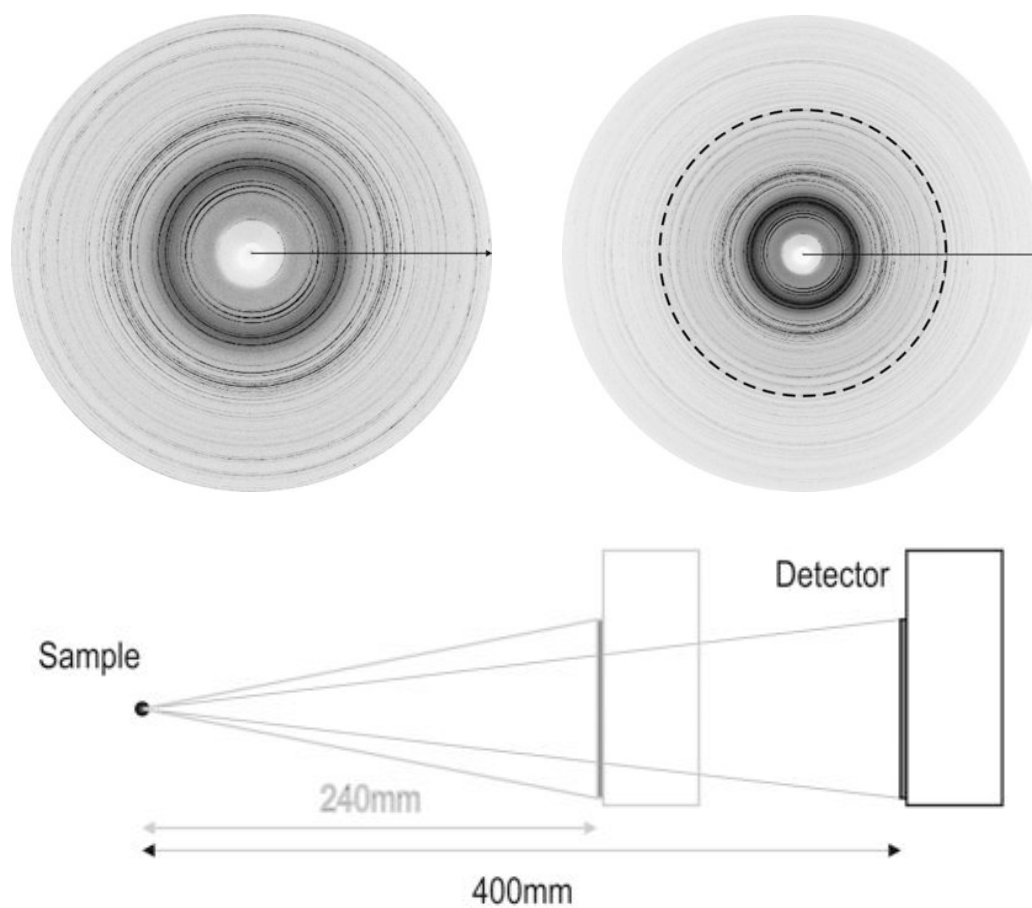Figure 2.5: Image plate frames collected at sample-to-detector distance of 400 mm (left) and at 240 mm (right). Dashed line indicates the 2θ limit for the 400 mm distance (Prokić, 2004)

3 Sample Preparation

The main requirement for the successful application of the texture method, besides a suitable data collection setup, is the availability of a polycrystalline sample with a high degree of preferred orientation. (Hedel *et al.*, 1997) found from their simulations, that an increase in texture strength goes hand in hand with an increase in the quality of the structure factors extracted. Their observation was later confirmed by Prokić (2004). In principle, a wide variety of crystal properties can be used to induce preferred orientation. These include electric and magnetic properties, spontaneous organization (self-assembly), crystal morphology, or the properties of a matrix material mixed with the sample of interest. In this investigation the emphasis was on the latter two approaches.

3.1 Materials

One possibility for inducing preferred orientation, involves mixing the sample with a small amount of a polymeric material that can serve as a matrix. The polymer fullfills two main needs: (1) any shear forces applied to it are transferred to the crystallites of the sample and (2) the specimen becomes self-supporting. Amorphous polymers must be used, otherwise reflections arising from the matrix material are superimposed on the diffraction pattern of the material of interest. For the different tests described in the following sections, some partially crystalline polymers have been investigated, see table 3.1.

Table 3.1: Polymeric materials investigated

Polymer	Average M_W	Manufacturer
ultra-high molecular weight polyethylene (UHMWPE, GUR® 4120)	5'000'000	Ticona GmbH
polyethylene oxide (PEO)	5'000'000	Polysciences Inc.
polyvinyl alcohol (PVA) (87-89 % hydrolyzed)	146'000 - 186'000	Sigma-Aldrich Inc.
polystyrene (PS)	280'00	Sigma-Aldrich Inc.

The diffraction pattern of a pure polystyrene (PS)-foil drawn in hot air at about 100°C is shown in figure 3.1, to illustrate the form of the amorphous background originating from the PS matrix.
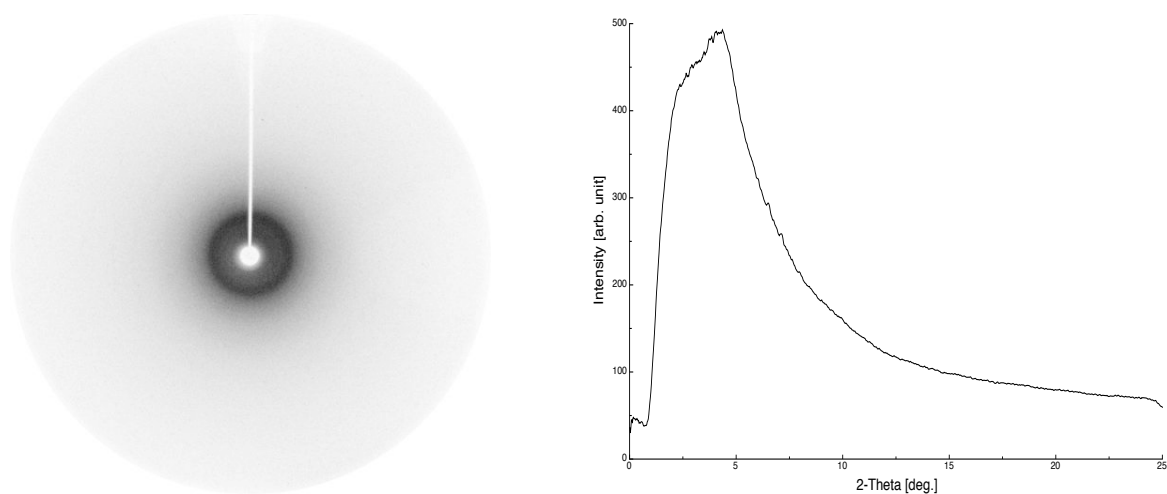

Figure 3.1: Diffraction pattern collected on a pure PS-foil drawn in hot air of about 100°C(left) and the corresponding powder pattern integrated from the image plate frame (right)

The following solvents (all obtained from Fluka Inc.) were used to dissolve the different polymers (table 3.2):

Table 3.2: Solvents

Solvent	Chemical formula
tetrahydrofuran (THF)	C_4H_8O
xylene	C_8H_8
methanol	CH_4O
chloroform	$CHCl_3$

3.2 Tensile Testing

The first experiments were performed in collaboration with the Polymer Technology Group in the Department of Materials at ETH Zurich. Ultra-high molecular weight polyethylene (UHMWPE)-foils containing different weight fractions of crystallites of the zeolite offretite were prepared. The UHMWPE was dissolved in xylene at 100°C. After one day, the appropriate amount of offretite was added to the polymeric solution and the mixture was poured into an aluminum form and dried for another day. From the resulting foils, small strips (70 mm x 10 mm) with a thickness of about 1 mm were tensile tested

(stretched) at 100°C to induce an orientation of the crystallites. To eliminate the sharp reflections originating from the crystalline domains in UHMWPE, foils with PS (dissolved in tetrahydrofurane (THF) at room temperature) in place of UHMWPE as the matrix material were cast and tensile tested under exactly the same conditions. Diffraction patterns from samples prepared in this way are shown in figures 3.2 and 3.3.
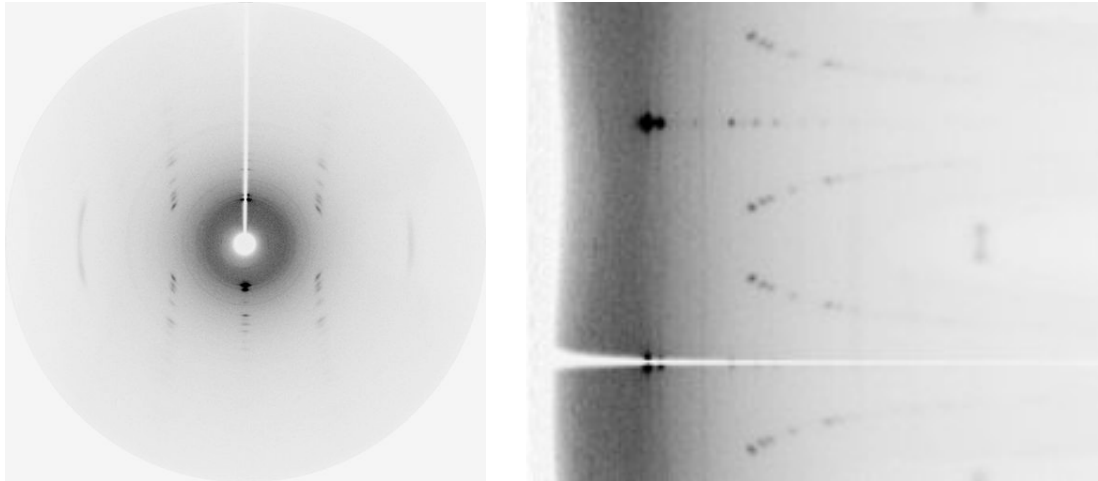

Figure 3.2: Diffraction pattern of a UHMWPE/Offretite-foil tensile tested at 100°C (left), unrolled pattern 2θ vs. azimuth 0-360° (right)
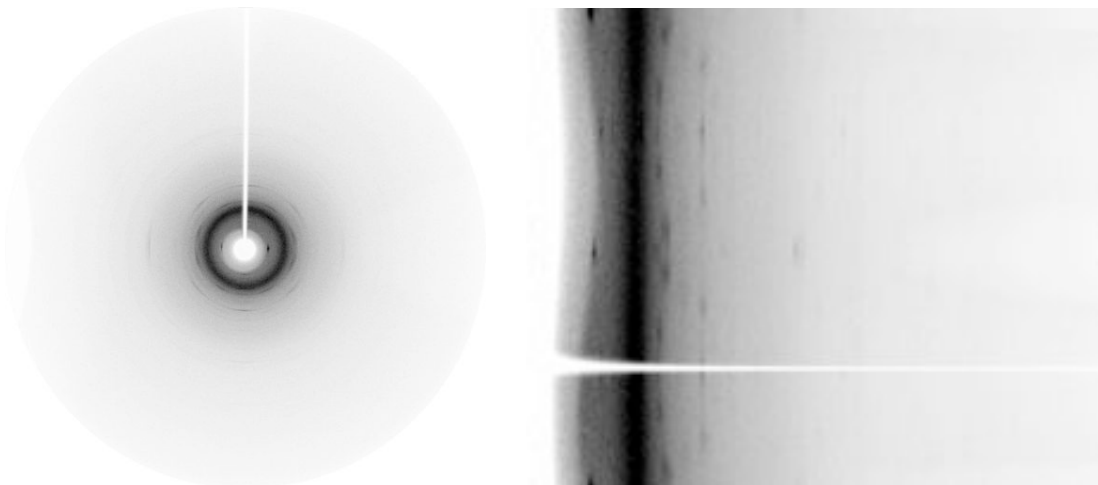
Figure 3.3: Diffraction pattern of a PS/Offretite-foil tensile tested at 100°C (left), unrolled pattern 2θ vs. azimuth 0-360° (right)

In view of the weak diffraction patterns obtained in these first tests, it was apparent that increasing the amount of sample and decreasing the amount of matrix material, was essential. Also it was thought hot drawing rather than tensile testing might further improve the preferred orientation in the samples. To reduce the amount of matrix material to a minimum, composite samples, consisting of a small amount of sample paste with PS matrix between two pure

UHMWPE-foils, were produced and tested.

During tensile testing, poor or no elongation of the samples was observed. This is probably because of the low tensile strength of the amorphous PS-matrix. However, alignment took place in at least some of the samples. In contrast, the UHMWPE-foils exhibited a very high tensile strength, but the sample material content could not be pushed above 0.5 wt.%, which is far too little. An additional problem, in the case of the composite samples, was the separation of the layers, because of the high tensile strength of the outer UHMWPE-layers compared to the inner layer containing only the sample crystallites and the PS matrix.

3.3 Modified Matrix-Smear Method

The matrix-smear method originally applied by Wessels *et al.* (1999) and further developed by Prokić (2004), was again modified. Disaggregated crystallites (using pulsed ultra-sound) were mixed with a solution of PS in THF (50 wt.%) and spread layer by layer, onto an elastic band, rather than on a glass slide. After about 10 minutes, when the sample mass exhibited a gel-like state, the rubber band was stretched to about double its original length and fixed. The main benefit of this method, is to pass additional shear forces to the sample mass, in a state where a lot of the solvent has already evaporated, i.e. the sample mass exhibits a higher viscosity than the initially prepared solution. With this method, samples of several different materials were prepared. Examples are shown in figures 3.4 and 3.5.

Figure 3.4: Synchrotron diffraction data of a PS/Offretite sample prepared by the modified matrix-smear method (left), unrolled pattern 2θ vs. azimuth 0-360º (right)

Some additional samples were prepared using polyethylene oxide (PEO) as the matrix material in place of PS, because self-supporting samples could be obtained with solutions containing only 0.5 -1 wt.% PEO. Although PEO exhibits a partially crystalline character, it was hoped that the small amount of
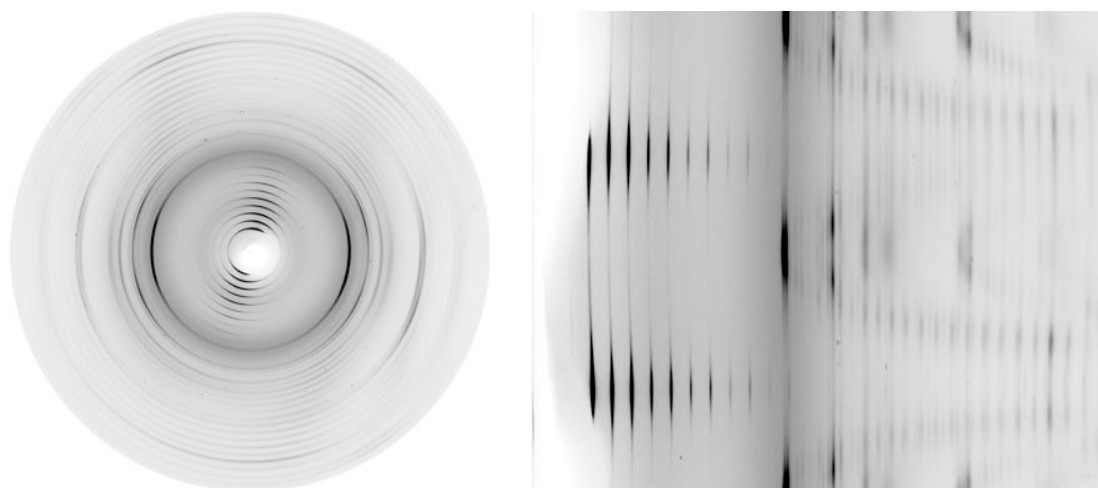
Figure 3.5: Synchrotron diffraction data of a PS/Ag-Behenate sample prepared by the modified matrix-smear method (left), unrolled pattern 2θ vs. azimuth 0-360º (right)

matrix material in the sample would be undetectable in the X-ray measurements. Unfortunately, in all the test measurements PEO peaks were present (figure 3.6).
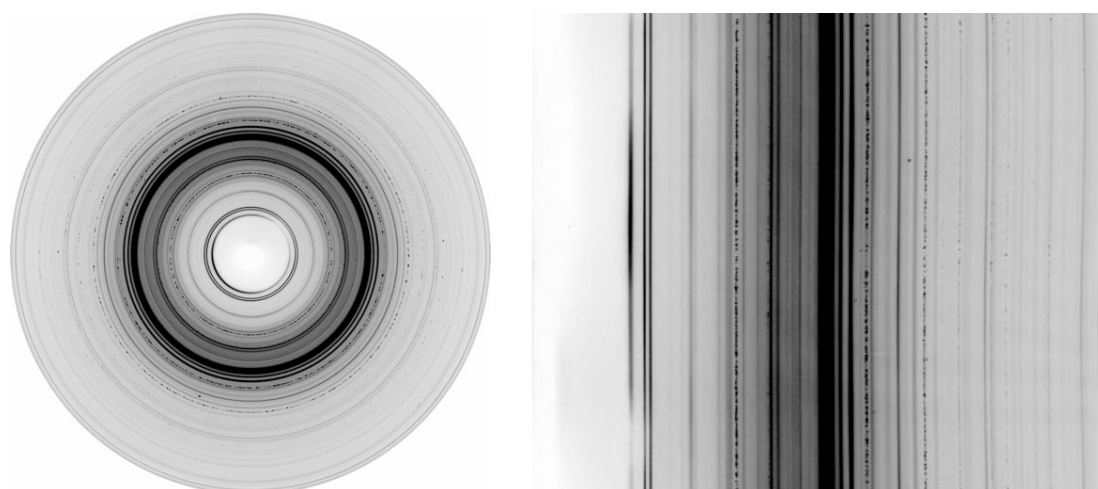
Figure 3.6: Synchrotron diffraction data of a PEO/IM-5 sample prepared by the modified matrix-smear method (left), unrolled pattern 2θ vs. azimuth 0-360º (right).

3.4 Micelles

A procedure for aligning of protein molecules for nuclear magnetic resonant NMR measurements has been reported (Tjandra & Bax, 1997) and it was thought that it might be adapted to the situation here. The magnetic field-

induced orientation behavior of buffered mixtures of the detergent 3-(chlor-amidopropyl)dimethylammonio-2-hydroxy-1-propane sulfonate (CHAPSO) and 1,2-dimyristoyl-*sn*-glycero-3-phosphocholine (DMPC) has been studied by Sanders & Prestegard (1990). 1:5 mixtures of CHASPO:DMPC containing water in the range of at least 65-85 % form micellar systems, which switch from a liquid gel into a nematic liquid crystal phase (with the crystals oriented along a particular direction), if a magnetic field is applied. Just above room temperature, this crystal phase consists of disc-shaped particles (so-called bicelles). Bicelles have diameters of several hundred angstroms and thicknesses of about 40 Å . Because of their diamagnetism, bicelles can be oriented with their plate-axis parallel to an applied magnetic field.

Solutions of CHAPSO and DPMC with different molar ratios were prepared according to instructions from Avanti Polar Lipids (Avanti Polar Lipids, Inc.) in a 10 mM phosphate buffer and 0.15 mM sodium azide aqueous solution. Unfortunately, no stable solutions of CHAPSO and DPMC were obtained, and no sign of preferred orientation was found in the samples produced and dried in a permanent magnetic field. A possible explanation is the collapse of the ordered liquid crystal phase during the drying process resulting in (re)agglomeration of the crystallites.

3.5 Bakery-Folding

A further possibility for introducing a strong alignment, especially with crystallites with plate-like morphologies involves mixing the sample with as little matrix material as possible, and then subjecting the mixture to pressure molding. This procedure was initially tested using a ca. 70 mm x 10 mm x 1 mm form. Later, a special die was constructed so that the sample mass, placed in the middle of the die, was forced along a narrow channel as pressure was applied. The die consists of a channel with a width of 5 mm and a corresponding punch, leaving a gap of 0.3 mm (the desired sample thickness) if fully pressed into the die (see figure 3.7).
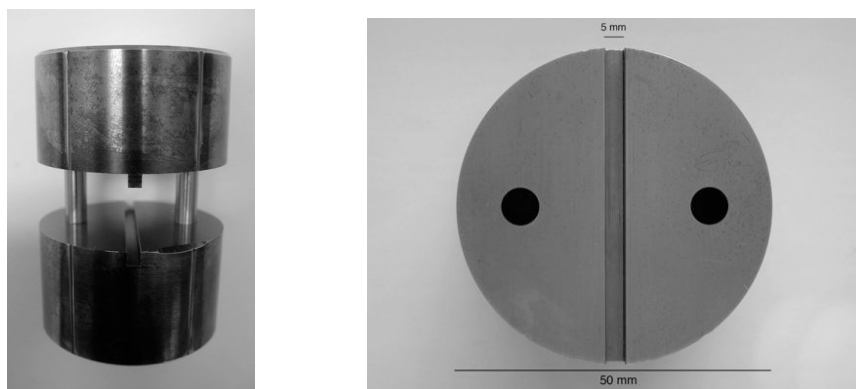

Figure 3.7: Die designed for repetitive pressure molding

A gel-like sample mass (dried for 2-3 hours from a solution) was pressed at

room temperature. In some cases, the resulting foil was cut into equal pieces after it had dried, and then stacked in the die and pressed again at 100°C. In some experiments the procedure was repeated several times (so-called bakery-folding), to further increase the strength of the preferred orientation. Tests were performed with crystallite contents in the range of 20 - 80 wt.% to identify the optimal press parameters and sample composition. Finally, a ratio of 1:1 between polymer matrix and sample material proved to work best.

In an attempt to improve the texture strengths obtained with the bakery-folding procedure, sodium dodecyl sulfate (SDS) was added to prevent (re)agglomeration of the crystallites. A sample of the zeolite IM-5, which had resisted all previous attempts to prepare a textured sample was prepared in this way, and as can be seen from the diffraction data, shown in figure 3.8, the crystallites could finally be aligned.

Figure 3.8: Data from a PS/IM-5 sample prepared using the repetitive pressure molding collected using the 2-dimensional PILATUS 6M detector on the X06SA PX beamline at the SLS (left), and the unrolled pattern 2θ vs. azimuth 0-360°. Note the intensity variations corresponding to different sample orientations indicating that preferred orientation had been induced.

3.6 Fiber Spinning

Khavari et al. (Khavari, 1990) was able to spin fibers from a PEO-ZrO_2 solution using a continuous dry-spinning process. Initial tests for dry-spinning pure PEO-fibres from solutions of 1 to 2.5% PEO in chloroform, were performed using the setup shown in figure 3.9. An automatic syringe pump *Model A-99* from Razel Scientific Instruments, Inc., was used to extrude polymer solutions at constant flow rates. Fibers exhibiting a maximum thickness of about 20 μm could be produced. However, when the standard sample was addded to the solution, no fibers could be produced under controlled spinning conditions. In further tests, polyvinyl alcohol (PVA) and PS were tried in an

effort to produce thicker fibers with oriented crystallites. Unfortunately, PS fibers could not be produced, because the PS/sample mixture proved to be too unstable for the dry spinning process. A modified version of the process developed by (Yamaura *et al.*, 2004) for the production of PVA-fibers using solution spinning into a methanol bath at -30ºC, led to stable fibers, but at the cost of PVA reflections in the diffraction data.
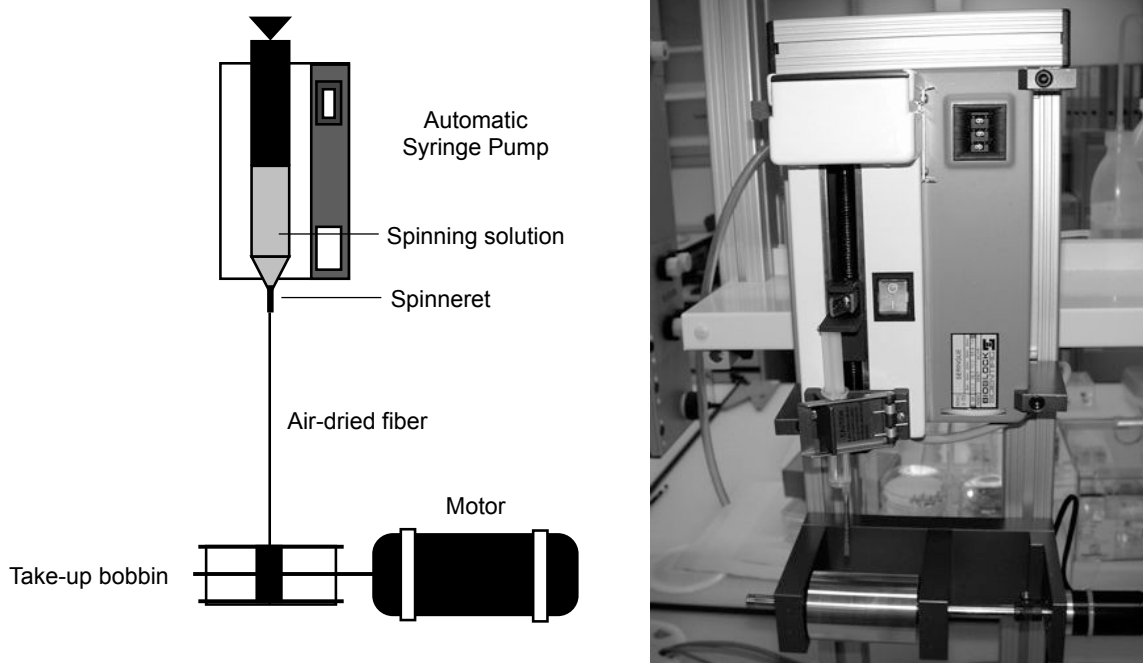

Figure 3.9: Schematic (left) and laboratory setup used for the fiber spinning experiments (right)

3.7 Crystal Growth

If the crystals to be analyzed exhibit fiber morphology, a textured powder sample can sometimes be prepared by simply aligning the fibers mechanically (e.g. using of tweezers). This method was used to prepare a textured sample of viologen vanadate, which crystallizes as thin fibroid crystals, see figure 3.10. In the case of the zeolite IM-12 (**UTL** framework type) the crystallites grew as stacked platelets, which lead to oriented agglomerates with a size of about 100 μm x 100 μm x 80 μm, which could be mounted and measured directly (figure 3.11).

The main advantage of these special morphologies is that there is no need to use a matrix material to produce a self-supporting sample. Of course this method is only applicable to a special group of materials, but is highly effective, because the diffraction data only reflects the sample to be analyzed and is not altered by any additional diffraction phenomena from a matrix material or other additives.
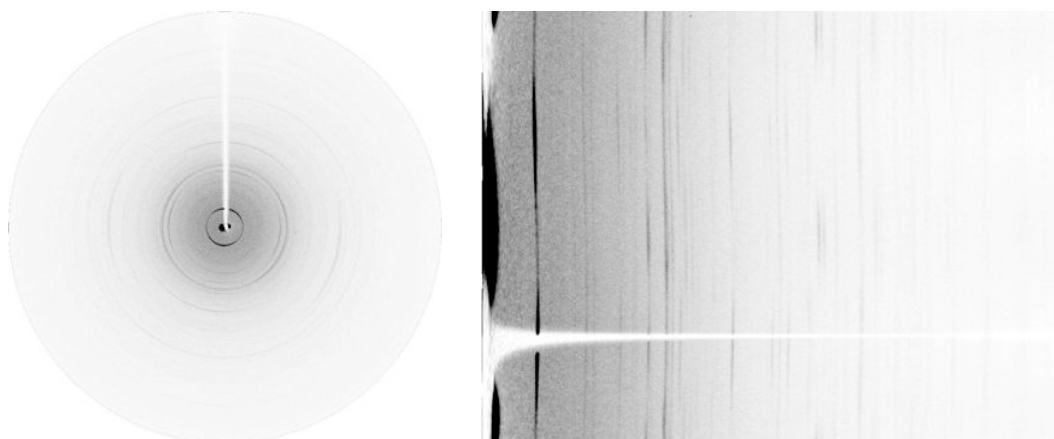
Figure 3.10: Laboratory diffraction data of a pure viologen-vanadate sample prepared by simply aligning the fiber-like crystals (left), unrolled pattern 2θ vs. azimuth 0-360º(right)
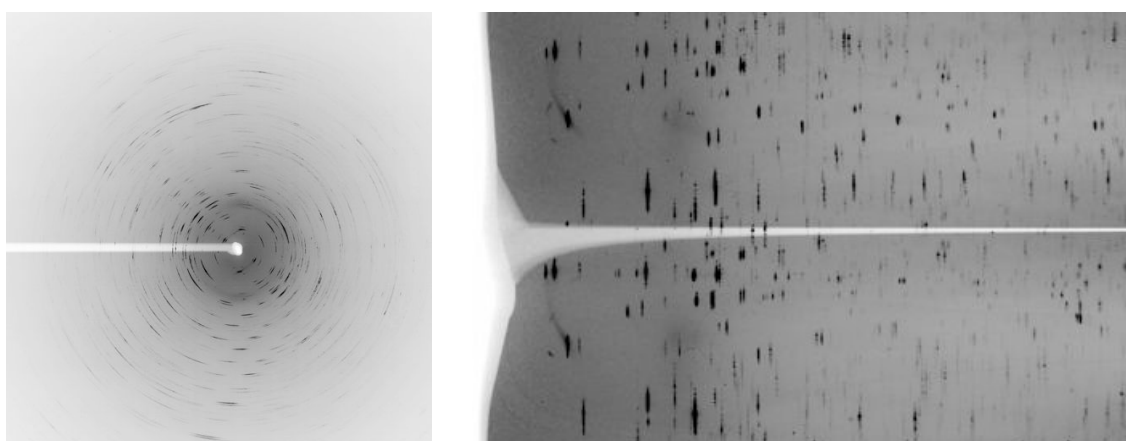

Figure 3.11: Data from a single IM-12 agglomerate, collected using the 2-dimensional PILATUS 6M on the X06SA PX beamline at the SLS (left), and the unrolled pattern 2θ vs. azimuth 0-360º (right)

3.8 Summary

By far the best results, a single-crystal like texture, was obtained for the single agglomerates of IM-12, which fortunately grew as a stacked order of platelets. From the 'man-made' methods, the repetitive pressing procedure performed best. With the zeolite offretite, several samples with the crystallites oriented along a fiber axis could be produced. For the samples of IM-5 (figure 3.8) and AM11 (figure 3.12), even a 3-dimensional texture was obtained. Advantages of this method are: (1) that texture samples can be produced in standardized procedure and (2) its independence from the person preparing the sample.
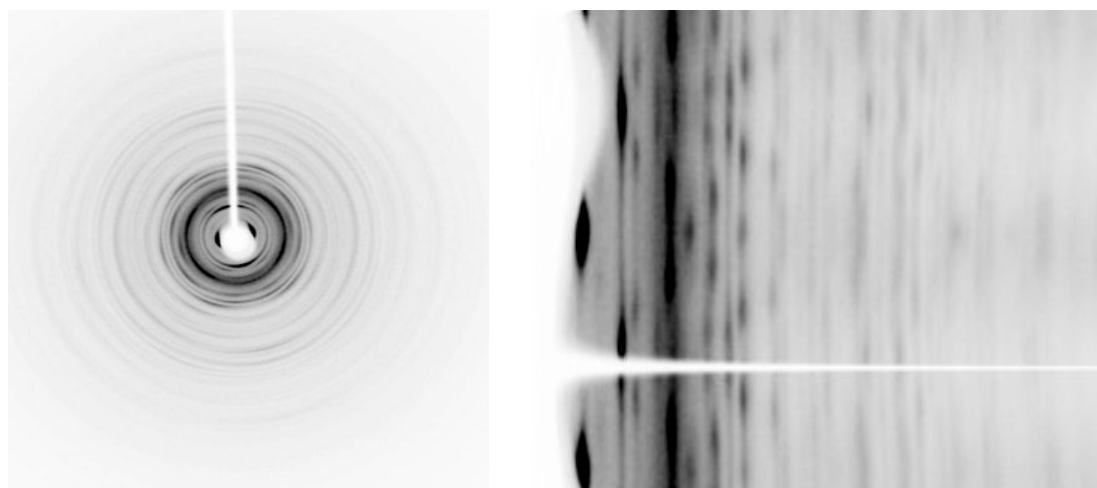
Figure 3.12: Data from a PS/AM11 sample prepared using the repetitive pressure molding collected on an *Oxford Diffraction Xcalibur* single crystal diffractometer (left), and the unrolled pattern 2θ vs. azimuth 0-360°. Note the intensity variations corresponding indicating that preferred orientation had been induced.

4 Data Collection

For this project, synchrotron data were collected on both Swiss Norwegian Beamlines (SNBL) at the European Synchrotron Facility (ESRF) in Grenoble (France) and on the Material Science beamline the Swiss Light Source (SLS) in Villigen (Switzerland). Data collection at both facilities was performed in transmission mode using approximately spherical samples, with a diameter of ca. 0.3 mm. The advantages of the imaging plate detector used at SNBL are twofold: the counting statistics are good even for higher 2θ angles, and a complete tilt series for a specific sample rotation is collected in a single shot. The microstrip detector at SLS is superior in both d-resolution (2θ range) and peakwidth, but because this detector is linear, a Eulerian cradle is needed to orient the sample. The Material Science Beamline has a minigap wiggler that produces hard X-rays in the energy range 5-40 keV (Patterson *et al.*, 2004). SNBL has a similar spectral range, but is situated on a conventional bending magnet source.

Additionally, test datasets were collected with the Pilatus 6M pixel detector (Hülsen *et al.*, 2006), installed on the X06SA protein crystallography beamline at SLS, to evaluate its suitability for texture measurements.

4.1 Experimental Setup on the SNBL Beamline BM01 A

To calibrate the experimental setup at SNBL, data were collected on a standard NIST 640a silicon sample before any experiment. The spherical samples of interest, comprised of preferrentially oriented crystallites in a polystyrene matrix, were mounted on a conventional single-crystal goniometer and centered. Data were then collected as a function of sample rotation (ψ) from 0-360º in 5º steps using a *Mar345* image-plate detector system. The pixel-size was set to 100 μm. With this setting the detector has 3450 active pixels, which require a readout time of ca. 100 seconds. To obtain the best possible resolution in peakwidth and an acceptable 2θ-range, the imaging plate detector was displaced diagonally (see schematics in figure 4.1) with respect to the primary beam.

 At the maximum sample-to-detector distance of 400 mm, this arrangement yields a 2θ range of about 0-35º and FWHM's in the range of 0.06º2θ for a wavelength of 0.8 Å. If the rotation ψ is done over the full 360º, the single quadrant contains the complete pole figure data needed for an ODF calculation (Prokić, 2004).
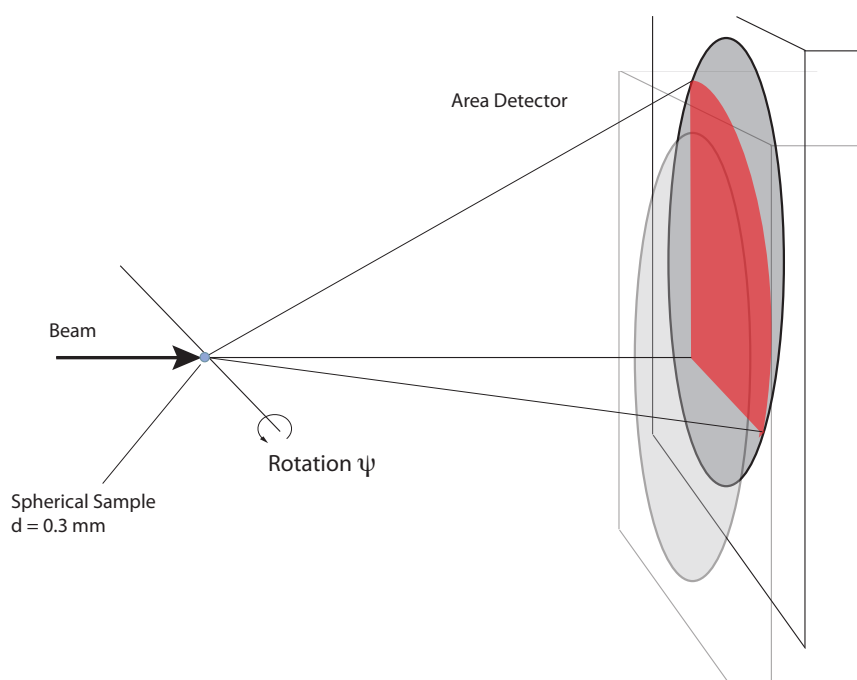
Figure 4.1: Conventional transmission setup with an image-plate area detector, superimposed the diagonally shifted position of the detector

4.2 Experimental Setup on the Material Science Beamline at SLS

4.2.1 The Si-microstrip detector

To extend the applicability of the texture method to even more complex structures, data needed to be collected at higher resolution, in both 2θ-range and peakwidth. Therefore, an experimental setup with the 1-dimensional Si-microstrip detector at the SLS was devised. The microstrip detector covers 60º in 2θ with an intrinsic resolution of about 0.004º (Schmitt *et al.*, 2004). The peakwidth of course, is dependent upon the diameter of the sample and its crystalline quality. For a 0.3 mm sample, a resolution of about 0.03º2θ could be expected. This was confirmed in the initial test measurements. The detector consists of 12 modules, each with 1280 silicon sensor strips and electronic components for read-out (figure 4.2). Between the individual modules there is a gap of ca. 0.2º, which results in 'blind' regions in the diffraction pattern. The time to read out the entire detector (a total of 15360 channels) is just 250 μsec.

4.2.2 The Setup

In order to access all of the 1368 orientations necessary for a texture measurement (0º $\leq \psi \leq$ 360º and 0º $\leq \delta \leq$ 90º), a Eulerian cradle was used. The setup at the beamline is shown in figure 4.3. B. Schmitt, who is developing the microstrip detector, kindly wrote a script to rotate the sample from 0 to 360º

in 5º steps and to tilt it from 0º to 90º also in 5º steps. At each orientation, the sample was oscillated around both axes by ±0.5º (for samples with large crystals, even ±2.5º) while the diffraction patterns were collected.
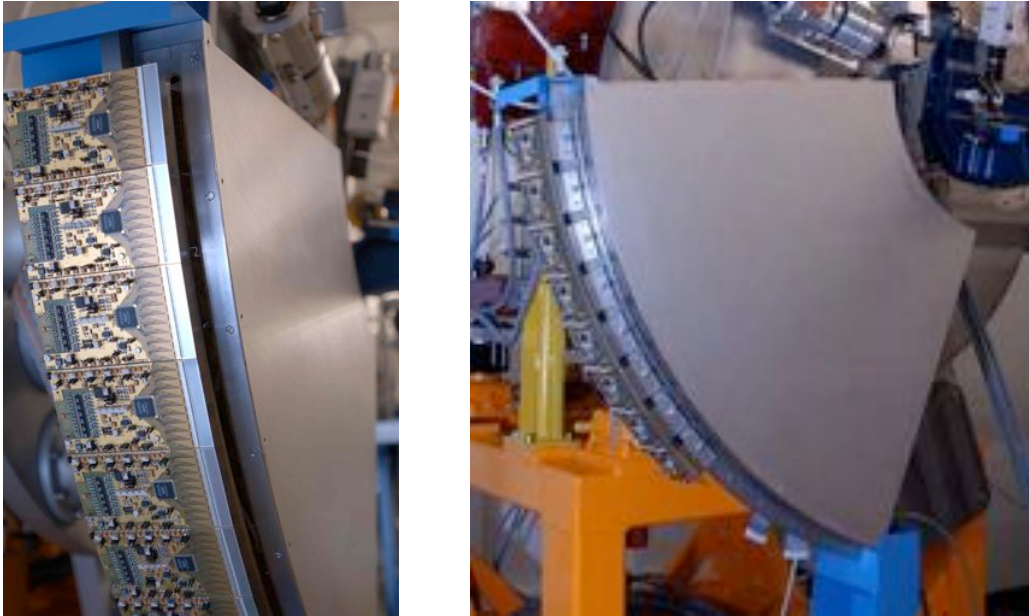

Figure 4.2: The individual modules at the back of the detector (left), and the detector, equipped with 8 modules, installed on the Material Science beamline at SLS (right)

The sample was oscillated to smooth any graininess present in the sample and thereby to improve the statistics and smoothness of the texture. Because of the gaps between the detector modules, two datasets collected with different detector positions, have to be merged to obtain a full dataset. To collect data in such a way, about 12h are needed. In all experiments, the maximum reflection intensity had to be restricted to ca. 30'000 counts, because the prototype detector used became overloaded at higher fluxes. This was done by inserting filters between the primary beam and the sample.

In the first experiments, it became apparent that the homogeneity of the synchrotron beam was critical, because of the movement of the sample in the cross-section of the beam and the sphere of confusion that is present in any Eulerian cradle. Therefore, a de-focused beam of ca. 0.6 mm x 0.6 mm was used for subsequent measurements. A diffuser (rotating sheets of paper) was also inserted into the beam to further homogenize the beam. The X-ray eye mounted on the microstrip arm was used to check the intensity distribution in the photon beam. The goal was to provide a large homogenous area in the primary beam (see figure 4.4), so that the sample could be centered and oriented within it, without causing any intensity changes related to beam inhomogeneity.

Figure 4.3: The setup on the Material Science beamline at the SLS, showing the beam pipe, the Eulerian cradle with the rotation axis ψ and the tilt angle δ and, indicated at the back, the entry slit to the micostrip detector

4.2.3 Calibration

Before starting the texture measurements, the homogeneity of the attenuated beam was checked with an untextured sample of the cubic Zeolite-A (*a=12.4 Å*) mixed with polystyrene. Diffraction patterns were collected at the rotation angles ψ: 0º, 90º, 180º and 270º for both tilt angles δ: 0º and 90º. Reflection intensities were compared for differences between different sample orientations. If necessary the beam was further equalized until no differences were found. To minimize the displacement of the texture sample in the cross-section of the beam during data collection, each sample was carefully aligned. In the setup shown in figure 4.3, with a tilt angle δ of 0º (horizontal position), rotating an unaligned sample about the ψ-axis, results in a shift of the entire diffraction pattern. By carefully measuring the positions of the diffraction peaks for different angles ψ, the position of the sample can be adjusted to coincide with the ψ axis. Similarly, by keeping the rotation angle ψ constant and measuring data for the tilt angles δ = 0º and 90º the height of the sample can be corrected. Finally, the data collection script was launched to collect full diffraction patterns at all 1368 orientations ($0º \leq \psi \leq 360º$ and $0º \leq \delta \leq 90º$).

4.2.4 Data Collection in Combination with a Cluster Analysis

To improve the counting statistics for the patterns used for the final intensity extraction, a different data collection strategy was developed. First, data for all
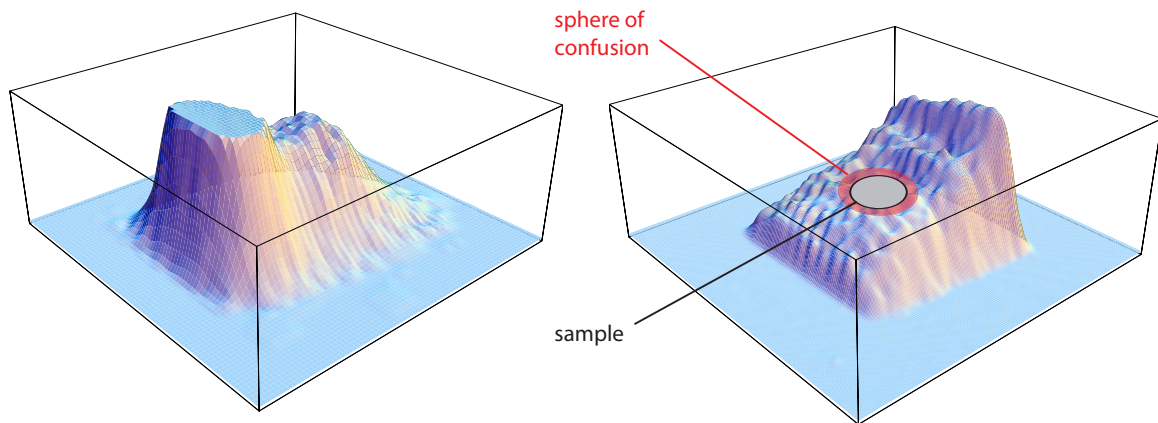
Figure 4.4: 3-dimensional profiles of the shape of the photon beam, badly equalized (left) and de-focused for a texture measurement (right). The cross-section of a 0.3 mm sample and the sphere of confusion related to the Eulerian cradle are shown for comparison.

orientations are collected with a single detector position (carefully chosen so that the gaps do not occur at important peak positions) and integrated intensities are extracted from the diffraction patterns online during data aquisition. These data are used to calculate an ODF, and this ODF is used to identify 5-10 orientations with the highest intensity contrasts (see section 5.3). Data with good counting statistics are then collected at these sample orientations. This improved procedure was used to collect data on the following unknown materials of unknown structure: Ag-Behenate, AM11 and IM-5.

5 Data Analysis

5.1 Raw Data Processing

After data collection with the setups described in the previous chapter, several steps of raw data treatment are necessary before the data can be further evaluated. The raw data handling steps are specific to each of the experimental setups. From the imaging plate frames, patterns for the different tilt angles have to be integrated. From the Si-microstrip data, bad counting channels have to be eliminated and all patterns collected at the same sample orientation merged. For both setups the data have to be normalized.

5.1.1 SNBL *Mar345* Image Plate Frames

An advantage of the 2-dimensional image plate detector is that a complete tilt series for $0^o \leq \delta \leq 90^o$ for each rotation angle ψ, is contained in a single frame. A full dataset consists of 72 imaging plate frames, each integrated over a sample rotation ψ of 5° during data collection. The beam center, the sample-to-detector distance and the detector tilt angles are calibrated using the NIST 640a silicon data. Then for each frame, radial wedges covering a tilt angle of 5° are integrated, to yield 19 powder diffraction patterns corresponding to 19 tilt angles δ (figure 5.1). The wedges are integrated using the software package
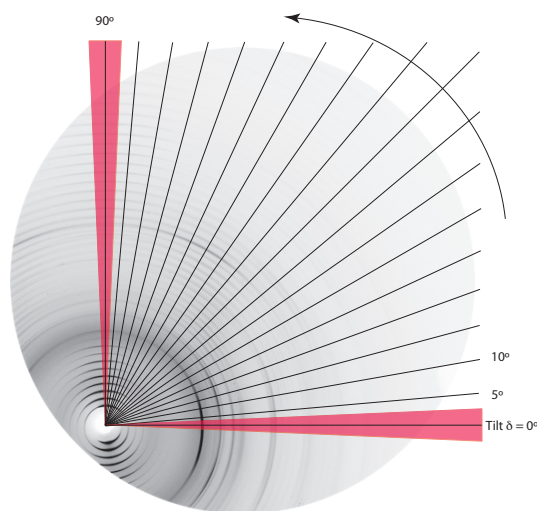

Figure 5.1: Integration of powder diffraction patterns for tilt angles δ 0-90° from an image plate frame collected for a rotation ψ of 5°. The wedges for 0° and 90° are indicated (solid), for the others only the center is indicated (solid line).

Fit2d (Hammersley *et al.*, 1996). The tilt angle, which is assigned to each integrated pattern, is the center angle of each wedge. For example the pattern at the tilt angle δ=0º is integrated from -2.5º to 2.5º. Usually, the patterns generated from the different image plate frames are normalized (corrected for the intensity decay of the primary beam during the measurement) using monitor counts of the image plate detector system. However, because the standard monitor counts were found to be rather inaccurate, a new scaling procedure has been implemented. The normalization factor for each frame, is determined from the averaged pattern intensities at user selected background points situated at low $2\text{-}\theta$ angles. By plotting the intensities as a function of the frame number (increasing rotation angle), the intensity decay of the primary beam is characterized, as illustrated in figure 5.2. From the characterization curve, the corresponding normalization factors for the patterns generated from each frame can be calculated.
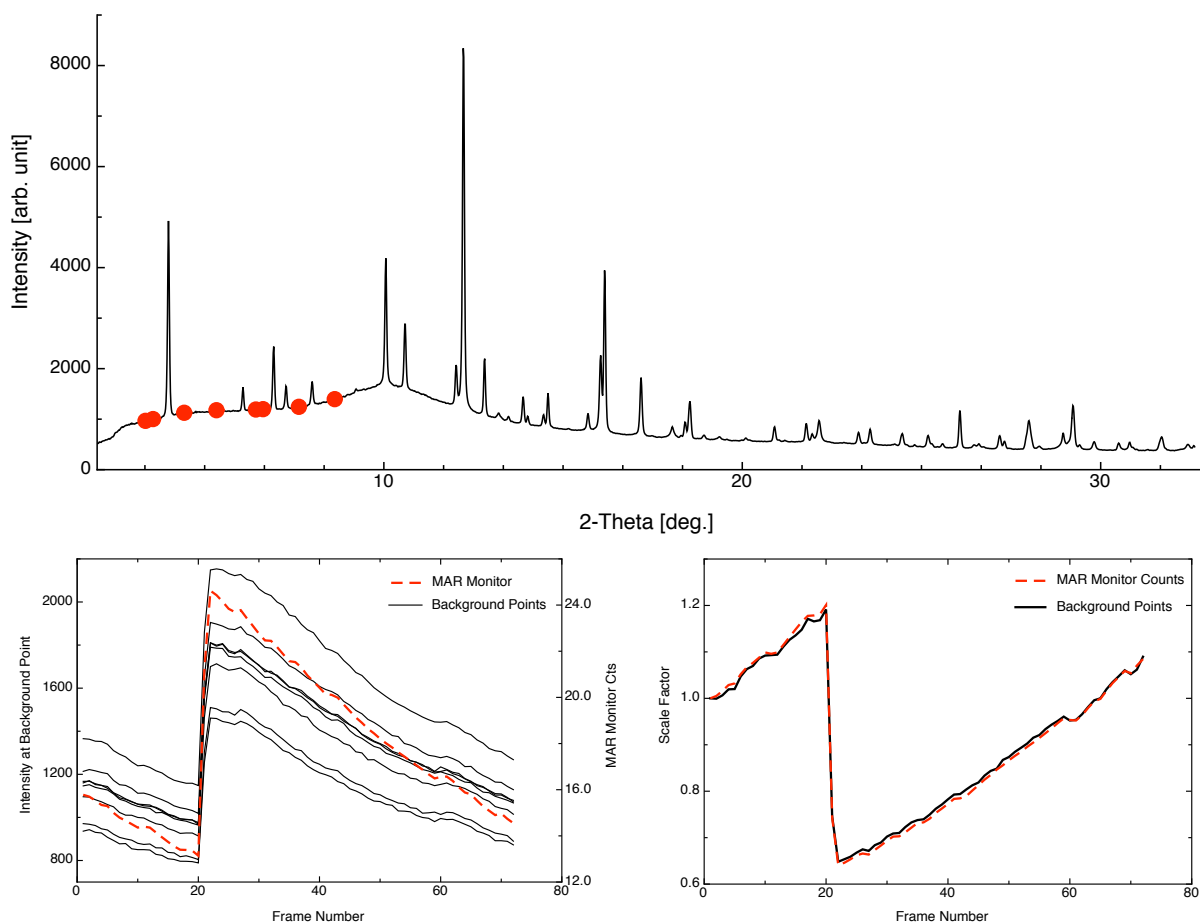

Figure 5.2: Background points selected for scale factor determination (top). Intensities for the background points (red circles) for $3.2º \leq 2\theta \leq 8.5º$ (bottom left) and the corresponding normalization factors determined for each frame (bottom right). Superimposed the results for the MAR monitor counts for comparison.

5.1.2 SLS Si-Microstrip Data

The microstrip detector is a one dimensional detector, so each orientation has to be measured individually, and because of the gaps between the detector modules two different detector position have to be used. As already stated in the previous chapter, the microstrip version used in this project was a proto-type. Before the two patterns collected at each orientation could be merged and normalized, the data had to be processed to remove spikes caused by defective channels. There are two different kinds of defective channels: dead channels, have no counts, e.g. the measured intensity is zero. Their removal from the data is straightforward. The second kind are the random hot channels, which yield randomly high intensities. These data points are removed, if their intensity exceeds the average of neighboring channel intensities (left and right) by more than a user-defined percentage. The limit is determined in a trial and error procedure. In most cases, most defective channels can be removed from the data in this way. Difficulties arise in cases where the random intensities are in the range of the 'real' diffraction intensities. These channels are not easy to identify and in some cases they had to be removed manually. After the data were corrected for dead and random hot channels, the patterns were normalized and the patterns collected at the same orientations merged and binned to $0.004°2\theta$. In figure 5.3, these typical data processing steps are illustrated.
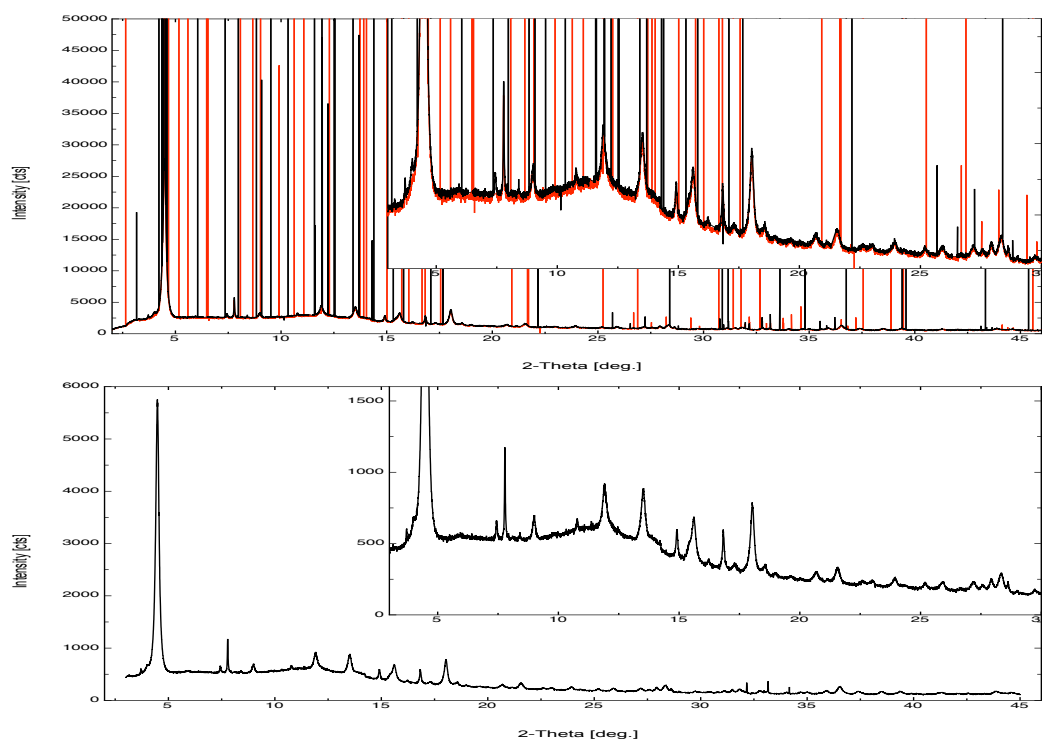

Figure 5.3: Raw data at 2 different detector positions (in black and red), inset scaled 4x (top). Note the random hot channels. The final pattern after removal of hot and dead channels, normalization, merging and binning (bottom)

5.2 Texture Analysis

Texture analysis as a tool, was first developed and applied in the fields of structural geology and physical metallurgy. It is used to relate preferred orientation in polycrystalline materials to their properties and to investigate processes, that lead to the presence of the anisotropy in the first place. In a conventional texture analysis, the orientation distribution function (ODF), a measure of the statistical distribution of the orientations of crystallites contained in a polycrystalline sample, is determined. Experimental measures of the ODF are so-called pole figures. They represent two dimensional projections along a certain path through the three dimensional ODF. To determine an accurate ODF for a cubic material, 3 to 4 pole figures are usually sufficient. However, depending on the method used for the computation of the ODF, more pole figures are necessary to obtain a reliable result for crystals with large unit cells or lower symmetry. For the ODF determinations in this project, only the discrete methods WIMV and E-WIMV, which perform computations in orientation space, were used. The WIMV method, developed by Matthies & Vinel (1982), computes the ODF, which is divided into a discrete number of regular 5° cells, in an iterative procedure. The extended WIMV method (so-called E-WIMV) can be used for computations with irregular or incomplete ODF coverage. X-ray or neutron diffraction pole figures are the most widely used, because their information is averaged over a statistically relevant number of crystallites, which provides quantitative information. In contrast, selected area electron diffraction (SAD) using transmission electron microscopy (TEM), provides only local information about single grains or small aggregates. Electron backscatter patterns (EBSP) produced with a scanning electron microscope (SEM) can be used to determine microstructural and crystal orientation information at specific locations in the surface layer of a sample, this technique is known as orientation imaging microscopy (Adams *et al.*, 1993). A certain area of the sample is scanned to generate orientation maps, which visualize the crystal orientations and the size of the grains in the investigated area.

5.2.1 Pole Figures

A pole figure is a measure of the distribution of the orientations (ϕ, χ) for the lattice plane (*hkl*). It shows the density distribution of a pole (normal to the lattice plane (*hkl*)) with respect to a fixed reference coordinate system *XYZ*. As illustrated in figure 5.4, a pole is the point of intersection between the lattice plane normal and the orientation sphere around the sample.
 The position on the orientation sphere of a pole can be described in spherical (the pole distance β and azimuth α) or in Cartesian ($x = sin\beta\ cos\alpha$, $y = sin\beta\ sin\alpha$ and $z = cos\beta$) coordinates. For visualization purposes, the upper hemisphere of the orientation sphere is usually projected onto the equatorial plane to show the pole density distribution for a given lattice plane (*hkl*). The most popular ways of mapping the pole distribution onto 2 dimensions are the stereographic (Lambert) and the equal-area (Schmid) projection. An advantage of the stereographic projection is that it produces a conformal mapping, i.e angles on the sphere are mapped identically to the projection. A Wulff net can be used to
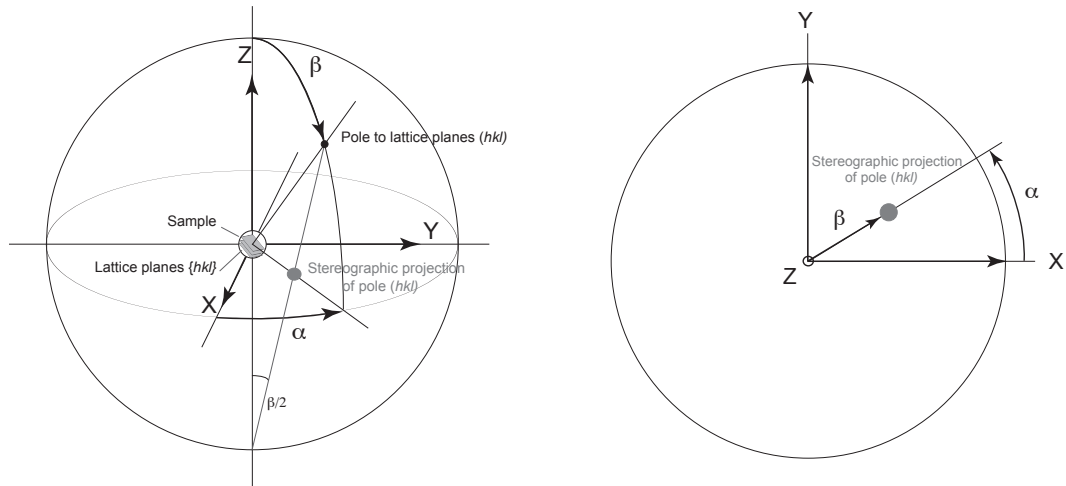
Figure 5.4: The pole of the lattice plane (*hkl*) with respect to the fixed coordinate system *XYZ* on the orientation sphere (left), and the corresponding point in the pole figure in stereographic projection (right)

determine the angle between two points or areas in the pole figures. In an equal area projection, in contrast, any mapped area is left unchanged. As a consequence, the mapped density distributions from the hemisphere appear with nearly no distortion effects. Every pole figure measured by conventional diffraction methods (diffraction geometries discussed in the next section) is a reduced pole figure. It is the superposition of the true pole figure of the reflection *hkl* with it's Friedel partner $\overline{hkl}$. Additionally, experimentally measured pole figures are almost always incomplete, because depending upon the experimental setup used, not all sample orientations are accessible. Whichever experimental setup is used to measure the pole figure, the rotation and tilt angles from the experiment have to be converted into the pole figure azimuth α and the pole distance β for data analysis.

5.2.2 Diffraction Geometries and Pole Figure Angles

Figure 2.3 shows a classical reflection setup. Individual pole figures are measured by setting the detector to the 2θ position of the reflection of interest, determined first in a conventional θ-2θ scan. Then the 5º x 5º grid (shown in figure 2.2) of sample rotations and tilts is scanned. In reflection geometry, the rotation angle ϕ corresponds directly to the pole figure azimuth α, and the tilt angle χ is equal to (90º - pole distance β) (Kocks *et al.*, 2000). The maximum measurable sample tilts are restricted to about 80º in a reflection measurement.

In transmission mode with a 2D detector, complete Debye-Scherrer rings (i.e. multiple sample orientations) are collected so the experiment is considerably faster. However, the information from the intensity variation around the Debye-Scherrer rings has to be converted into pole figure angles. This transmission setup is shown schematically in figure 5.5.
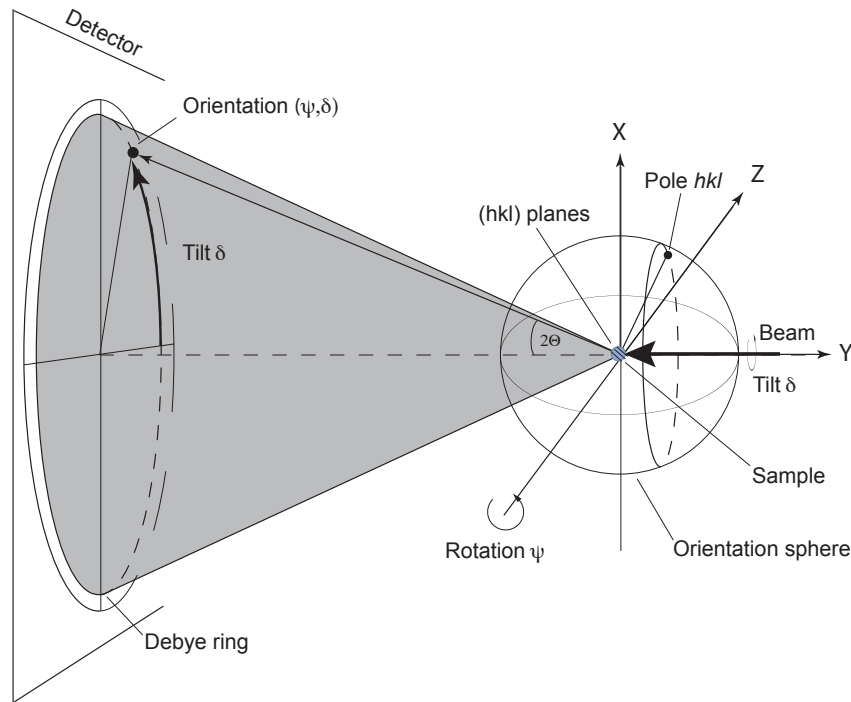
Figure 5.5: Setup used for data collection in transmission mode with a 2D detector (right) and the corresponding pole figure angles (left)

The sample was rotated about ψ (horizontal axis, perpendicular to the primary beam), the data at the different tilt angles was integrated directly from the 2D images. The same holds for the measurements with the 1D Si-microstrip detector at SLS, a Eulerian cradle, providing the angles $\{\sigma,\ \delta,\ \psi\}$ was used. The sample was rotated about ψ (horizontal axis, perpendicular to the primary beam), but also tilted about δ (in the plane perpendicular to the primary beam. The σ-axis was held at a constant position ($\sigma = 0°$) during the entire measurement.

For each reflection, the tilt angle δ and the rotation angle ψ are transformed into the pole figures angles α and β, according to the following equations (Heidelbach *et al.*, 1999):

$$cos\beta = cosc\ (\sqrt{(1 - \frac{sin^2\theta\ sin^2\delta}{1\ -\ cos^2c})(1 - \frac{sin^2\sigma\ sin^2\delta}{1\ -\ cos^2c})} - \frac{sin\sigma\ sin\theta\ sin^2\delta}{1\ -\ cos^2c} \qquad (5.1)$$

with

$$cosc = cos\theta\ cos\sigma + sin\theta\ sin\sigma\ cos\delta \qquad (5.2)$$

If, as is the case in our experiments, the sample is not tilted about the σ-axis ($\sigma = 0°$), cosc simplifies to

$$cosc = cos\theta \qquad (5.3)$$

and, solving equation 5.1 for the pole distance β, we get

$$\beta = arccos(cos\theta \ \sqrt{1 - \frac{sin^2\theta \ sin^2\delta}{1 - \ cos^2c}}) = arccos(cos\theta \ cos\delta) \tag{5.4}$$

The azimuth α in the pole figure can then be expressed as

$$\alpha = \psi + arccos(\frac{sin\theta}{sin\beta}) \tag{5.5}$$

As a result of the above transformation, a blind spot appears at the center of each pole figure, with a diameter of θ. For the determination of the ODF using the texture software (BEARTEX, MAUD), the pole figure angles (α,β) are interpolated back onto a 5º x 5º standard pole grid (New Berkeley format). The significance of the transformation to pole figure angles is illustrated in figure 5.6 below.
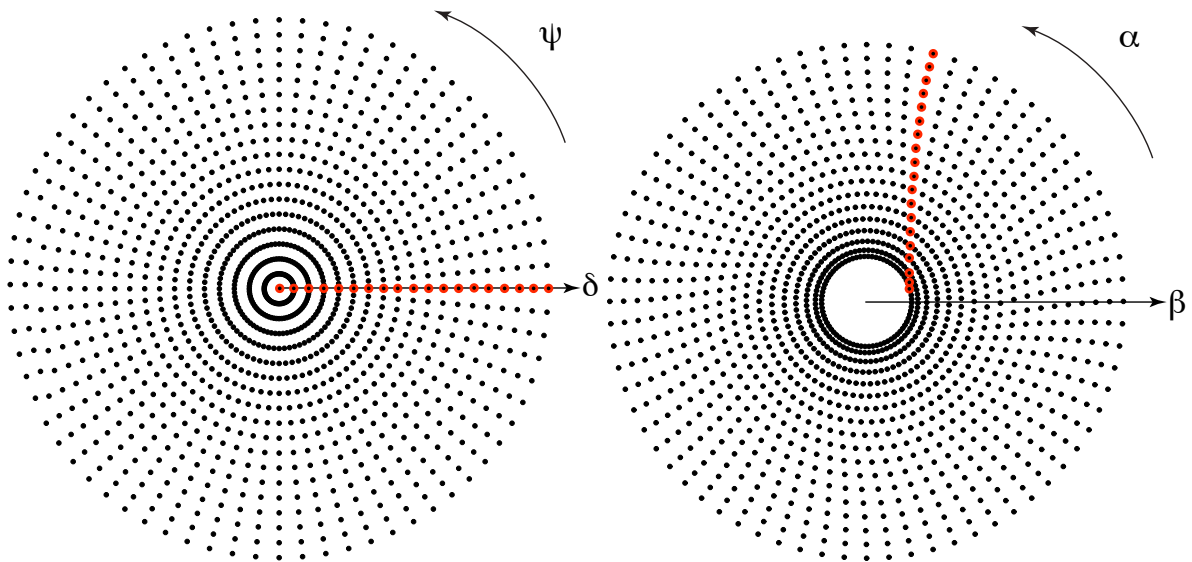

Figure 5.6: Conventional 5º x 5º pole grid for (ψ,δ) in (left) and its conversion to the pole figure angles (α,β) for a reflection at $2\Theta = 30º$ with a 15º blind spot at the center (right). For $\psi = 0º$ the tilt angles $0º \leq \delta \leq 90º$ are indicated in red.

5.2.3 The Orientation Distribution Function (ODF)

The orientation distribution function *f(g)*, as defined in equation 5.6, represents the statistical distribution of the orientations of all of the crystallites in the sample volume *V*. In the volume fraction *dV/V* of the sample, all the crystals exhibit the orientation *g* within *dg*.

$$f(g) \ dg \ = \ \frac{dV}{V} \tag{5.6}$$

The orientation *g* describes the orientation of the crystallite coordinate system *a, b, c* with respect to the sample coordinate system *X, Y, Z*. It rotates the crystallite system into the sample system and can be described by either a rotation matrix, by the Miller indices *(hkl)[uvw]* of two crystal directions parallel to the direction of rolling **RD** and its transverse **TD** (e.g. for rolled samples), or by the Euler angles $\{\alpha, \beta, \gamma\}$ (figure 5.7). There are different conventions for defining the sample coordinate system *X, Y, Z*. In metals, the definition is given by the forming process. In geological investigations, the choice is more arbitrary, but it usually follows crystallographic conventions (e.g. *Z*: [001], *Y*: perpendicular to [001] and [100] and *X*: perpendicular to *X* and *Z*) according to (Wenk & Van Houtte, 2004). The Euler angles bring the two orthogonal right-handed coordinate systems to coincidence by the three rotations (figure 5.7). The first rotation α is around the Z-axis, the second β around the X'-axis and the third γ around the Z'-axis.
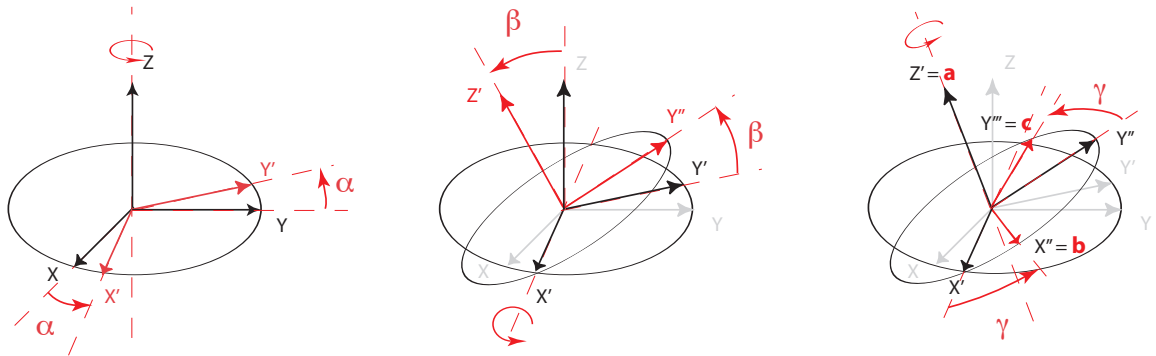

Figure 5.7: The Euler angles $\{\alpha, \beta, \gamma\}$ relating the two orthogonal coordinate systems (reference: X, Y, Z and the crystal: a, b, c)

The experimentally measured pole figures are 2 dimensional projections of the crystal direction **h** (perpendicular to the lattice plane (*hkl*)) of the 3 dimensional ODF. They represent the probability, in sample coordinates, of finding the pole of the lattice plane (*hkl*) in the sample direction **y**=(α,β). The volume fraction $dV_{\mathbf{h}\|\mathbf{y}}/V$ of crystals in the sample with their lattice plane normal [*hkl*] parallel to the sample direction (α,β), is:

$$P_{\mathbf{h}}(\mathbf{y}) = \frac{dV_{\mathbf{h}\|\mathbf{y}}/V}{\sin \alpha \ d\alpha d\beta} \tag{5.7}$$

The definition in equation 5.7 is independent of the rotation ψ about the diffraction vector parallel to the direction **h** with the angular element $\sin \alpha d\alpha d\beta$. The measured intensity is not changed by rotating the sample about the crystal direction **h**. Integration of the ODF about **h** with respect to **y** leads us to the pole figure:

$$P_{(hkl)}(\alpha, \beta) = \frac{1}{2\pi} \int_{\mathbf{h}\|\mathbf{y}} f(g) \ d\psi \tag{5.8}$$

To calculate the ODF, equation 5.8 has to be solved for a set of pole figures with different (*hkl*). For the calculations in the present work, only the WIMV

method developed by (Matthies & Vinel, 1982) and E-WIMV, a related algorithm capable of processing data with an incomplete ODF coverage, were used.

5.3 Cluster Analysis

Cluster analysis is a multivariate statistical analysis procedure for grouping similar objects in a dataset into clusters. It is by no means a new method in statistics, but has found growing interest for the evaluation of microarray data in biotechnologies. Complementary DNA microarrays comprised of tissue samples are used to measure expression levels in cells for thousands of genes simultaneously. Fluorescence levels over the arrays have to be analyzed for similarities between genes and between samples.

Our problem is a similar one. From powder data measured at more than a thousand sample orientations, integrated intensities are extracted for hundreds to thousands of reflections. The dataset for clustering analysis contains P-value differences for all sample orientations. A cluster analysis is used to group the orientations exhibiting similar differences. By finding the most representative orientations for each group, most of the accessible information about the overlapping reflections is contained in these few orientations.

5.3.1 Sample Orientations with Maximum Intensity Contrast

A simple and straightforward way to identify the sample orientations, at which the maximum differences for overlapping reflections occur, is to evaluate their difference pole figures within the overlap group. The overlapping reflections are grouped by applying an overlap factor *of* (typically 0.3) according to equation 5.9 (Grosse-Kunstleve, 1996).

$$(2\theta_{i+1} - 2\theta_i) \; < \; \frac{FWHM_{i+1} + FWHM_i}{2} \; of \tag{5.9}$$

The difference pole figures for all possible combinations of pole figure pairs within each overlap group are then calculated (an example for a single group is illustrated in figure 5.8). Then, these difference pole figures are summed over all groups, and the orientations giving the maximum differences are identified. A more pronounced definition of the orientations can be achieved by considering only the differences above a user-defined percentage level for the summation. A comparison between the two summation methods applied to an experimental dataset is shown in figure 5.9.

5.3.2 Hierarchical Clustering

Barr *et al.* (2004) integrated clustering methods into the commercial computer software *PolySNAP* for application in high-throughput powder diffraction. In that case, full patterns are matched, by treating them as bivariate data with n measured points (x_1, y_1) to (x_n, y_n). To match the patterns to each other, an n
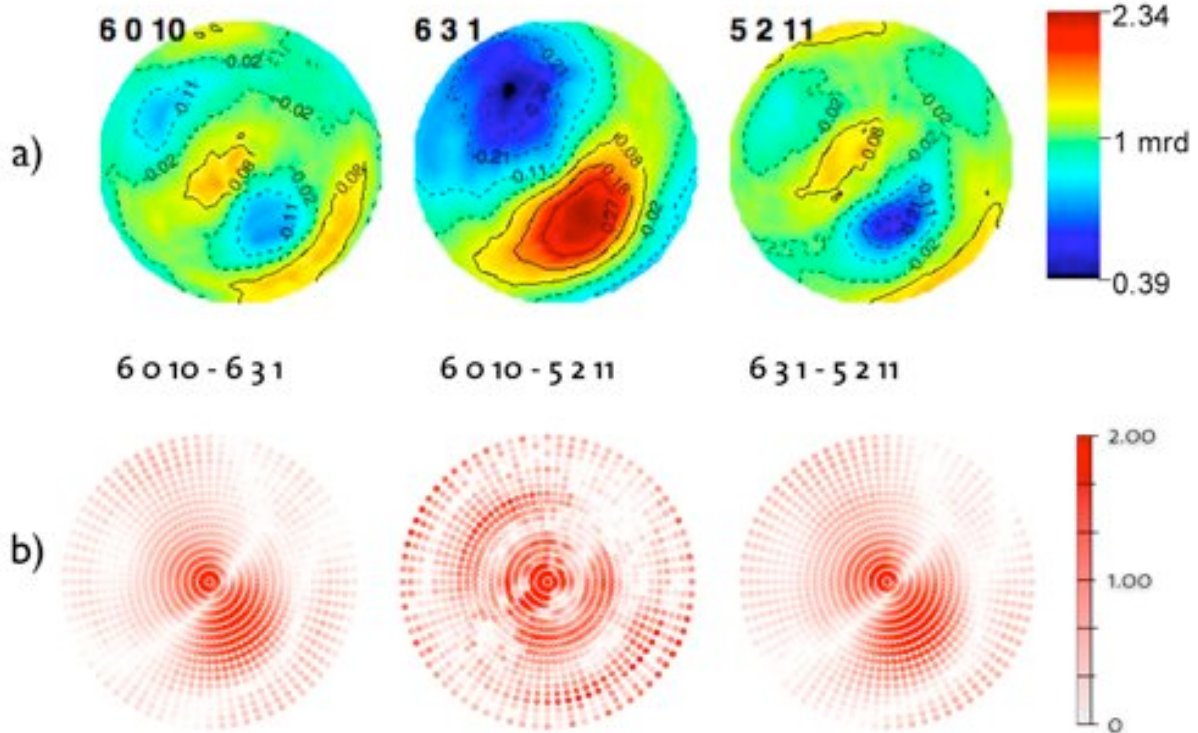
Figure 5.8: (a) Pole figures for the overlap group: 6 0 10 (2θ=34.045º), 6 3 1 (2θ=34.053º), 5 2 11 (2θ=34.055º), (b) difference pole figures for all possible combinations of pole figure pairs in the group
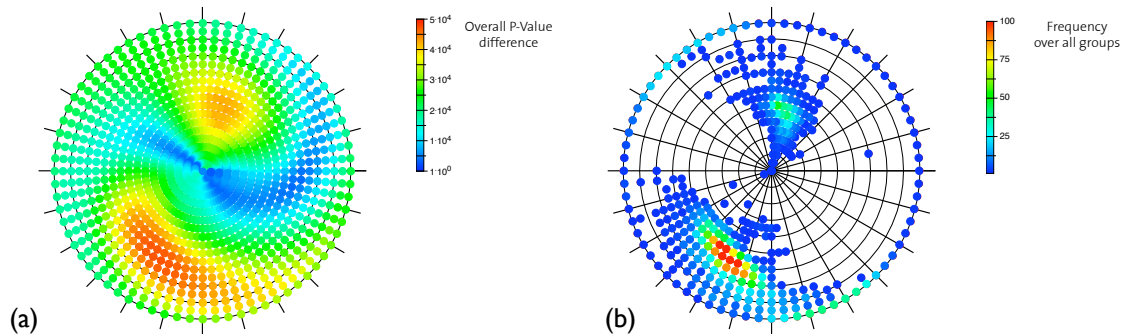

Figure 5.9: (a) Orientation factor (P-value) differences (log scale) summed over all overlap groups, (b) only differences that exceed 95% of the maximum difference in each group are used in the summation.

x n correlation matrix is generated, and then converted into a Euclidian distance matrix **d**. Agglomerative hierarchical clustering, using **d** to maximize the similarity in each class, is carried out. Besides the Euclidian distance, other distance measures are also used, a summary is given in table 5.1.

The Pearson correlation describes the degree of correlation between two series of datapoints (x,y), where $\bar{x}$ and $\bar{y}$ are the average values and σ_x and σ_x their standard deviations. The correlation value r is between -1 and 1, r = 1 means

Table 5.1: Distance measures

Name	Definition
Pearson correlation	$r = \frac{1}{n} \sum_{i=1}^{n} \left(\frac{x_i - \bar{x}}{\sigma_x} \right) \left(\frac{y_i - \bar{y}}{\sigma_y} \right)$
Euclidian distance	$d(x, y) = \sqrt{\sum_{i=1}^{n} (x_i - y_i)^2}$
Squared Euclidian distance	$d(x, y) = \sum_{i=1}^{n} (x_i - y_i)^2$
City-block (Manhattan) distance	$d(x, y) = \sum_{i=1}^{n} \mid x_i - y_i) \mid$

the datasets are identical, for r = 0 the datasets are completely unrelated and for r = -1 they are the perfect opposites. Besides the Pearson correlation, the Euclidian distance (the geometric distance between two points) is most widely used. The weighting for objects, that are further apart from each other can be increased by using the squared Euclidian distance. The city-block distance returns similar results as does the Euclidian distance, but damps the effect of outliers in a dataset.

An advantage of using hierarchical clustering methods is that they offer different levels of detail, i.e. they produce nested sequences of clusters (small clusters are nested into larger ones). One can choose the level of detail by focusing on either a few large clusters containing a lot of observations or a lot of small ones with a few observations. Additionally, the user does not have to decide on the number of clusters in advance. In the initial cycle, each object (in our case an orientation) is in a separate cluster. In such bottom-up methods, in each step the closest clusters are joined on the basis of one of the linkage rules (table 5.2).

Table 5.2: Linkage rules

Linkage rule	Inter-cluster distance
Single linkage	min. distance
Complete linkage	max. distance
Average linkage	average of all distances
Centroid linkage	centroids of each cluster

The procedure is repeated until all objects are in a single cluster. The results are usually graphically represented in tree plots (dendrograms). The degree of dissimilarity between the clusters is represented on the vertical axis. To illustrate the effect of the different linkage rules, the dendrograms resulting from

clustering the same dataset according to each of the previously discussed linkage rules, are shown in figure 5.10.
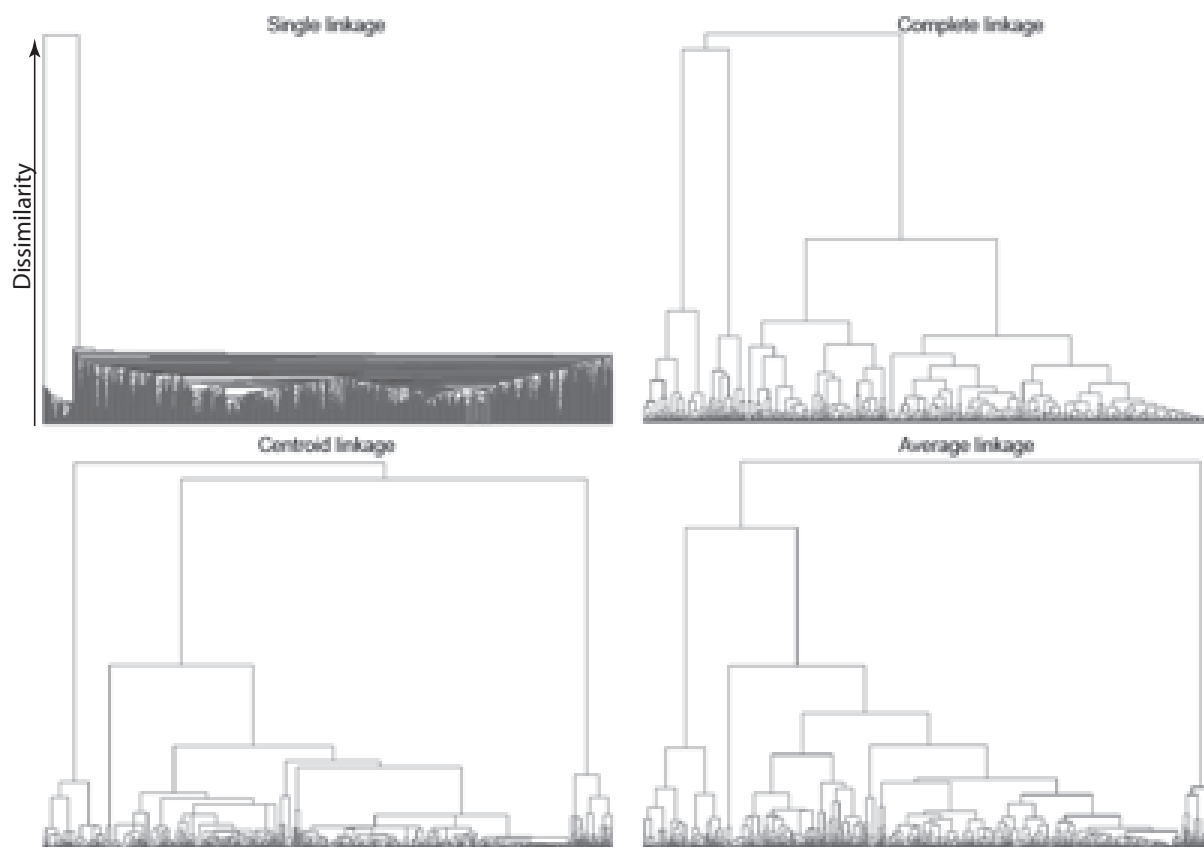

Figure 5.10: Trees generated with the four different linkage rules defined in table 5.2. The data was clustered using *Cluster3.0* (Eisen, 1999), the dendrograms were generated with *Java TreeView* (Saldanha, 2006). The dissimilarity increases vertically from bottom to top in each tree.

As shown in figure 5.10 above, single linkage results in long chains of clusters, complete linkage tends to produce compact clusters. Average and centroid linkage are a compromise of the two. To cluster the difference pole figures after computing the ODF, the Euclidian distance was used as a distance measure and the average linkage rule for agglomerative clustering of the data. Clustering was performed using the Cluster 3.0 software (Eisen, 1999). The level of detail (number of clusters) was selected by applying a horizontal line at a certain degree of dissimilarity. In figure 5.12, an example with 7 clusters is shown with the corresponding orientations plotted on the pole grid. For each cluster, the most representative orientations can be selected for measuring diffraction patterns with better counting statistics for the final joint refinement procedure.

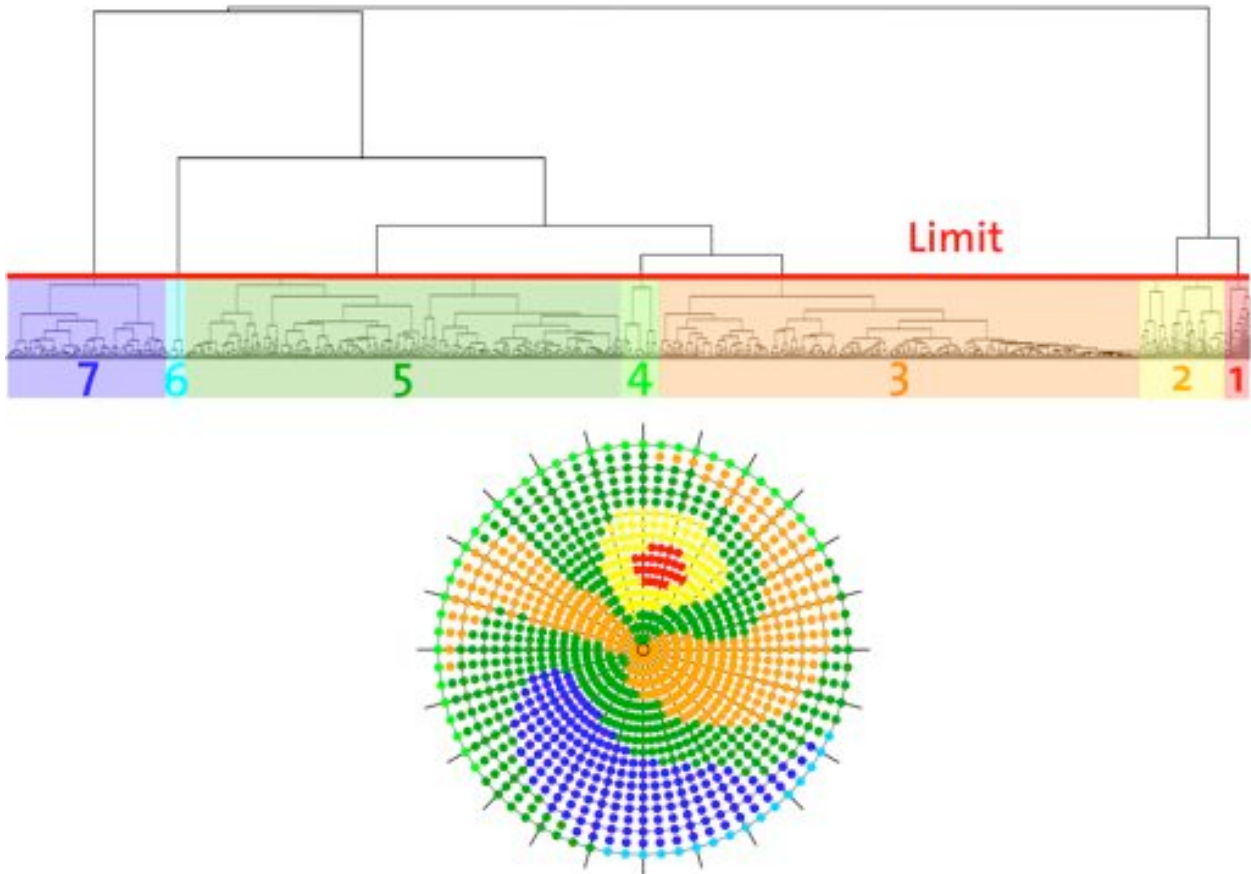In the final procedure, the two methods: (1) the summation of the difference

Figure 5.11: Dendrogram for a test dataset. Seven clusters chosen by drawing a horizontal line at the appropriate level of dissimilarity. Plotting the orientations, color coded according to their cluster affiliation, on a pole grid shows that each cluster represents a distinct group of orientations.

poles figures and (2) the cluster analysis of the difference poles figures, were combined in a complementary fashion. First, the orientations providing the maximum P-value differences were determined using the summation method considering only differences, that exceed 95% of the maximum difference. A drawback of the cluster analysis is, that it only provides information on the similarity, but not on the magnitude of the differences contained in each cluster. Therefore, the orientations determined via the summation procedure, were compared to the results from a cluster analysis to identify and confirm the clusters containing the orientations with the highest differences. If necessary, the list of sample orientations for the final data collection procedure was augmented to assure that these important clusters were represented.
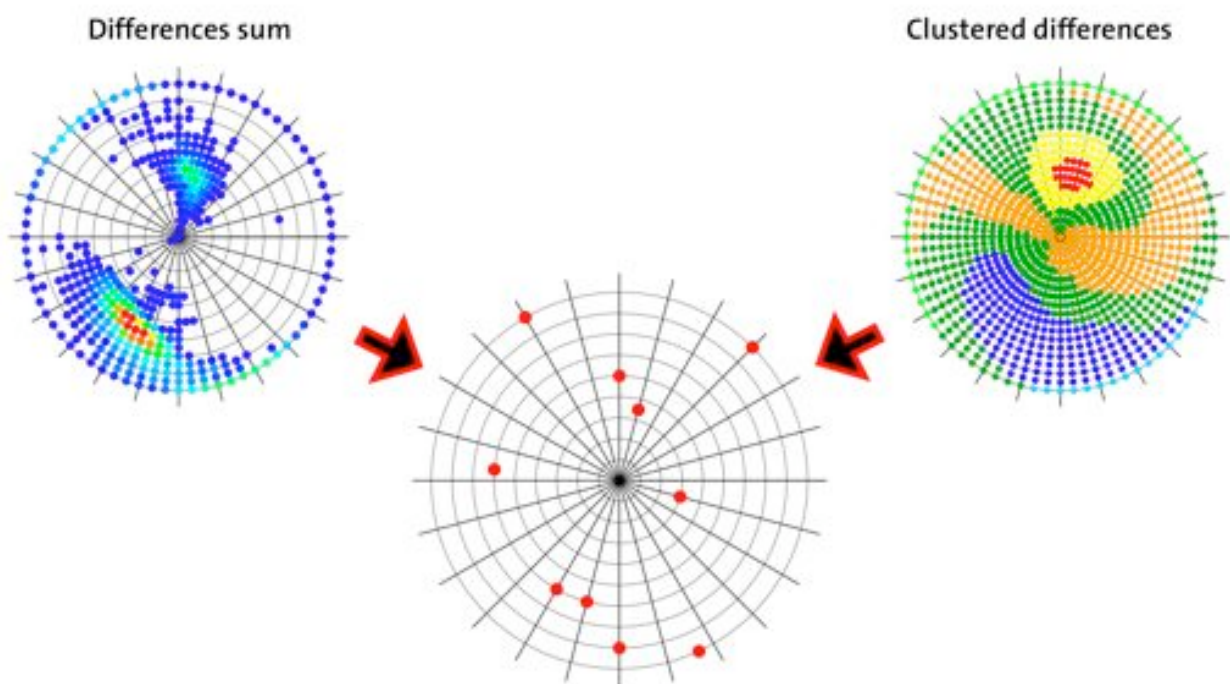
Figure 5.12: The final data collection grid (middle) in (ψ, δ), combined from the grids determined via the difference sum procedure (left) and the cluster analysis (right)

6 Test Structures

In this chapter, results from textured samples prepared from crystallites with known crystal structures, are discussed. The two test structures are: TMA-O, a synthetic zeolite with the **OFF** framework type and the extra-large pore zeolite IM-12 (**UTL** framework type). With these zeolites, experiments to optimize the data collection and analysis procedure and to test the new SLS setup were performed. Additionally, the effectiveness of different sample preparation procedures were evaluated.

6.1 Offretite

The crystal structure of the natural zeolite offretite was solved in 1967 by Bennet & Gard (1967) in a single crystal study. Offretite has the chemical composition [Al$_{5.2}$Si$_{12.8}$O$_{36}$]-**OFF**, space group $P\bar{6}m2$ and unit cell a=b=13.291 Å and c=7.582 Å. The structure has large 12-ring channels along the c-axis and smaller 8-ring channels perpendicular to them. Two views of the framework structure are shown in figure 6.1.
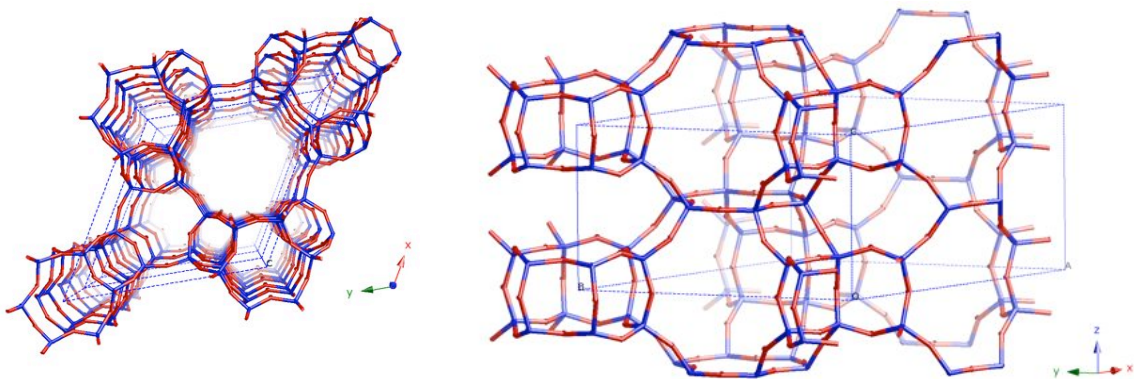

Figure 6.1: The framework structure along [001] (left) and the view perpendicular to it along [110] (right)

Grouping the reflections using an overlap factor of 0.3 (equation 5.9), down to a minimum d-spacing of 1.0 Å, only 9.6% of the reflections overlap. As shown in figure 6.2 the crystallites exhibit a stick-like shape with lengths of about 1 μm and a width of about 0.4 μm.
From the morphology of the crystallites, a textured sample can be expected to exhibit a fiber texture (i.e. the crystallites are oriented along a single axis, but randomly around it). Therefore this sample was a typical case for evaluating the different sample preparation techniques.
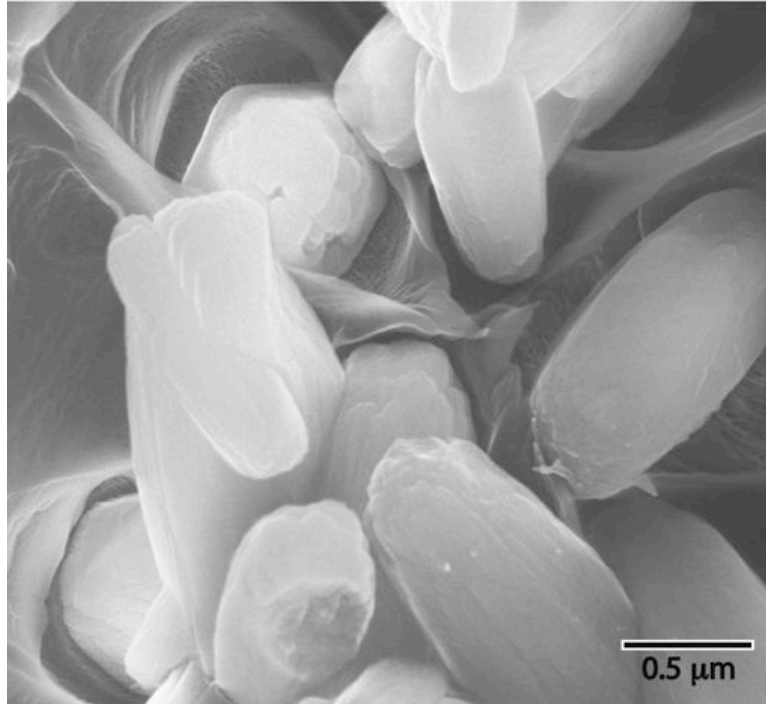
Figure 6.2: Scanning electron micrograph of offretite crystals embedded in a polystyrene matrix

6.1.1 Sample Preparation

Two different textured samples of synthetic |TMA| [Al-Si-O]-**OFF** were prepared. For the first sample (*OFF1*) 0.1 g of TMA-OFF were dispersed in THF using a pulsed ultrasonic treatment. Then 0.2 g of a solution of 50 wt.% PS in THF was added. The homogeneously mixed, milky dispersion was poured onto a piece of aluminum foil and dried for about 3 hours, until it formed a gel-like foil. From this foil, strips of about 5 mm width were cut, stacked and pressed using a pressure mold specially manufactured for bakery-folding (see section 3.5). From the resulting specimen, a ca. 0.3 x 0.3 x 0.3 mm^3 sample was cut for the texture measurement. The second sample (*OFF2*) was prepared in the same way as the first one but large agglomerates were removed in a sedimentation procedure before the crystallites were dispersed and a different texturing procedure was applied. For this sample, texture was induced by shearing the sample foil between two glass slides after heating it above the glass-temperature of polystyrene (T_g 100ºC). Finally, a 0.3 x 0.3 x 0.3 mm^3 sample was cut from the bulk.

6.1.2 Data Collection

For both samples, data were collected at the SNBL using the transmission setup with a diagonally shifted image plate detector. For the pressure-molded sample, *OFF1*, an additional dataset was collected with the microstrip detector at the SLS for comparison, using a second small sample cut from the same bulk sample. Details are listed in table 6.1.

Table 6.1: Datasets collected on the textured sample prepared from TMA-OFF

Texture Data	
Textured Sample	OFF1
Synchrotron Facility	SNBL BM01A
Wavelength	0.8000 Å
Sample to detector distance	400 mm
Sample Rotation ψ (72 frames)	0-360º in 5º steps
2θ range	2.5-32.5º
Time per frame	180 s
Textured Sample	OFF2
Synchrotron Facility	SNBL BM01A
Wavelength	0.8000 Å
Sample to detector distance	400 mm
Sample Rotation ψ (72 frames)	0-360º in 5º steps
2θ range	2.5-32.5º
Time per frame	180 s
Textured Sample	OFF1(2)
Synchrotron Facility	SLS MS
Wavelength	0.9250 Å
Beam size	0.6 x 0.6 mm^2
Sample Orientations	72 x 19 =1368
Rotation ψ	0-360º in 5º steps
Tilt δ	0-90º in 5º steps
Sample Oscillation in ψ and δ	±0.5º
Si-microstrip detector positions	2
2θ range	2.5-56.3º
Time per pattern	10 s
High Resolution Data	
Synchrotron Facility	SLS MS
Wavelength	0.9250 Å
Diffraction Geometry	Debye-Scherrer
Analyzer Crystals	Si 111
Sample	rotating 1 mm capillary
2θ range	2.0 - 54.0º
Step size	0.003º2θ

6.1.3 Data Analysis

The ODFs for all three measurements were calculated from data collected on the non-overlapping reflections 100, 001, 110, 101, 200, 201, 210 & 102 (see figure 6.3), using the WIMV method included in the *MAUD* package. All of the data were converted to the pole figure angles (α,β) using the conversion according to (Heidelbach *et al.*, 1999) discussed in section 5.2. In figures 6.4 to 6.6, these pole figures are shown together with those calculated from the ODF. The left pole figure of each pair is the experimentally measured one and the right one is calculated from the ODF. All the pole figures are log-scale and equal area projections.
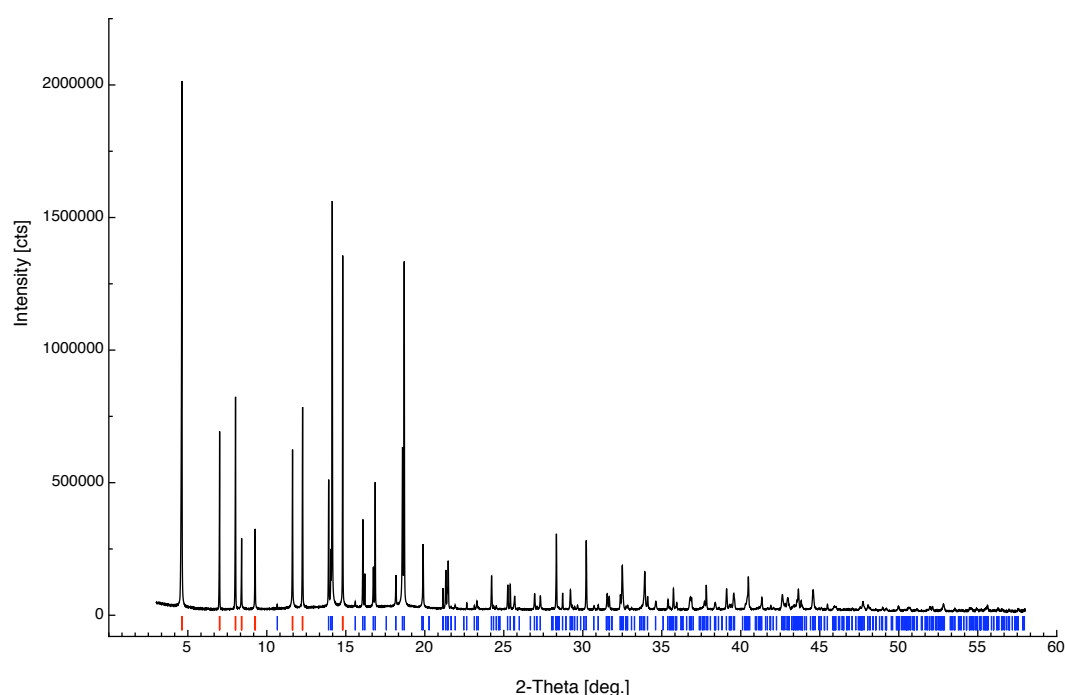

Figure 6.3: High resolution data collected at the Swiss Light Source, λ=0.9250 Å (reflections used for the ODF calculations are indicated in red)
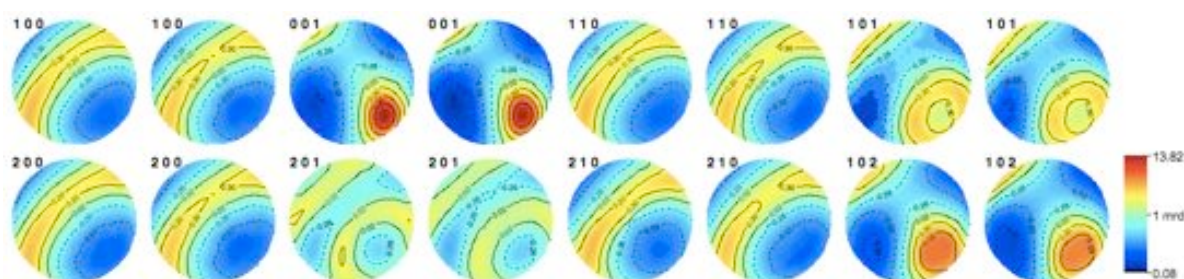

Figure 6.4: Experimental and calculated pole figure pairs for *OFF1*; SNBL Data; texture Index: 4.22 mrd; Rp-Value: 8.8%
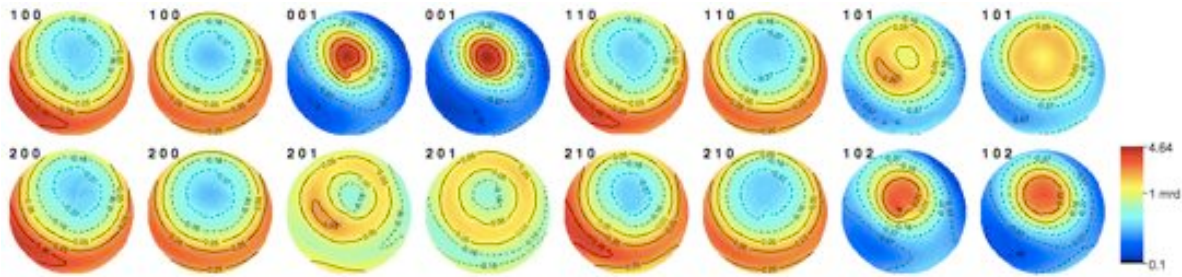
Figure 6.5: Experimental and calculated pole figure pairs for *OFF2*; SNBL Data; texture Index: 2.65 mrd; Rp-Value: 14.1%
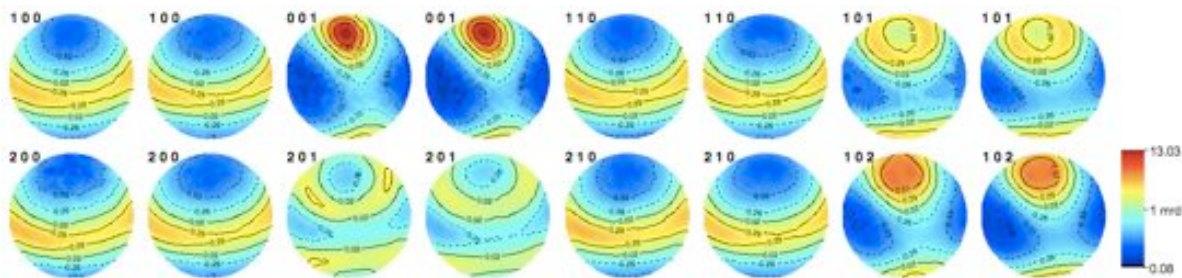

Figure 6.6: Experimental and calculated pole figure pairs for *OFF1(2)*; SLS Microstrip Data; Texture Index: 4.10 mrd; Rp-Value: 7.3%

6.1.4 Discussion

A rather strong texture was induced in the *OFF1* sample using the bakery folding technique. In all samples, fiber textures along the [001]-direction are present. Additionally, it was shown for the sample *OFF1* that the texture information obtained from the data collected with the setup at SLS (figure 6.6), match that from the SNBL data (figure 6.4).

The structure could be solved from the joint refined sets of intensities using conventional direct methods programs in all cases. To assess the quality of the joint refined F-values, the structure factors calculated from the known structure, those extracted from high-resolution data collected on a capillary sample (figure 6.7), and those from the joint refinement procedure, were compared. A second set of single-crystal like intensities was extracted in combination with a high-resolution powder diffraction pattern collected on a sample with randomly oriented crystallites. The comparison of the calculated and extracted structure factors is shown in figure 6.8. It can be seen that the quality of the F-values extracted in combination with a high-resolution powder diffraction pattern is superior, especially for the weak reflections, which are mostly zero if extracted without the high-resolution data.
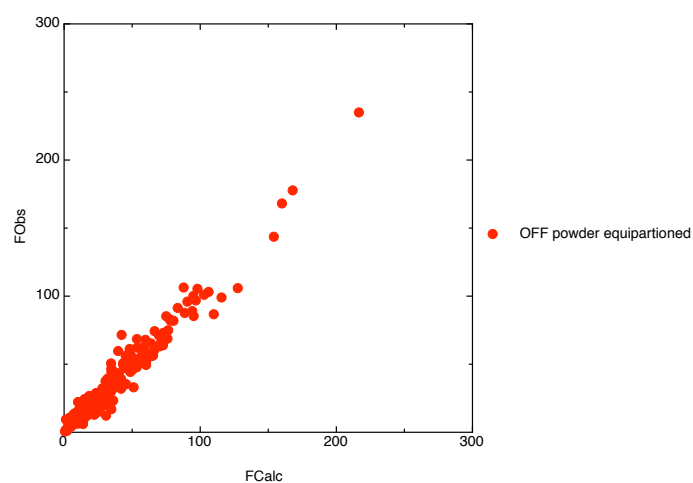
Figure 6.7: Comparison of calculated structure factors with the experimentally determined ones, extracted from high-resolution data collected on a capillary sample.
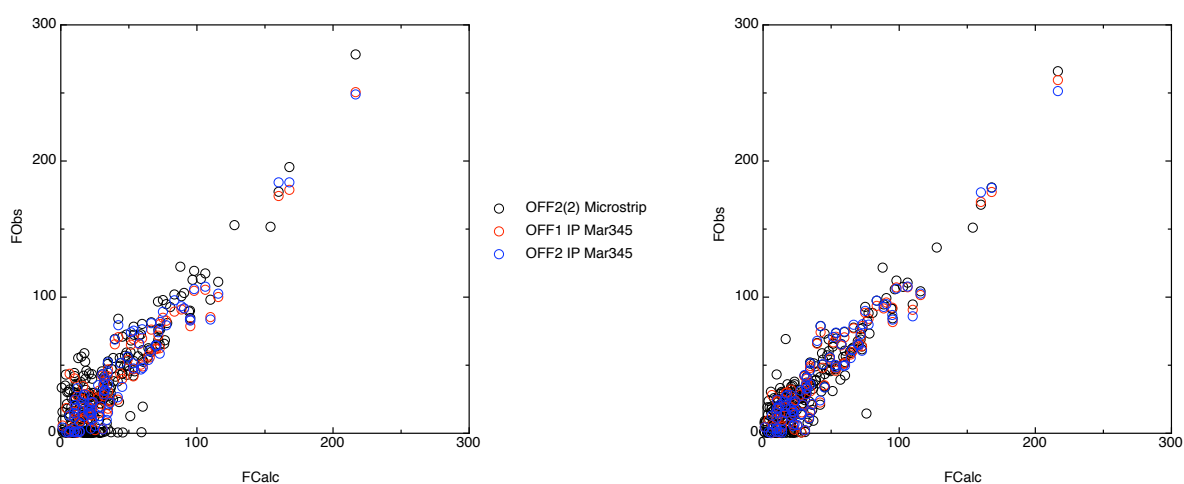

Figure 6.8: Comparison of calculated structure factors with the experimentally determined ones. Left: using only data from a textured sample. Right: including high-resolution powder diffraction data.

6.2 IM-12

The structure of the extra-large pore zeolite IM-12 (**UTL** framework) was solved from laboratory powder diffraction data (Paillaud *et al.*, 2004). IM-12 has a monoclinic unit cell: a=29.8004 Å, b=13.9926 Å, c=12.3926 Å and γ=105.185º. The space group is *C2/m* and the chemical composition $Ge_{13.8}Si_{62.2}O_{152}$. There are 12 (Ge, Si)-atoms in the asymmetric unit. The framework structure can be described as having a 2-dimensional channel system with 14-ring pore openings along the *c*-axis intersecting with 12-ring pores along the *b*-axis, see figure 6.9.
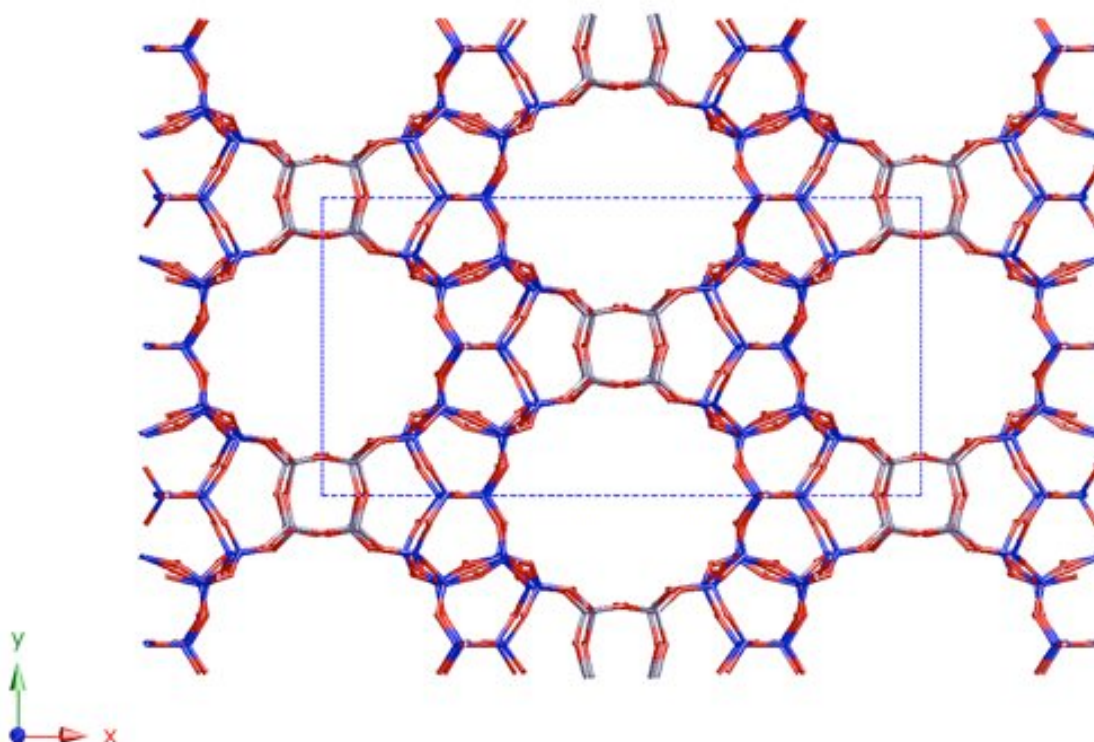

Figure 6.9: A projection of the **UTL** framework along the 14-ring channels down the c-axis [001]. Note the Ge-atoms (grey) and Si-atoms (blue).

6.2.1 Sample Preparation

The IM-12 sample used in this study was kindly provided by Jean-Louis Paillaud (Université de Haute Alsace, Mulhouse, France). The morphology of the individual IM-12 crystals is plate-like with dimensions of ca. 2 x 5 μm (figure 6.10). During the static synthesis, the platelets agglomerated perpendicular to the platelet-plane up to a thickness of about 10 μm and ca. 60 x 40 μm in the plane (figure 6.10). For the texture measurements, an isolated agglomerate (ca. 100μm x 100μm x 80μm) was placed in a protein cryo-loop and mounted on a Eulerian cradle.
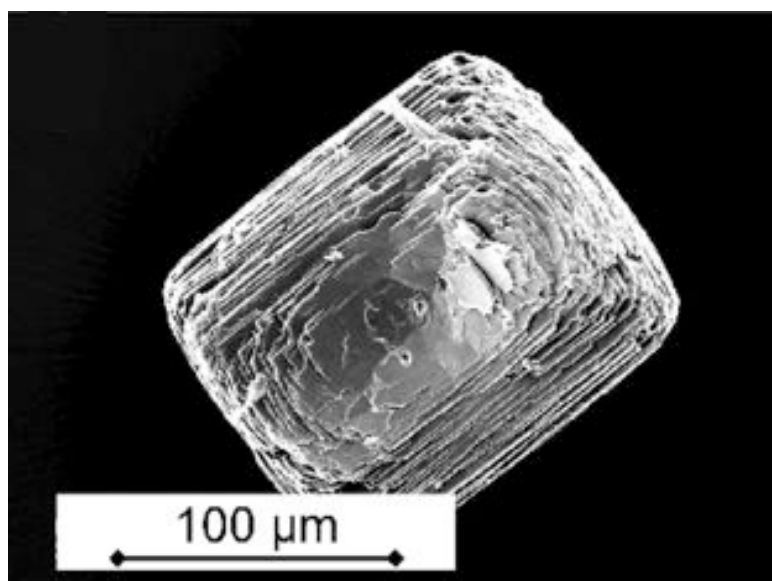
Figure 6.10: Scanning electron microscopy picture of agglomerated IM-12 crystallites from (Paillaud *et al.*, 2004)

6.2.2 Data Collection and Analysis

Two different kinds of texture measurements were performed at the SLS. In addition to the normal measurement using the Si-microstrip detector on the MS beamline, a second dataset was collected using the 2-dimensional Pilatus 6M detector installed on the Protein Beamline (PX1).

SLS Si-Microstrip Data

With the microstrip detector, a complete texture dataset was measured with a 5° x 5° grid. An ODF was determined from the extracted intensities of the non-overlapping reflections: 011, $\bar{1}$00, $\bar{1}$20 and $\bar{1}$11, and the ODF was determined. This ODF had a texture index of 218.3 and an Rp-Value of 57.1% (see figure 6.11). Details for both data collection procedure are given in table 6.2.

SLS Pilatus 6M Data

The Pilatus 6M pixel detector on the PX1 Beamline is a protoype detector developed for protein crystallography, rotation measurements (sample rotation 0° - 360° in 5° steps) have been performed to evaluate this detector's suitability for texture measurements. The detector has a size of 2463 x 2527 pixels, each with a size of 172 μm^2. It contains 5 x 12 individual modules, so data for each orientation were collected with 3 different detector positions, and then merged. Figure 6.12 shows an example of the three individual datasets and the final merged one for the one sample orientation. Data collection details are given in table 6.3.
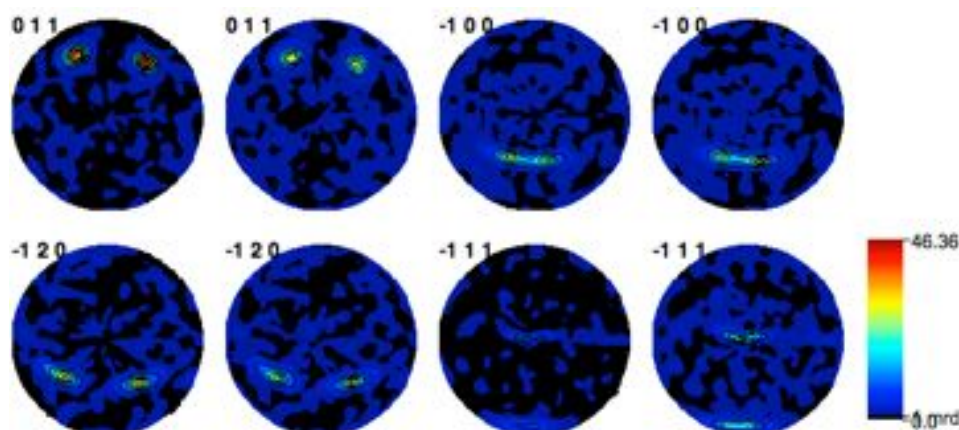
Figure 6.11: Experimental (left) and calculated (right) pole figures pairs for the normal measurement using the microstrip detector.

Table 6.2: Datasets collected on a textured agglomerate of IM-12

Texture Data Set 1	
Texture Sample	IM-12-3
Synchrotron Facility	SLS MS
Wavelength	0.925 Å
Beam size	0.6 x 0.6 mm^2
Sample Orientations	72 x 19 = 1368
Rotation ψ	0-360º in 5º steps
Tilt δ	0-90º 5º steps
Sample Oscillation in ψ and δ	±0.5º
Si-microstrip detector positions	1
2θ range	2.5-56.3º
Time per pattern	10 s

From the frames of the Pilatus rotation measurement, 19 individual powder patterns (radial wedges covering 5º each) were integrated for the tilt angles from 0º to 90º using *Fit2d*. Intensities were extracted from all the patterns using the software *Expol*. The pole figure data extracted with *Expol* were converted to pole figure coverage using the conversion used by the *MAUD* program ((Lutterotti, 2007)). Then the ODF calculation was performed using the *E-WIMV* method, because this method is not only able to process data with incomplete coverage, but is also more suitable for strong textures. However, it seems that the data are not good enough to allow a reasonable ODF to be calculated, even using the *E-WIMV* algorithm. The experimental pole figures (0 2 0, 0 1 1, 1 0 0, $\bar{1}$ 2 0, $\bar{1}$ 1 1, 2 2 0 and 0 4 2) are shown in figure 6.13.

Table 6.3: Datasets collected on textured agglomerates of IM-12

Pilatus 6M Texture Dataset	
Texture Sample	IM-12-3
Synchrotron Facility	SLS PX1
Wavelength	0.76507 Å
Beam size	0.12 x 0.12 mm^2
Sample to detector distance	204.9 mm
Rotation ψ (72 frames)	0-360º in 5º steps
2θ range	2.5-32.5º
Time per pattern	1 s

6.2.3 Discussion

The experiments in this section were performed to investigate, wether or not samples with a very sharp single crystal-like texture can be evaluated by the procedure. The problem with data measured with a 5º grid is, that neither the *WIMV* nor the more flexible *E-WIMV* algorithm are able to calculate a reliable ODF. A possible solution would be to acquire the data with higher resolution, i.e. scanning the orientation space in 2.5º or even 1º steps or oscillate the sample more during the measurement. The second problem, which is only relevant for the Pilatus 6M detector, is that the pixelsize is too large compared with the peakwidth of the data. The low angle peaks, which are normally used for determining the ODF, are defined by only 3 or 4 datapoints and this is not enough. This may be another reason for the inconsistencies in the texture determination procedure. It has to be stated that samples with a very strong degree of preferred orientation, like the IM-12 samples, cannot be handled by the texture method at its current stage of development.
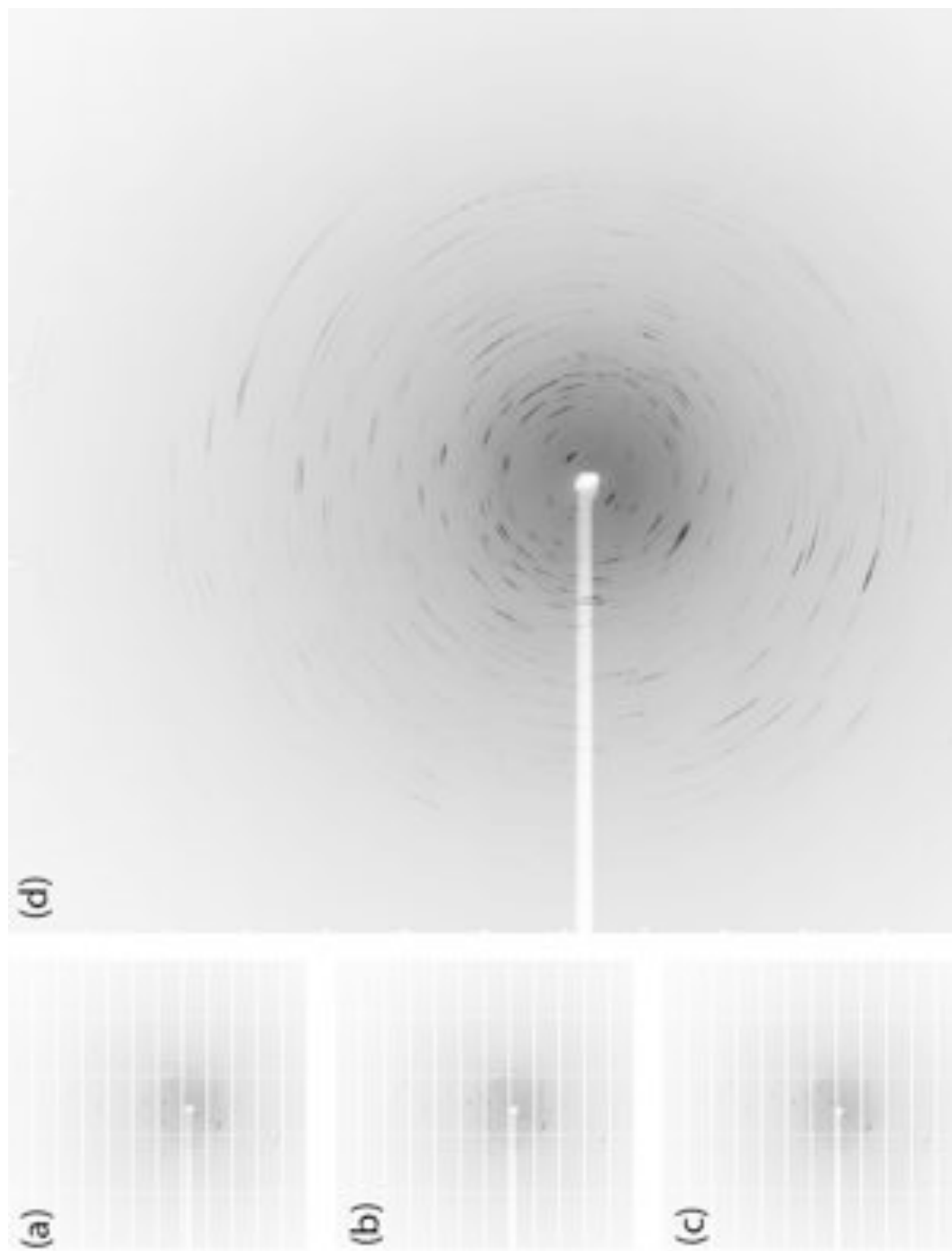
Figure 6.12: Data collected using the Pilatus detector: (a) - (c) individual frames for one same sample orientation and three detector positions, (d) data merged from the three frames.
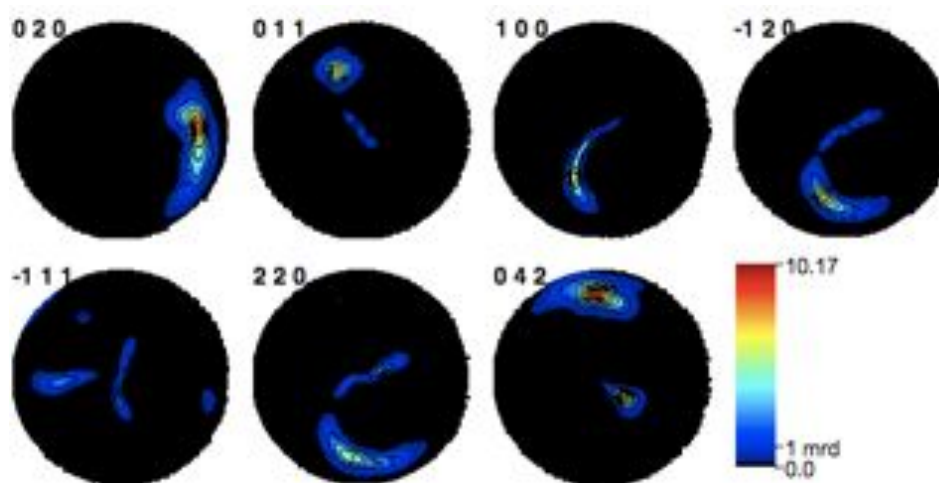
Figure 6.13: Experimental pole figures (pole figure coverage, equal area projection) extracted using *Expol*

7 Layered Silicate DLM-2

The sample of the layered silicate DLM-2 was kindly provided by Martin A. Zwijenburg, TU Delft. Details on the synthesis can be found in Massüger *et al.* (2007).

7.1 Sample Preparation

As shown in figure 7.1, the particles of as-synthesized DLM-2 exhibit a platelet-like shape, varying in size from ca. 1 μm to 10 μm. This is of course an ideal shape to prepare a textured sample. To dissaggregate and homogeneously
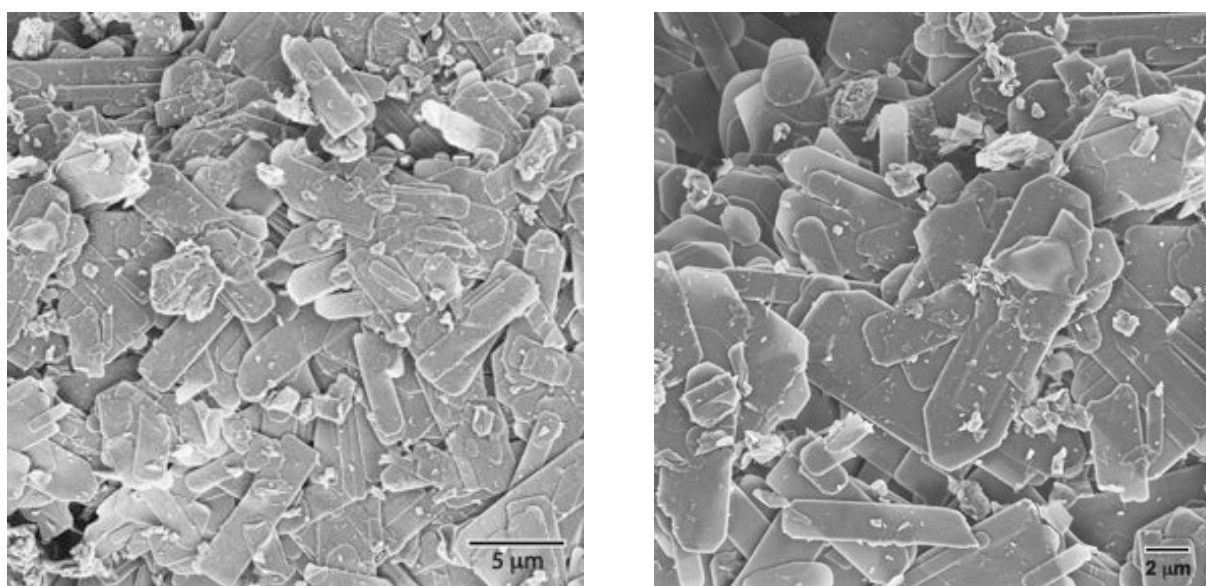

Figure 7.1: Scanning electron micrographs of DLM-2 crystals

disperse the crystals, they were suspended in Tetrahydrofuran (THF) and subjected to pulsed ultrasonic treatment. These treatments of ca. 10-20 s each were repeated several times. A solution of polystyrene PS (50 wt.%) in THF was then added. The resulting mixture was spread layer by layer onto a rubber strip. Each layer was allowed to solidify partially before applying the next one. When a thickness of ca. 0.5 mm was reached, the whole assembly was dried for another 30 minutes, before the strip was stretched to ca. three times it's original length and fixed. After 24 hours, a sample with a diameter of 0.3 mm was cut from the bulk material. For data collection, the sample was mounted in a cryo-crystallography loop and fixed with Araldite highly diluted with alcohol.

7.2 Data Collection

High-resolution synchrotron powder diffraction data were collected on a capillary sample of DLM-2 using the analyzer setup at SNBL. Details are given in table 7.1.

For the texture measurement at the SLS, a homogenized, unfocused beam with a cross-section of about 0.6 x 0.6 mm^2 was used. Complete pole figure data (1368 orientations at 2 detector positions) were collected (details in table 7.1). At each sample orientation, the sample was oscillated in ψ and δ by $\pm$ 0.5º.

Table 7.1: Datasets collected on DLM-2

High Resolution Data	
Synchrotron Facility	SNBL BM01B
Wavelength	0.5007 Å
Diffraction Geometry	Debye-Scherrer
Analyzer Crystal	Si 111
Sample	rotating 1 mm capillary
2θ range	1.020-30.501º
Step size	0.003º2θ
Time per step	1.0 s
Texture Data	
Synchrotron Facility	SLS MS
Wavelength	0.925 Å
Beam size	0.6 x 0.6 mm^2
Sample Orientations	72 x 19 = 1368
Rotation ψ	0-360º in 5º steps
Tilt δ	0-90º in 5º steps
Sample Oscillation in ψ and δ	± 0.5º
Si-microstrip detector positions	2
2θ range	2.5-56.3º
Time per pattern	10 s

7.3 Data Analysis

The high-resolution data were indexed with an orthorhombic unit cell, a = 11.496 Å, b = 8.413 Å and c = 27.923 Å, using the program TAUP (Taupin, 1973) from the Crysfire suite of indexing programs (Shirley, 2000) by Prokić (2004). The space group was ambiguous, but *Imma* was assumed initially.

Using an overlap factor of 0.3 (equation 5.9), 53 % of all reflections in the *d*-range from 4.7 to 0.95 Å are overlapping (534 out of 900).

The two diffraction patterns collected on the textured sample at each orientation, were normalized using the monitor counts and then merged.

Reflection intensities were extracted from these patterns. The pole figure angles (ψ,δ) of six well-separated reflections (002, 011, 200, 202, 114 & 204) were converted to ODF angles (α,β), and then a full texture analysis was performed using the *MAUD* program (Lutterotti *et al.*, 1997). A texture index of 1.88 m.r.d (multiples of random distribution) with an average Rp value of 6.94 % was obtained. A comparison between the measured and calculated pole figures is shown in figure 7.2. This ODF was then used for the extraction of a single set of reflection intensities using all 1368 patterns simultaneously.
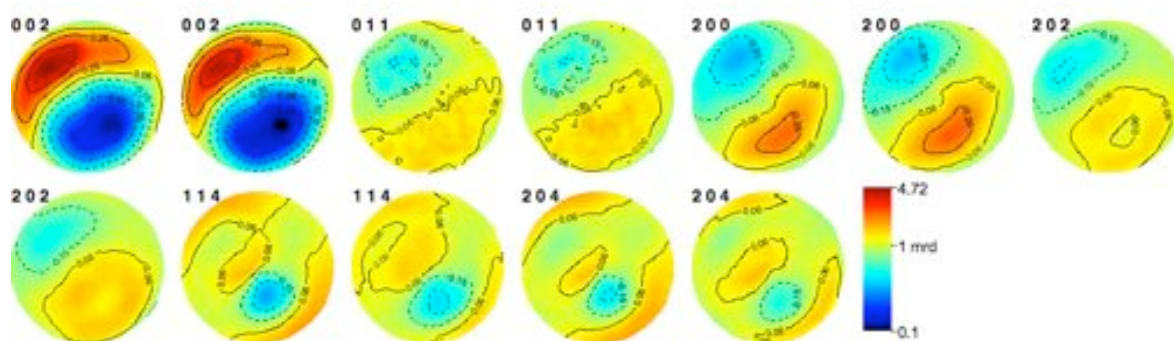

Figure 7.2: DLM-2 texture analysis, observed (left) and calculated (right) pole figures pairs (equal area projection)

All attempts to solve the structure using the direct methods packages *EXPO* (Altomare *et al.*, 1999) and *SHELXS97* (Sheldrick, 1997) from these intensities failed. Because the space group was unclear and there was a minor violation of the body-centering, all primitive, centrosymmetric subgroups of *Imma* were also tried, but without success. Then the new symmetry-independent structure solution method charge flipping see (1.2.3), was applied and the structure finally solved. The correct space group proved to be non-centrosymmetric (*Ima2*) and that possibility had not been considered in the direct methods trials.

7.4 Rietveld Refinement

A Rietveld refienement of the model obtained from the electron density map produced by the charge-flipping program *Superflip* (Baerlocher *et al.*, 2007a), was performed using the program XRS-82 (Baerlocher & Hepp, 1982-2003) and the high-resolution powder diffraction data. Geometric restraints were placed on the bond lengths and angles of the atoms in the silicate layer and the TMA$^+$ cations, and on the distances between the H-bonding O atoms. Additionally, a preferred orientation factor along the [001]-direction had to be included. The refinement proceeded smoothly and converged with R$_F$=0.049

and R_{wp}=0.136 (R_{exp}=0.121). The details for the refinement are given in table 7.2, the fit of the profile calculated from the refined structure to the experimental data is shown in figure 7.3, and the final atomic parameters are given in table 7.3.

Table 7.2: Rietveld Refinement of the structural model for DLM-2

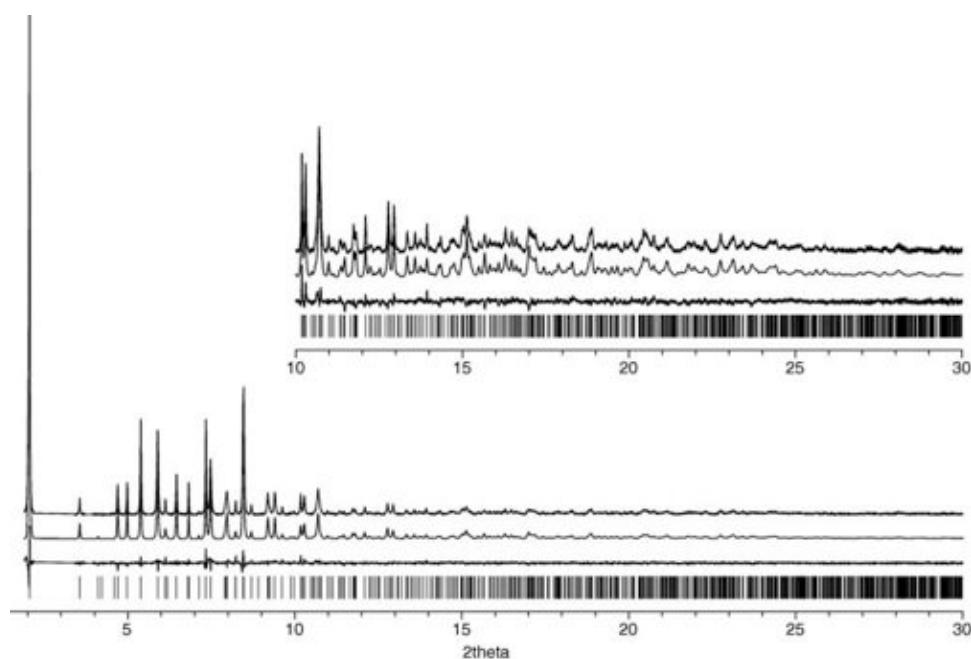| **Rietveld Refinement**		
Number of observations		8979
Number of contributing reflections		842
Number of geometric restraints		56
Si-O	1.61(1) Å	12
N-C	1.48(1) Å	6
O-O	2.70(3) Å	6
O-Si-O	109.5(1.0)°	18
Si-O-Si	145(8.0)°	6
C-N-C	145(1.0)°	8
Number of structural parameters		57
Number of profile parameters		9
R_F		0.049
R_{wp}		0.136
R_{exp}		0.121

Figure 7.3: Observed (top), calculated (middle) and difference profiles (bottom) for the Rietveld refinement of the DLM-2 structure. The tick marks indicate the reflection positions.

Table 7.3: Atomic Parameters for DLM-2[a]

Atom	x	y	z	$\mathbf{U}_{iso}$ ($\mathring{A}^2$)
Si(1)	0.0	0.0	0.2100	0.0145(6) [b]
Si(2)	0.1121(4)	0.8043(7)	0.2895(3)	0.0145 [b]
Si(3)	0.1135(4)	0.3011(8)	0.1678(3))	0.0145 [b]
Si(4)	0.0	0.5	0.2477(3)	0.0145 [b]
O(1)	0.0803(8)	0.1171(10)	0.1770(3)	0.017(1) [c]
O(2)	0.0939(8)	0.0890(12)	0.2430(3)	0.017 [c]
O(3)	0.25	0.7746(15)	0.2970(7)	0.017 [c]
O(4)	0.0554(8)	0.6366(8)	0.2801(4)	0.017 [c]
O(5)	0.0550(10)	0.8851(15)	0.3357(5)	0.017 [c]
O(6)	0.25	0.3074(17)	0.1580(6)	0.017 [c]
O(7)	0.0430(10)	0.3687(16)	0.1217(5)	0.017 [c]
O(8)	0.0914(8)	0.4005(12)	0.2160(4)	0.017 [c]
N(1)	0.25	0.6885(19)	0.5841(7)	0.015(2) [d]
C(11)	0.3507(6)	0.5909(20)	0.5749(7)	0.015 [d]
C(12)	0.25	0.8283(24)	0.5520(9)	0.015 [d]
C(13)	0.25	0.7422(25)	0.6354(7)	0.015 [d]
N(2)	0.25	0.1850(18)	0.8820(7)	0.015 [d]
C(21)	0.25	0.1471(25)	0.8296(7)	0.015 [d]
C(22)	0.3525(6)	0.1204(20)	0.9049(7)	0.015 [d]
C(23)	0.25	0.3591(20)	0.8892(10)	0.015 [d]
O(51)	0.1294(7)	0.6979(24)	0.9252(8)	0.030(2) [e]
O(52)	0.0	0.5	0.9803(16)	0.030 [e]
O(53)	0.1286(7)	0.2807(26)	0.0319(8)	0.030 [e]

[a] Numbers in parentheses are the esd's in the units of the least significant digit given. Values without an esd were not refined.
[b–e] Thermal parameters with the same superscript were constrained to be equal.

7.5 Discussion

The refined structure is shown in figure 7.4. It consists of silicate layers hydrogen-bonded to one another by water molecules with the TMA$^+$ encapsulated in the voids. The silicate layer consists of partial sodalite cages forming cups, which point up and down alternately along both the *a*- and the *b*-axes. Each cup hosts a TMA$^+$ cation, approximately in the middle of what would be a complete sodalite cage. Oberhagemann and co-workers (1996) reported a very similar structure, RUB-15. The only difference lies in the space group (*I2cb* with the DLM-2 unit cell setting) and the resulting arrangement of the water molecules between the silicate layers.
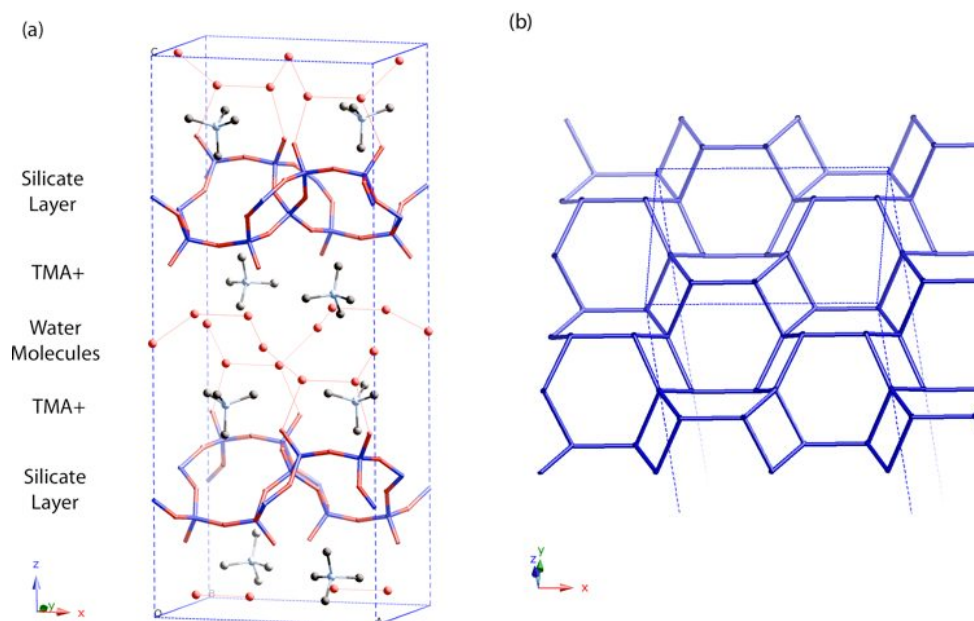

Figure 7.4: The structure of DLM-2 (a) viewed down the *b*-axis showing the arrangement of the silicate layers, TMA$^+$ cations and water molecules, (b) projection of the silicate layer perpendicular to the *a*-axis (TMA$^+$ cations, water molecules and bridging oxygens removed for clarification)

To validate the ODF calculation procedure and the angle conversion, the texture data collected for DLM-2 at SLS were also evaluated using the *MAUD* program. Intensities were extracted from all 1368 patterns. The ODF was again calculated and refined using the *WIMV* method. A texture strength of 1.95 and an Rp-Value of 4.3% was determined and refined using nine well-separated reflections in the 2θ range: 3.0 - 14.25° (002, 112, 200, 202, 114, 204, 020, 121 & 116). The experimental and calculated pole figures pairs are shown in figure 7.5. A comparison of the ODFs calculated from the two texture analyses shows that the texture information obtained is identical. The only difference between the two evaluations is that the conversion from (ψ, δ) to (α, β) according to (Heidelbach *et al.*, 1999) that was used in the first analysis
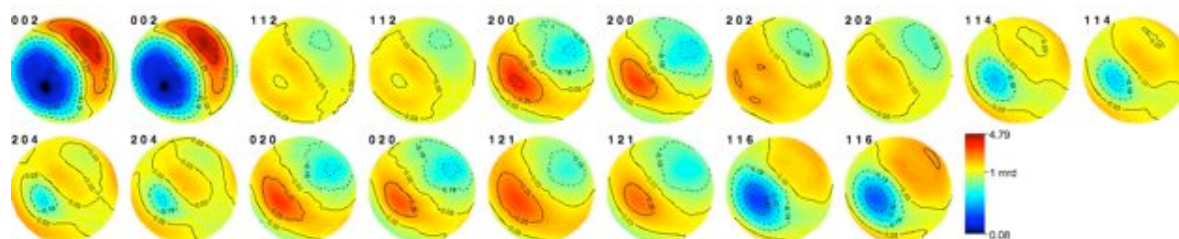
Figure 7.5: Observed and re-calculated pole figures (log-scale, equal area projection) of DLM-2 texture analysis with Maud

results in a 90°-roation in α in all the pole figures with respect to that used in *MAUD*, which is performed according to (Von Dreele, 1997) and (Lutterotti, 2007).

From the reflection intensities extracted in the correct space group, the structure of DLM-2 could also be solved using with conventional direct methods. To further investigate the quality of the jointly refined intensities, a comparison between the structure factors calculated from the refined structure and those obtained experimentally in the joint-refinement procedure, is shown in figure 7.6.
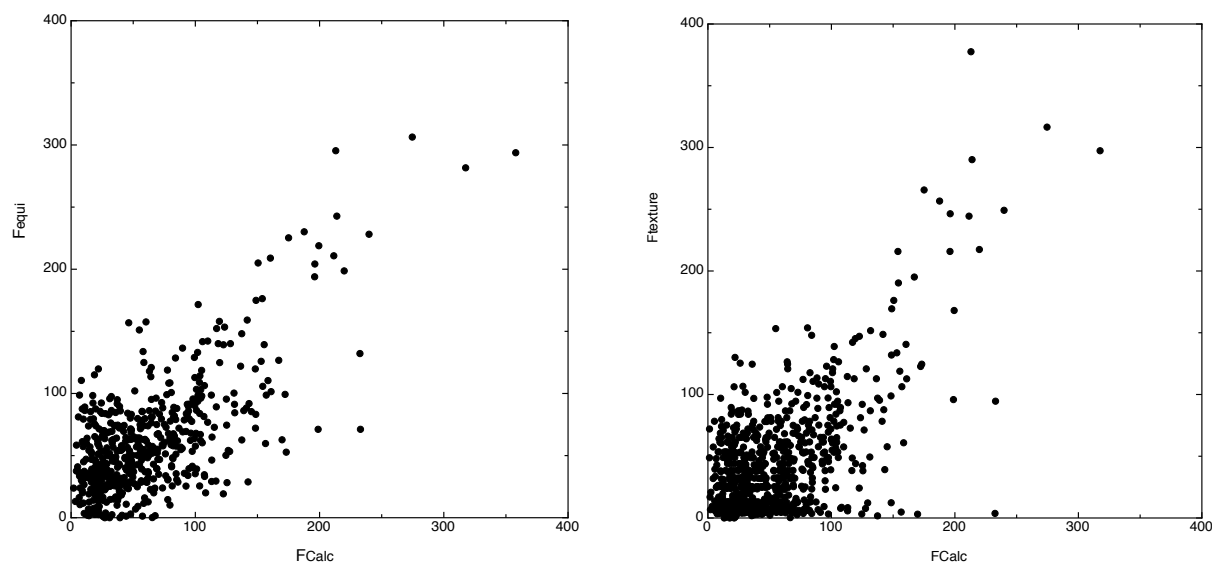

Figure 7.6: Comparison between calculated and extracted structure factors with equipartitioning (left) and structure factors joint refined using the texture method (right).

It can be seen that the medium to strong F-values are comparable, but the weak ones are mostly zero or wrong. A joint extraction together with the high-resolution powder diffraction data was not attempted, because a preferred orientation factor along the [001]-direction had to be included in the Rietveld refinement. Another joint refinement was performed using only 6 patterns, which had been identified as most useful in a cluster analysis (see 5.3). As

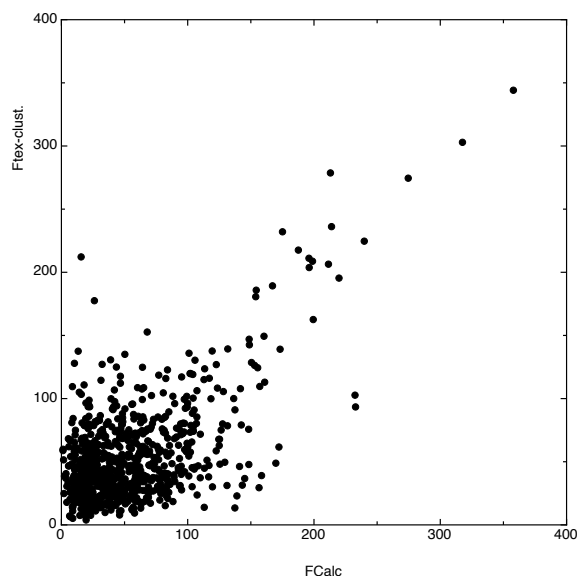shown in figure 7.7, some improvement could be achieved this way.

Figure 7.7: Comparison between calculated and structure factors joint refined using the texture method and only 6 single patterns from the complete dataset.

For a more thorough investigation, powder diffraction patterns for specific orientations were calculated using the known structure and the P-values (orientation factors) calculated from the ODF (figure 7.8) At low angles, the patterns match quite well, but at high 2θ angles, the magnitude of the reflection intensities is in the range of the (poor) counting statistics of the experimental data.

A reason for the discrepancies between the F-values extracted using the information from the texture analysis and those calculated using the structure, could originate from the nature of the texture. To check this, the pole figures from different groups of overlapping reflections were compared. It was found that in many of the groups, the lattice planes are nearly parallel (e.g. 0 0 6 and 0 1 5 figure 7.9.a) or 2 4 10, 2 5 1, 0 1 17, 0 2 16 and 7 1 0 figure 7.9.b)). As a consequence, the pole figures of these reflections do not help in the deconvolution process.
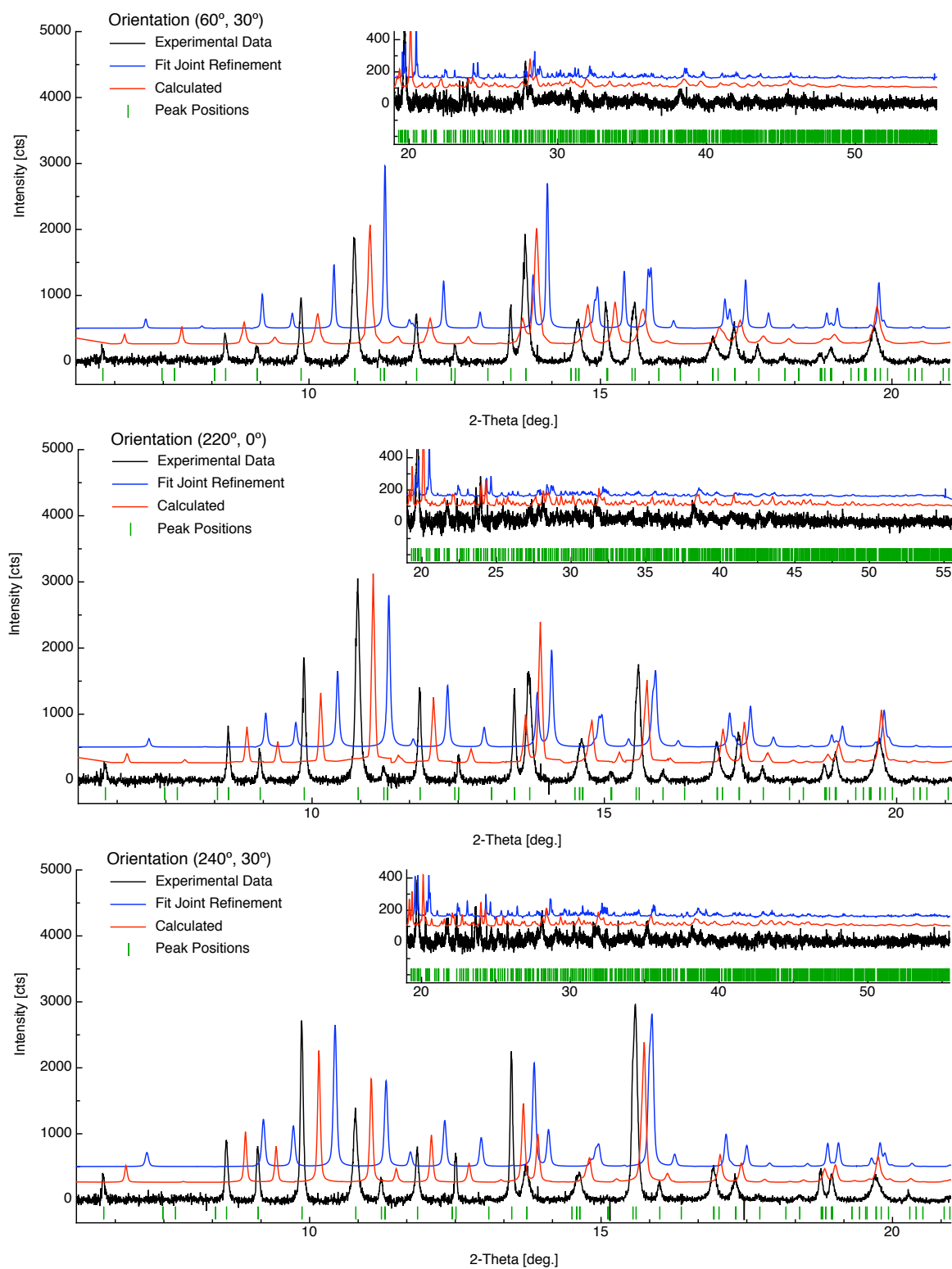
Figure 7.8: Plots of the experimental data for 3 different sample orientations (ψ,δ) (black), the pattern calculated from the structure and P-values (red), and the pattern calculated from the extracted intenisities and the P-values (blue). Tick marks indicate the reflection positions (green)
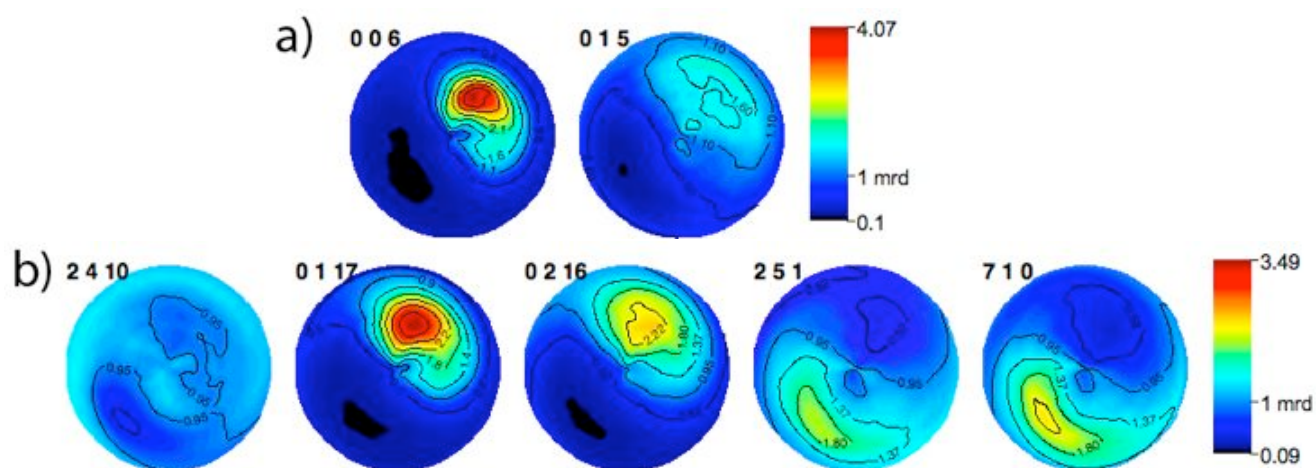
Figure 7.9: Pole figures for 2 groups of overlapping reflections for the DLM-2 texture sample. a) 0 0 6 & 0 1 5, b) 2 4 10, 0 1 17, 0 2 16, 2 5 1 and 7 1 0

8 IM-5

The polycrystalline zeolite catalyst IM-5 (**IMF** framework type) was synthesized in 1998, but it's crystal structure was only solved recently (Baerlocher *et al.*, 2007b) by using intensities extracted from high-resolution powder diffraction data in combination with phases calculated from high-resolution transmission electron microscopy data. Attempts to apply the texture approach to the IM-5 problem were also made.

8.1 Sample Preparation

Several attempts to prepare a textured sample of IM-5 failed. As can be seen in figure 8.1 the IM-5 crystalites are very small and exhibit a needle-like shape with longest dimensions of less than 1 μm.
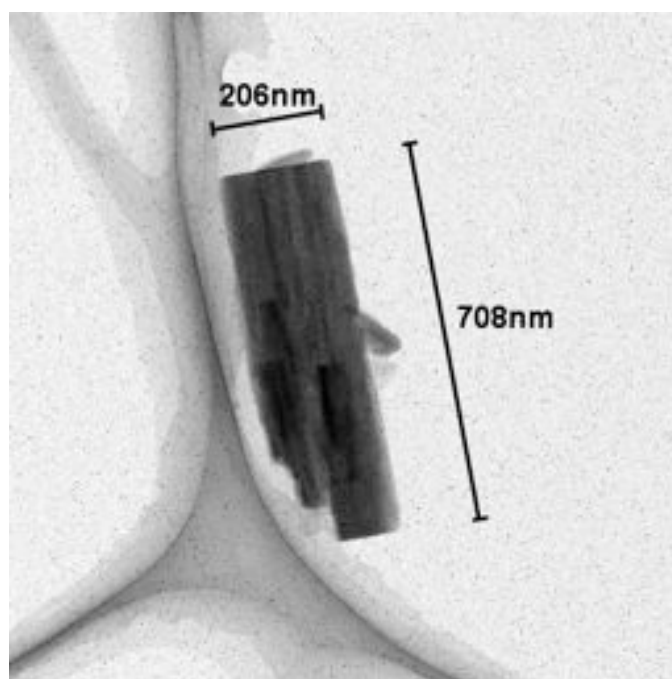

Figure 8.1: Transmission electron micrograph of typical a IM-5 crystal

By adding the surfactant sodium dodecyl sulfate (SDS) to the dispersed crystallites, a textured sample with a moderate degree of preferred orientation was finally prepared. The crystallites were first suspended in THF and disaggregated and dispersed by applying pulsed ultrasonic treatment. Then ca. 2 wt.% of SDS was added and the ultrasonic treatment was repeated (10-20 s at a time) until the resulting suspension was homogeneous and milky. Finally, a

50 wt.% solution of PS in THF was added to the suspension. A bakery-folding procedure was repeated 3 times and after ca. 24 h, a sample of *ca.* 0.3 mm diameter was cut from the final strip (in the middle of the tip of the sample strip) and mounted in a nylon loop.

8.2 Data Collection

Several high-resolution powder diffraction patterns were collected on different samples of IM-5 at both the SNBL and the SLS. Powder diffraction patterns on the textured sample were collected at the SLS (details, table 8.2) using the optimized data collection strategy described in 4.2.4.

Table 8.1: High-resolution data collection details for IM-5

High Resolution Data 1	
Synchrotron Facility	SLS MS
Wavelength	0.9265 Å
Diffraction Geometry	Debye-Scherrer
Analyzer Crystal	Si 111
Sample	rotating 1 mm capillary
2θ range	3.0-43.9º
Step size	0.003º2θ
Time per step	1.0 s

High Resolution Data 2	
Synchrotron Facility	SNBL BM01B
Wavelength	0.5006 Å
Diffraction Geometry	Debye-Scherrer
Analyzer Crystal	Si 111
Sample	rotating 1 mm capillary
2θ range	1.0-30.0º
Step size	0.003º2θ
Time per step	1.0 s

The cluster analysis was performed to identify the orientations best suited for resolving overlapping reflections (see 8.3), and then high-quality data were collected at these 12 orientations. At each orientation, 60 powder patterns at 10 different detector positions (a total of 600 patterns) were taken to improve the counting statistics and reduce the likelihood of "hot channels". Details are given in table 8.2.

Table 8.2: Texture data collection details for IM-5

Texture Data Set 1 (ODF calculation)	
Synchrotron Facility	SLS MS
Wavelength	0.9250 Å
Beam size	0.6 x 0.6 mm^2
Sample Orientations	72 x 19 = 1368
Rotation ψ	0-360º in 5º steps
Tilt δ	0-90º in 5º steps
Sample Oscillation in ψ and δ	±0.5º
Si-microstrip detector positions	1
2θ range	2.5-56.3º
Time per pattern	10 s

Texture Data Set 2	
Synchrotron Facility	SLS MS
Wavelength	0.9250 Å
Beam size	0.6 x 0.6 mm^2
Sample Orientations ψ/δ	12
(1) 0º/ 20º	60 x 10s
(2) 355º/ 35º	60 x 10 s
(3) 160º/ 60º	60 x 10 s
(4) 180º/ 60º	60 x 10 s
(5) 155º/ 80º	60 x 10 s
(6) 180º/ 80º	60 x 10 s
(7) 225º/ 70º	60 x 10 s
(8) 205º/ 70º	60 x 10 s
(9) 260º/ 80º	60 x 10 s
(10) 55º/ 90º	60 x 10 s
(11) 225º/ 90º	60 x 10 s
(12) 270º/ 90º	60 x 10 s
Sample Oscillation in ψ and δ	±0.5º
Si-microstrip detector positions	10
2θ range	2.5-56.3º
Total time per orientation	6000 s

8.3 Data Analysis

The indexing of the high-resolution data (figure 8.2) proved to be quite a challenge, because the unit cell (*a*=14.3100 Å, *b*=57.4030 Å and *c*=20.1420 Å) is unusually large and impurity peaks are present in the pattern.

With an overlap factor of 0.3 (equation 5.9), 3614 (about 91 %) of the 3970 reflections to a $d_{min.}$ of 1.06 Å overlap. This enormous degree of overlap results
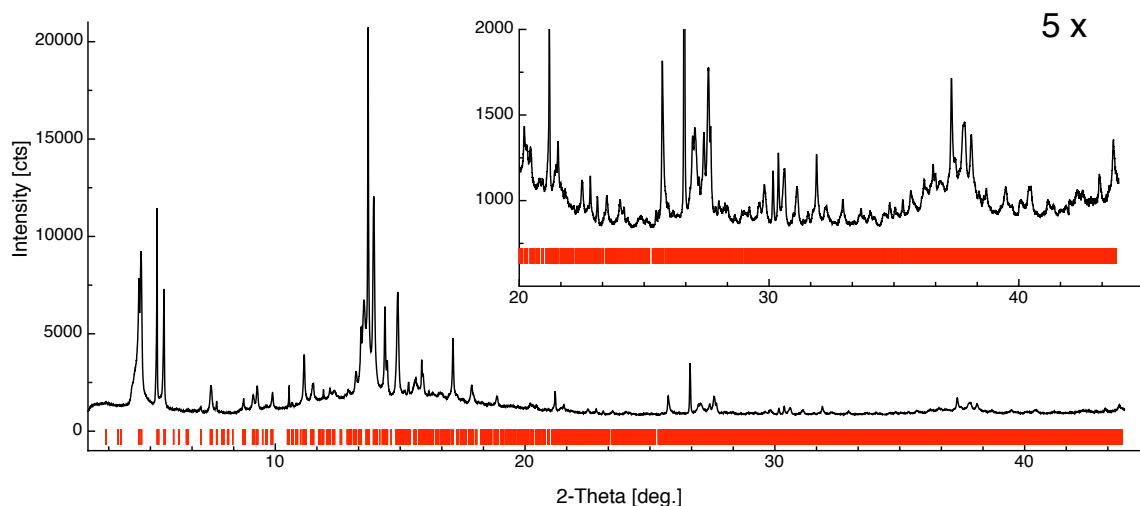
Figure 8.2: High-resolution data collected on a 1 mm capillary sample at the SLS, tick marks indicate reflection positions

from the very large unit cell and approximate relationships between the unit cell axes ($b \sim 4a$ and $c \sim \sqrt{2}a$).

Reflection intensities were extracted from the datasets collected for the ODF determination using the program *Topas* (Coelho, 2003), refining anisotropic line broadening (sharpest peaks along [00l]-direction). A full texture analysis using the pole figure data for the four non-overlapping reflections 041, 130, 002 and 060 was performed using *E-WIMV* implemented in the *MAUD* software package (Lutterotti *et al.*, 1997). The ODF coverage was not sufficient for the conventional *WIMV* algorithm (Matthies & Vinel, 1982). A texture strength of 2.3 with an Rw-Value of 13.8 % was determined. Experimental and calculated pole figures are shown in figure 8.3.
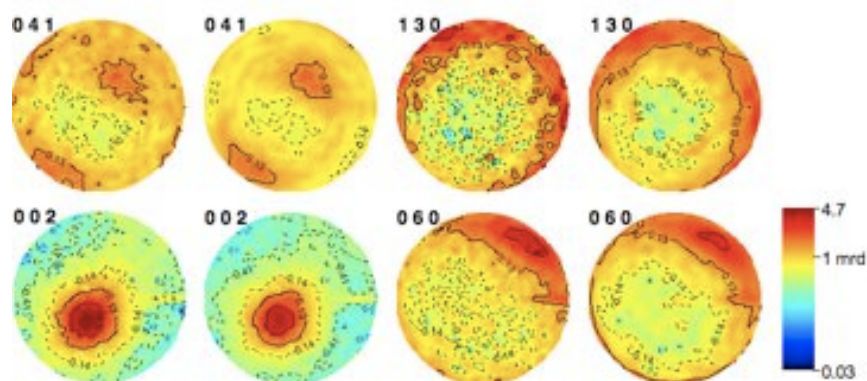

Figure 8.3: IM-5 texture analysis with MAUD: Observed (left) and calculated (right) pole figures (log-scale, equal area projection) in pairs

The P-values calculated from the ODF, were exported and converted back to the data collection angles (ψ,δ). The final data collection grid (shown in figure 8.4) was determined in a cluster analysis. For comparison, the results

from the cluster analysis of the intensity differences for each overlap group, performed using the program *Cluster 3.0* (Eisen, 1999) is shown in figure 8.5.
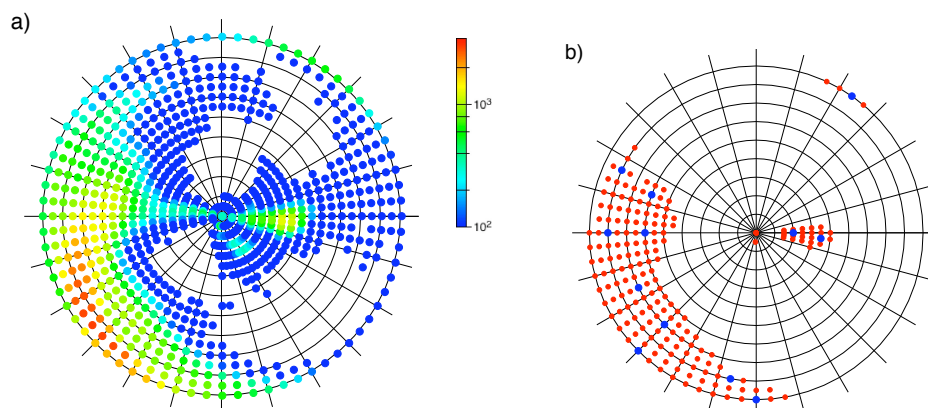

Figure 8.4: (a) Sum of difference pole figure values exceeding 95 % of the max. intensity differences for each group (log-scale), (b) data points determined by a cut-off of 500 hits (red), superimposed on the final measurement grid (blue)
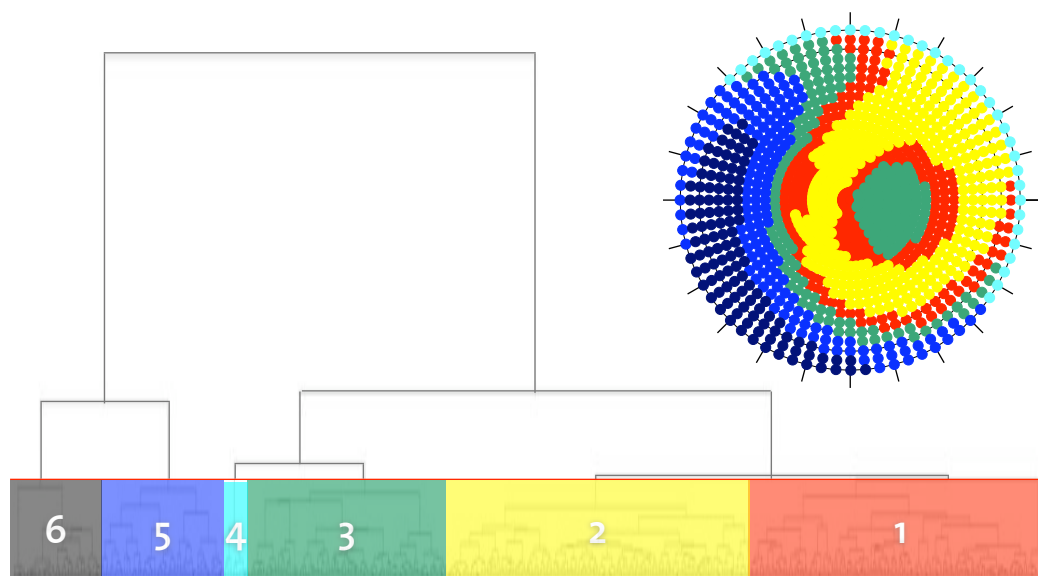

Figure 8.5: Cluster Analysis of the difference pole figures calculated for each overlap group, 7 clusters were chosen by a horizontal at a certain degree of dissimilarity

The final 12 patterns were used for the joint refinement of a single set of reflection intensities. This set of intensities was used as input to *SHELXS* (Sheldrick, 1997), but no sensible solution was obtained. In another attempt, the intensity set was extended to the space group *P1* and used as input into the charge-flipping program *Superflip.* Some of the electron density maps exhibited partially sensible frameworks, but none could be interpreted to a level, sufficient for structure solution. The structure was finally solved, using

integrated intensities extracted from high-resolution powder diffraction data (after removal of analcime impurity peaks) combined with phases obtained from HRTEM images taken along the three main zone axes in a charge-flipping algorithm.

8.4 Discussion

Figure 8.6, shows eight of the twelve datasets collected with improved counting statistics. Intensity differences indicative of preferred orientation are clearly apparent. In figure 8.7 one of these patterns (merged from 600 individual patterns) is compared to the data collected for the ODF determination (one pattern per orientation) and a test measurement performed on the same sample with the high resolution setup also available at SLS (the high-resolution measurement was merged from 5 scans from 0-20º2θ, scan speed 0.375º/min., total time ca. 4.4 h). This comparison shows, that texture data with a quality comparable to the high-resolution data measured with an analyzer setup can be obtained by collecting data repeatedly at certain sample orientations. The amount of time needed for these measurements compared to a conventional texture measurement did not increase.
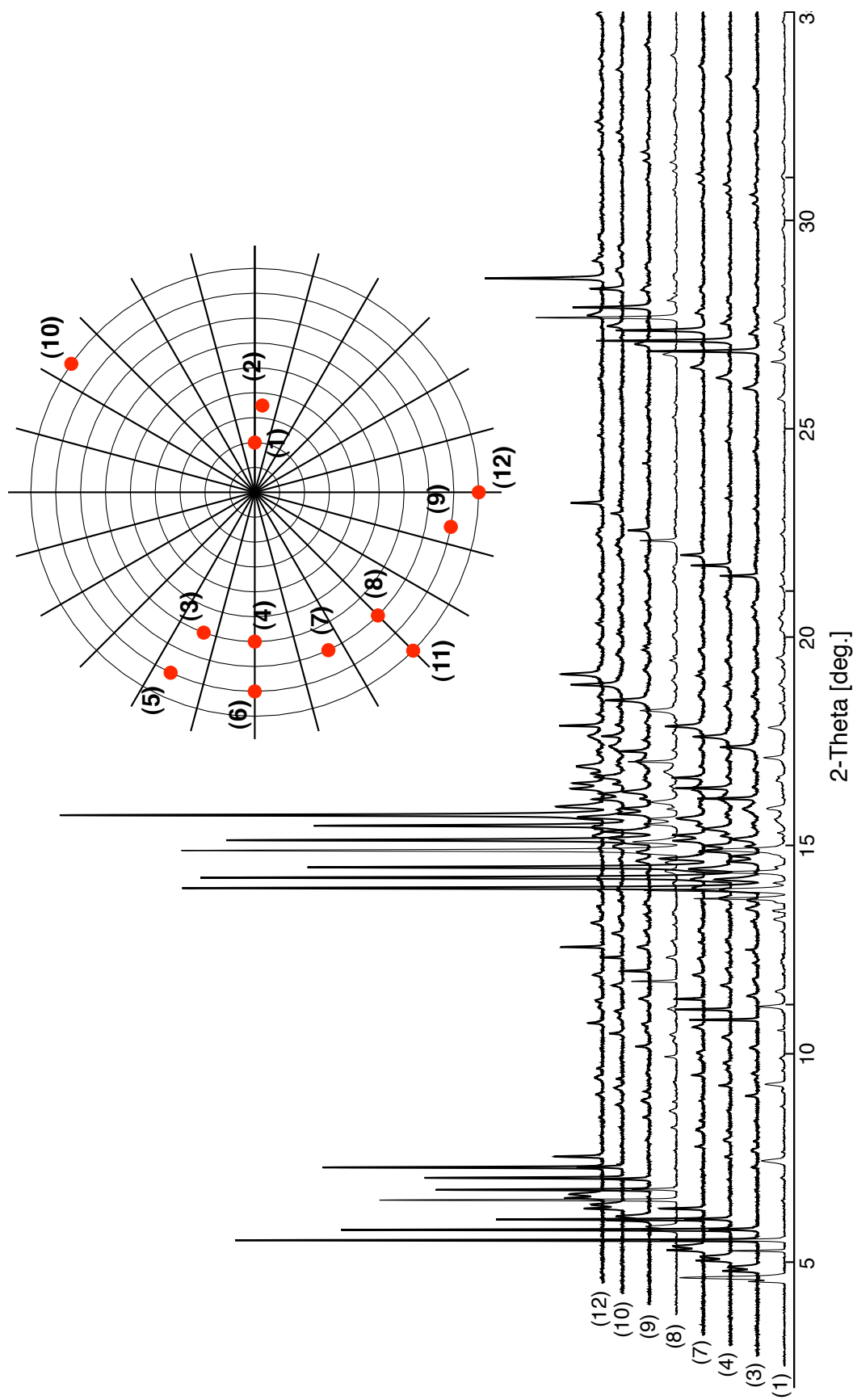
Figure 8.6: Data collected at selected orientations with improved counting statistics, the background has been removed from all the patterns for the joint-extraction (the numbering of the orientations corresponds to the listing given in table 8.2)
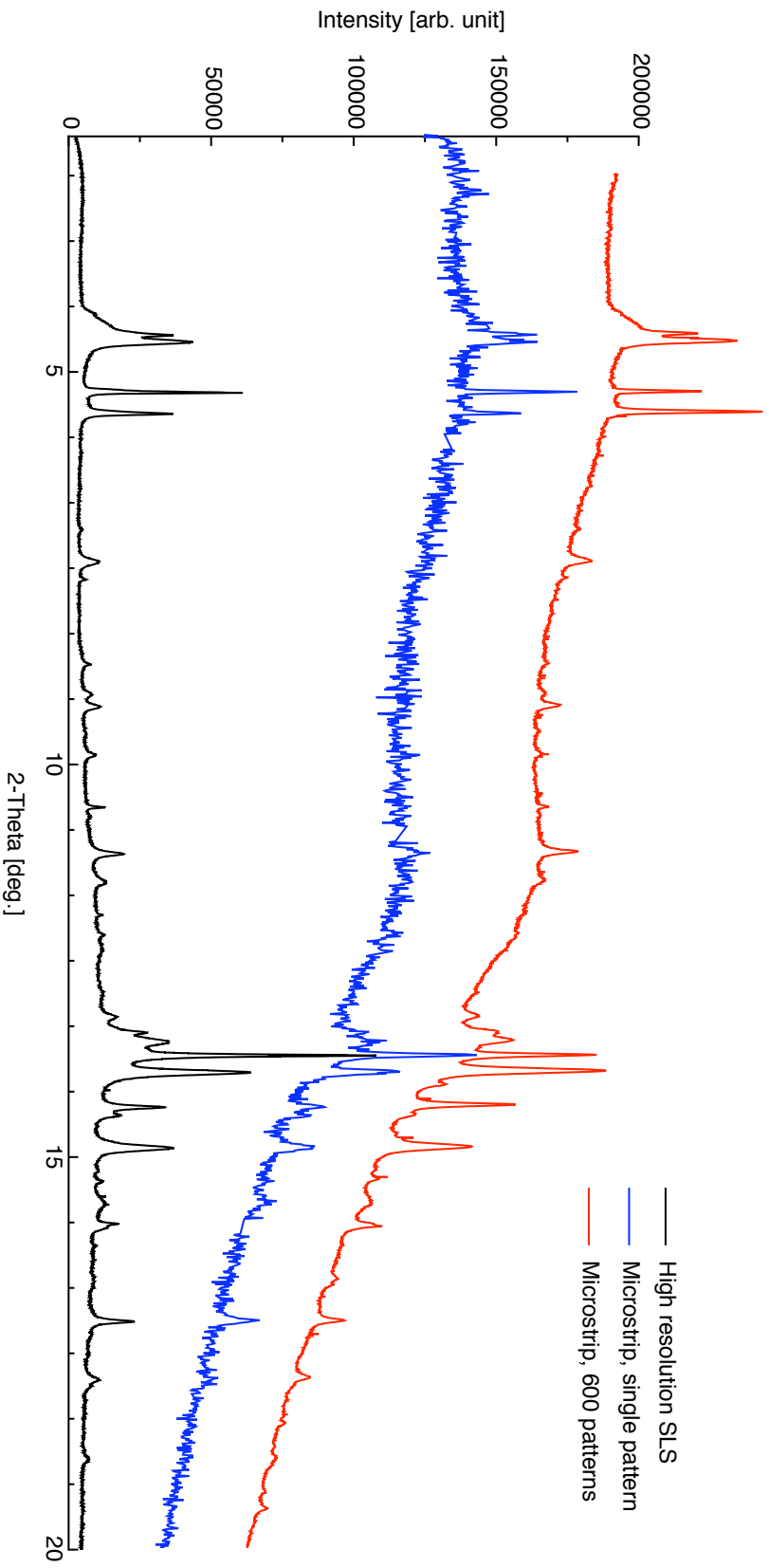
Figure 8.7: Comparison between data collected with the high-resolution analyzer setup at SLS, and data collected with the microstrip detector (a single pattern and one merged from 600 patterns) on the IM-5 texture sample at orientation($\psi = 235°, \delta = 80°$).

9 Silver Behenate

Silver behenate [$CH_3(CH_2)_{20}$ COOAg] was first analyzed and discussed as a possible low-angle diffraction standard by Huang *et al.* (1993). They determined the long unit cell axis by fitting the [*00l*]-peaks in synchrotron x-ray data, with d_{001}=58.380(3) Å. After these successful tests, Keiderling and co-workers (1999) discussed the application of silver behenate for determining the wavelength in small-angle neutron scattering (SANS) experiments.
However, the other two dimensions of the unit cell were not determined. As shown in fig. 9.1, the crystallites of silver behenate, exhibit a plate-like morphology (ca. 0.2 x 2 x 0.1 μm^3).
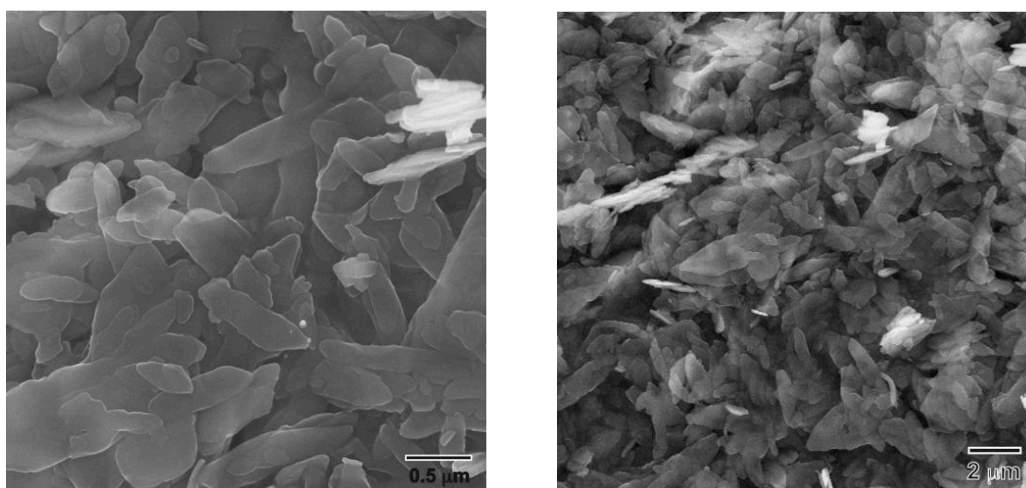

Figure 9.1: Scanning electron microscopy images of silver behenate crystals

9.1 Sample Preparation

The sample of silver behenate was kindly provided by Daniel Louër in 2005. A first texture sample was produced using the modified matrix-smear method (SB-MS) and a second one using the bakery-folding procedure (SB-BF), described for IM-5 in the previous chapter.

9.2 Data Collection

High-resolution data were collected on an untextured (capillary) sample at SNBL in Grenoble (table 9.2). Some of the last runs of the measurement had to be excluded from the binning procedure, because the sample deteriorated during the measurement.

9 Silver Behenate

Conventional texture measurements were performed on two samples taken from SB-MS preparation. One was measured using the setup with the diagonally shifted imaging plate, and the other with the microstrip detector (details in table 9.1).

Table 9.1: Data collected on Ag-Behenate (SB-MS)

High Resolution Data	
Synchrotron Facility	SNBL BM01B
Wavelength	0.5004 Å
Diffraction Geometry	Debye-Scherrer
Analyzer Crystal	Si 111
Sample	rotating 1 mm capillary
2θ range	1.0-32.0º
Step size	0.005º2θ
Time per step	1 s

Texture Data SNBL	
Textured Sample	Matrix-Smear (1)
Synchrotron Facility	SNBL BM01A
Wavelength	0.8000 Å
Sample to detector distance	400 mm
Rotation ψ (72 frames)	0-360º in 5º steps
2θ range	2.5-32.5º
Time per frame	180 s

Texture Data SLS	
Textured Sample	Matrix-Smear (2)
Synchrotron Facility	SLS MS
Wavelength	0.9250 Å
Beam size	0.6 x 0.6 mm^2
Sample Orientations	72 x 19 = 1368
Rotation ψ	0-360º in 5º steps
Tilt δ	0-90º in 5º steps
Sample Oscillation in ψ and δ	±0.5º
Si-microstrip detector positions	2
2θ range	2.5-56.3º
Time per pattern	10 s

For the SB-BF sample, first a complete dataset was collected with a single detector position for the ODF determination, and then 60 patterns with 11 different detector positions at each of the eight selected orientations were

measured.

Table 9.2: Data collected on Ag-Behenate (SB-BF)

Texture Dataset for ODF calc.	
Textured sample	SDS + Bakery folding
Synchrotron Facility	SLS MS
Wavelength	0.925 Å
Beam size	0.6 x 0.6 mm^2
Sample Orientations	72 x 19 = 1368
Rotation ψ	0-360º in 5º steps
Tilt δ	0-90º in 5º steps
Sample Oscillation in ψ and δ	±0.5º
Si-microstrip detector positions	1
2θ range	2.0-50.3º
Time per pattern	10 s

Final Dataset	
Synchrotron Facility	SLS MS
Wavelength	0.925 Å
Beam size	0.6 x 0.6 mm^2
Sample Orientations ψ/δ	8
(1) 165º/ 0º	60 x 10 s
(2) 320º/ 5º	60 x 10 s
(3) 335º/ 10º	60 x 10 s
(4) 300º/ 20º	60 x 10 s
(5) 0º/ 35º	60 x 10 s
(6) 10º/ 40º	60 x 10 s
(7) 85º/ 70º	60 x 10 s
(8) 100º/ 70º	60 x 10 s
(9) 115º/ 75º	60 x 10 s
(10) 190º/ 85º	60 x 10 s
Sample Oscillation in ψ and δ	±0.5º
Si-microstrip detector positions	11
2θ range	2.0-50.3º
Total time per orientation	6600 s

9.3 Data Analysis

As can be seen in the high-resolution data collected at SNBL (figure 9.2), a series of high intensity reflections dominate the low angle region. The inset, scaled-up 6.5 times, shows more detail of the high angle region.
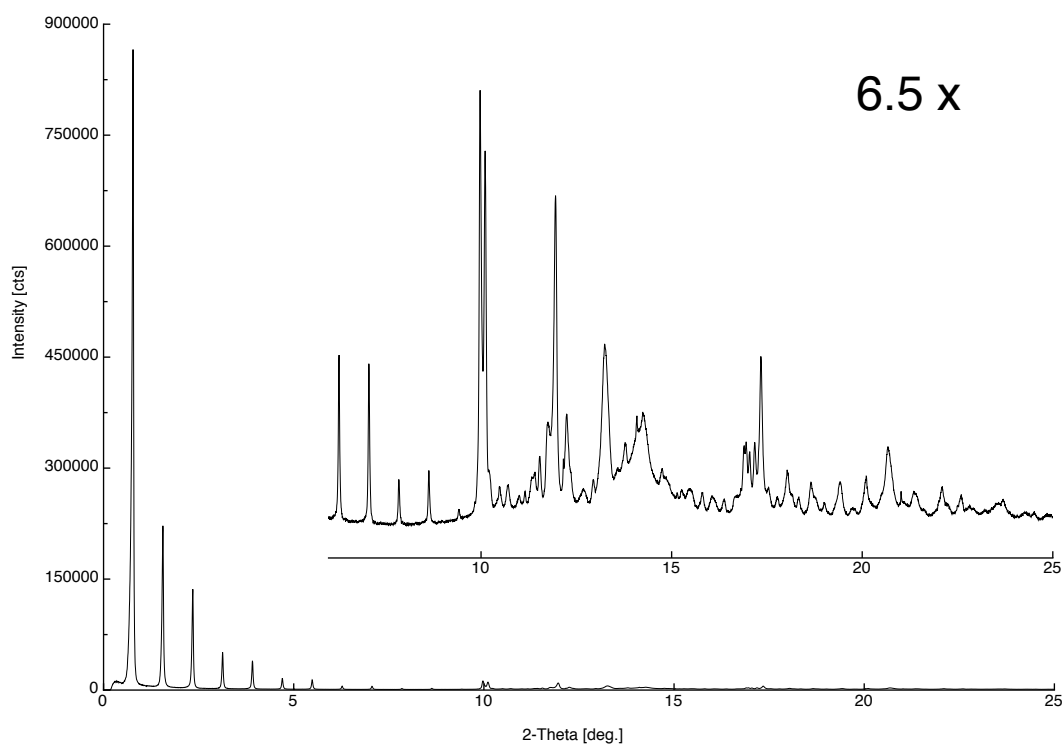

Figure 9.2: High-resolution data collected on a 1 mm capillary sample at the SNBL

With the help of the texture measurements, an orthorhombic unit cell with *a*=58.3103 Å, *b*=8.1159 Å and *c*=5.5533 Å could be determined. The series of strong low angle reflections are all *h00* reflections, so the determination of *a* is straightforward (58.3103 Å). From an image plate frame collected at SNBL, a pattern perpendicular to the *h00*-direction was integrated (figure 9.3). The *d*-spacing for the first reflection of the direction perpendicular to *a* was determined with ca. 5.5 Å. All the attempts to index the pattern using *DICVOL04* did not succeed. Finally, in an attempt with *TOPAS*, the *b*- and *c*-axis could be determined. The space group is ambiguous, first *A222* was assumed.

The ODF was determined for the two conventional texture measurements with the image plate and the microstrip detector using the orthorhombic cell. Experimental and calculated pole figures are shown in figures 9.4 and 9.5.

From the data collected at a single detector position from the SB-BF sample, the extracted intensities of the reflections: 500, 011, 211 & 520 were used to determine the ODF. The converted pole figures were imported into *MAUD* and a texture strength of 6.5 with an Rp-Value of 22.3 % was determined. The experimental and calculated pole figures are shown in figure 9.6.
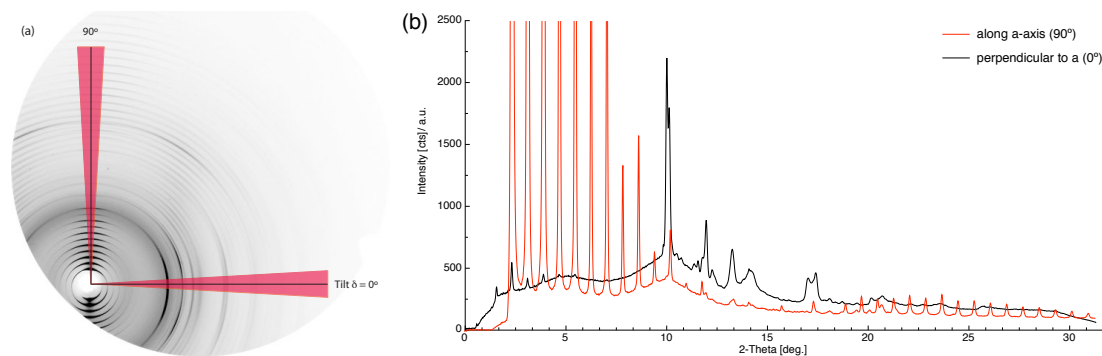
Figure 9.3: (a) Image plate frame collected on a textured sample at SNBL, (b) powder patterns integrated along the *a*-axis and perpendicular to it.
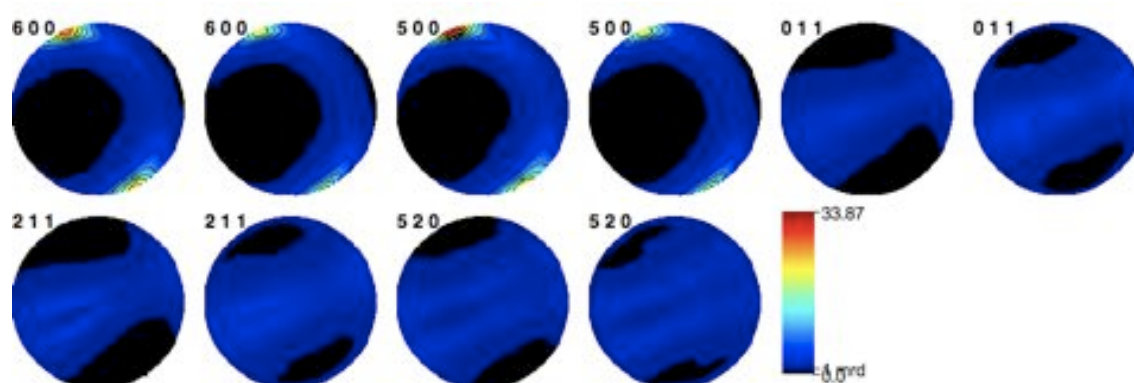

Figure 9.4: Experimental (left) and calculated (right) pole figure pairs for Ag-Behenate *SB-MS(1)*; SNBL Data; texture Index: 7.2 mrd; Rp-Value: 18.5%;

9.4 Discussion

The Rp-Value for the calculated ODF is quite high, which is related to the very high intensities of the [*h00*] reflection compared to the others. Anyway, a joint refinement has been attempted, but the refined intensities did not yield a sensible solution for the structure. Further investigations, mainly on the indexing and space group for this compound are in progress, another evaluation using the space group *Pbam* will be done, because the molecule(s) would not fit in the unit cell with an *A*-centered space group.
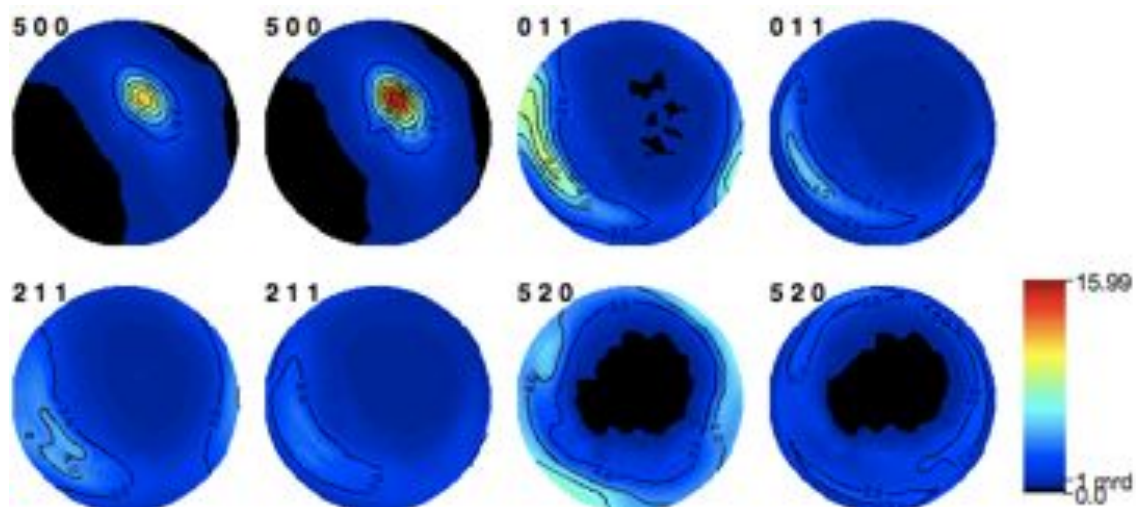
Figure 9.5: Experimental (left) and calculated (right) pole figure pairs for Ag-Behenate *SB-MS(2)*; SLS Microstrip Data; texture Index: 11.3 mrd; Rp-Value: 40.2%
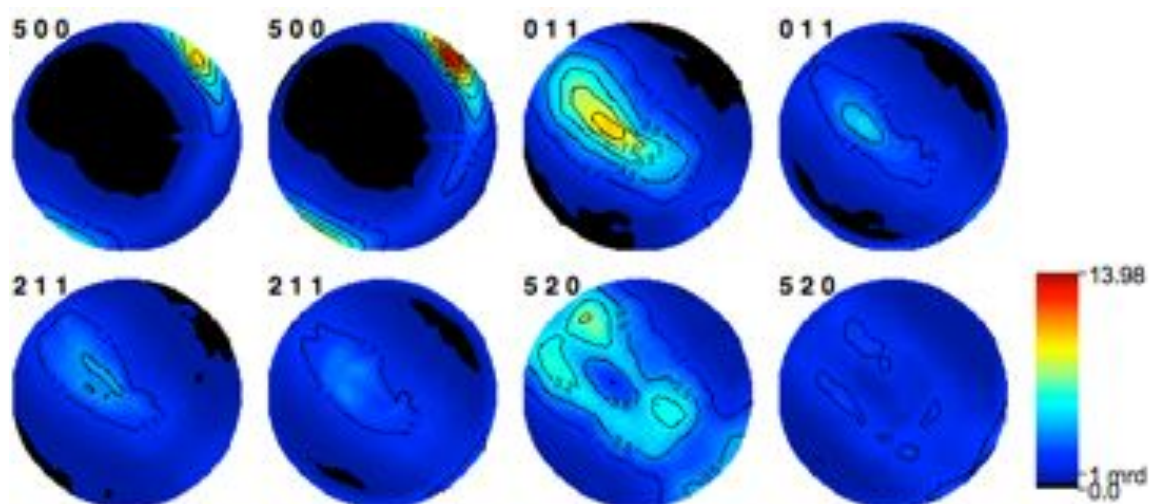

Figure 9.6: Observed (left) and calculated (right) pole figure pairs (equal area projection) for SB-BF; SLS Microstrip Data.
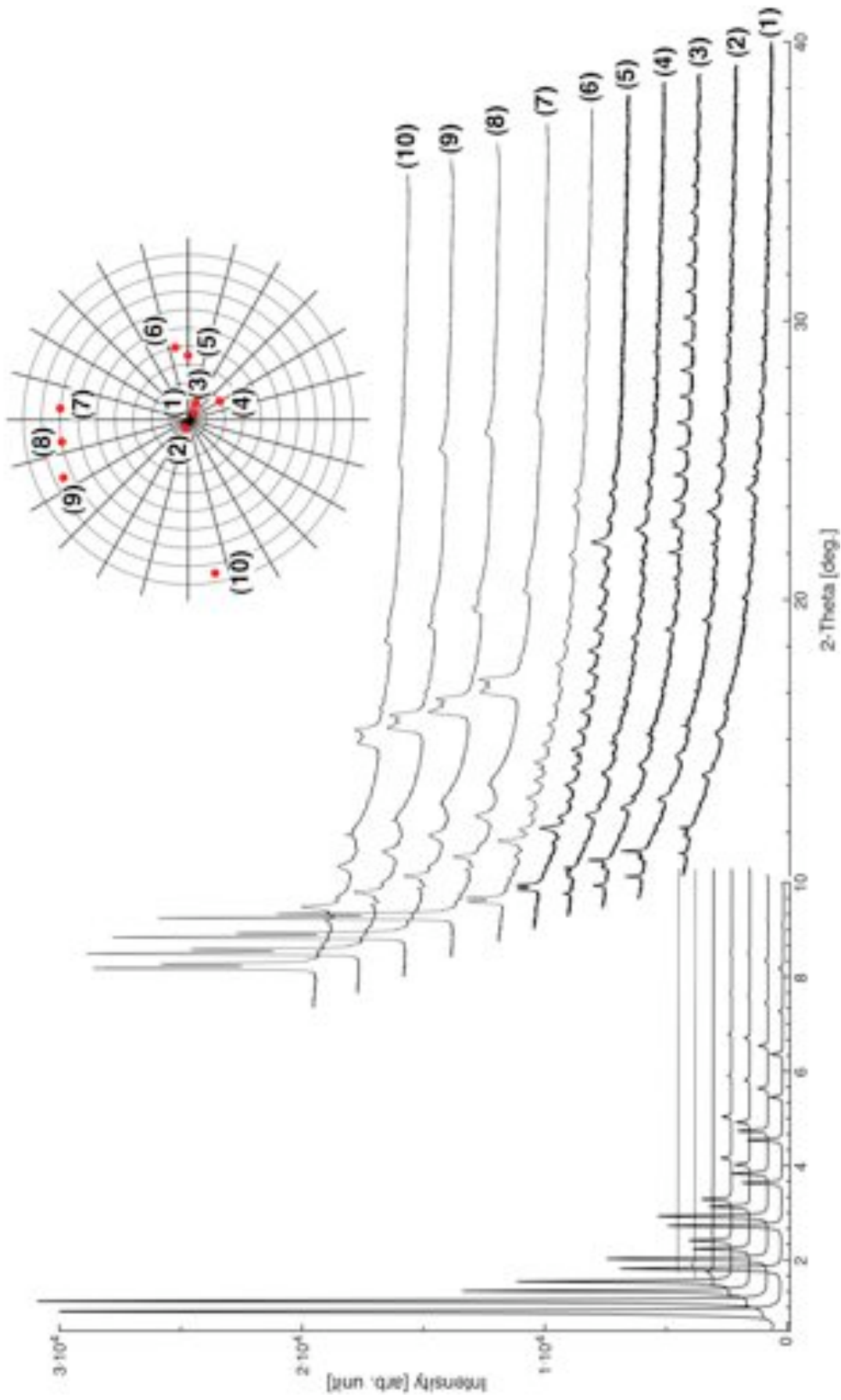
Figure 9.7: Patterns, each merged from 600 individual patterns, taken at the orientations determined in cluster analysis, specified in table 9.2. The high angle is shown at a magnification factor of 50.

10 AM11

During the course of a systematic study of microporous zirconium and niobium silicates, Rocha and co-workers (1998) synthesized a new niobium silicate, denoted AM-11. TEM investigations revealed that the AM-11 crystals are needles (figure 10.1) with an enormous aspect ratio (length ca. 1 μm, width ca. 0.02 μm).
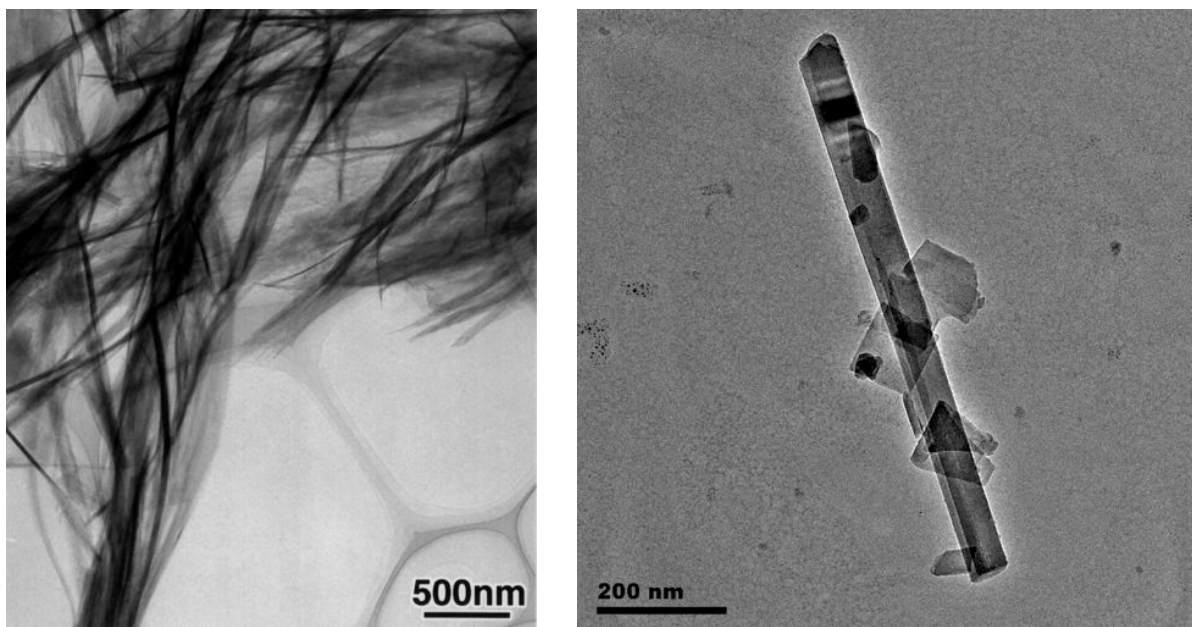
Figure 10.1: TEM images of AM-11 crystallites

10.1 Sample Preparation

A calcined and an as-synthesized sample of AM-11 were kindly provided by Antonió Moreira dos Santos. The textured sample for AM-11 was prepared by the bakery-folding procedure discussed in chapter 3.5. The sample preparation procedure is identical to the one used for IM-5 (chapter 8.1). The bakery-folding procedure was repeated 6 times. After the final sample strip was dried for about 24 hours, the sample of ca. 0.3 mm diameter was cut from the middle section at the very tip of the final strip.

10.2 Data Collection

High resolution data were collected on capillary samples of both the calcined and the as synthesized powder samples. Details are given in table 10.1.

Table 10.1: High-resolution data collection for AM-11

High Resolution Data: AM-11 (calcined)	
Synchrotron Facility	SNBL BM01B
Wavelength	0.5004 Å
Diffraction Geometry	Debye-Scherrer
Analyzer Crystal	Si 111
Sample	rotating 1 mm capillary
2θ range	1.0-32.0º
Step size	0.005º2θ
Time per step	1 s

High Resolution Data: AM-11 (as synthesized)	
Synchrotron Facility	SNBL BM01B
Wavelength	0.5007 Å
Diffraction Geometry	Debye-Scherrer
Analyzer Crystal	Si 111
Sample	rotating 1 mm capillary
2θ range	1.0-30.0º
Step size	0.003º2θ
Time per step	1 s

At the SLS, datasets were collected on the textured AM-11 sample using the optimized data collection strategy described in 4.2.4. Eight orientations were selected from the cluster analysis for high quality data collection. At each of these orientations, 60 powder patterns with 10 different detector positions (a total of 600 patterns) were taken to improve the counting statistics (table 10.2).

Table 10.2: Texture data collected on AM-11

Texture Dataset for ODF calc.	
Synchrotron Facility	SLS MS
Wavelength	0.9250 Å
Beam size	0.6 x 0.6 mm^2
Sample Orientations	1368
Rotation ψ (72 frames)	0-360º in 5º steps
Tilt δ (19 frames)	0-90º in 5º steps
Sample Oscillation in ψ and δ	±0.5º
Si-microstrip detector positions	1
2θ range	2.0-50.3º
Time per pattern	10 s

Final Dataset	
Synchrotron Facility	SLS MS
Wavelength	0.9250 Å
Beam size	0.6 x 0.6 mm^2
Sample Orientations ψ/δ	8
(1) 340º/ 15º	60 x 10 s
(2) 350º/ 35º	60 x 10 s
(3) 250º/ 40º	60 x 10 s
(4) 0º/ 45º	60 x 10 s
(5) 50º/ 70º	60 x 10 s
(6) 150º/ 80º	60 x 10 s
(7) 175º/ 85º	60 x 10 s
(8) 265º/ 85º	60 x 10 s
Sample Oscillation in ψ and δ	±0.5º
Si-microstrip detector positions	10
2θ range	2.0-50.3º
Total time per orientation	6000 s

10.3 Data Analysis

The high-resolution data collected on an untextured sample of the as-synthesized material (figure 10.2) could be indexed with three different unit cells: orthorhombic (a=23.5826 Å, b=13.6020 Å, c=7.47 Å), monoclinic (a=12.4116 Å, b=13.6098 Å, c=7.47 Å , β=107.96º) and hexagonal (a=b=27.2181 Å , c=7.47 Å). The relationship between the three unit cell is shown in figure 10.3.

Integrated intensities were extracted from the data collected for the ODF determination, using the commercial software *TOPAS* (Coelho, 2003) and the peak positions from the hexagonal unit cell with the space group $P6_3/mmc$ and the orthorhombic cell with *Pmma*. The pole figures for the reflections with the following 2θ angles: 4.5º, 7.5º, 7.8º, 9.0º, 10.8º, 11.9º, 14.2º, 14.2º and 15.6º are shown with the hexagonal and orthorhombic indexing in figures 10.4 and 10.5, respectively.

With the hexagonal unit cell, the indices of the reflections at 7.8º and 15.6º are 220 and 440, respectively. As 440 is just a higher order of 220, its pole figure should be the same, but this is not the case. Similarly, the 200 and 400 pole figures (4.5º and 9.0º) should be the same, but are not. With the orthorhombic indexing, the peak at 7.8º has the indices 020, but that at 15.6º includes both the 620 and 040 reflections. As the pole figure at 15.6º resembles that of 200 (at 4.5º), it can be assumed that the 620 reflection, whose pole figure is approximately parallel to 200, is stronger than 040. Similarly, the peak at 15.6º involves overlapping reflections in the orthorhombic system, so again there is no inconsistency. Using this reasoning, it can be concluded that the unit cell is not hexagonal. This is a nice example of how texture analysis can be used to resolve indexing ambiguities. Note that the pole figures for the 200, 020 and 002 reflections have maxima in mutually perpendicular directions, as expected for an orthorhombic system. The pole figures for the reflections 220, 202 and 620 were not used for ODF calculation, because either their intensity was too low or they overlap with neighboring reflections.
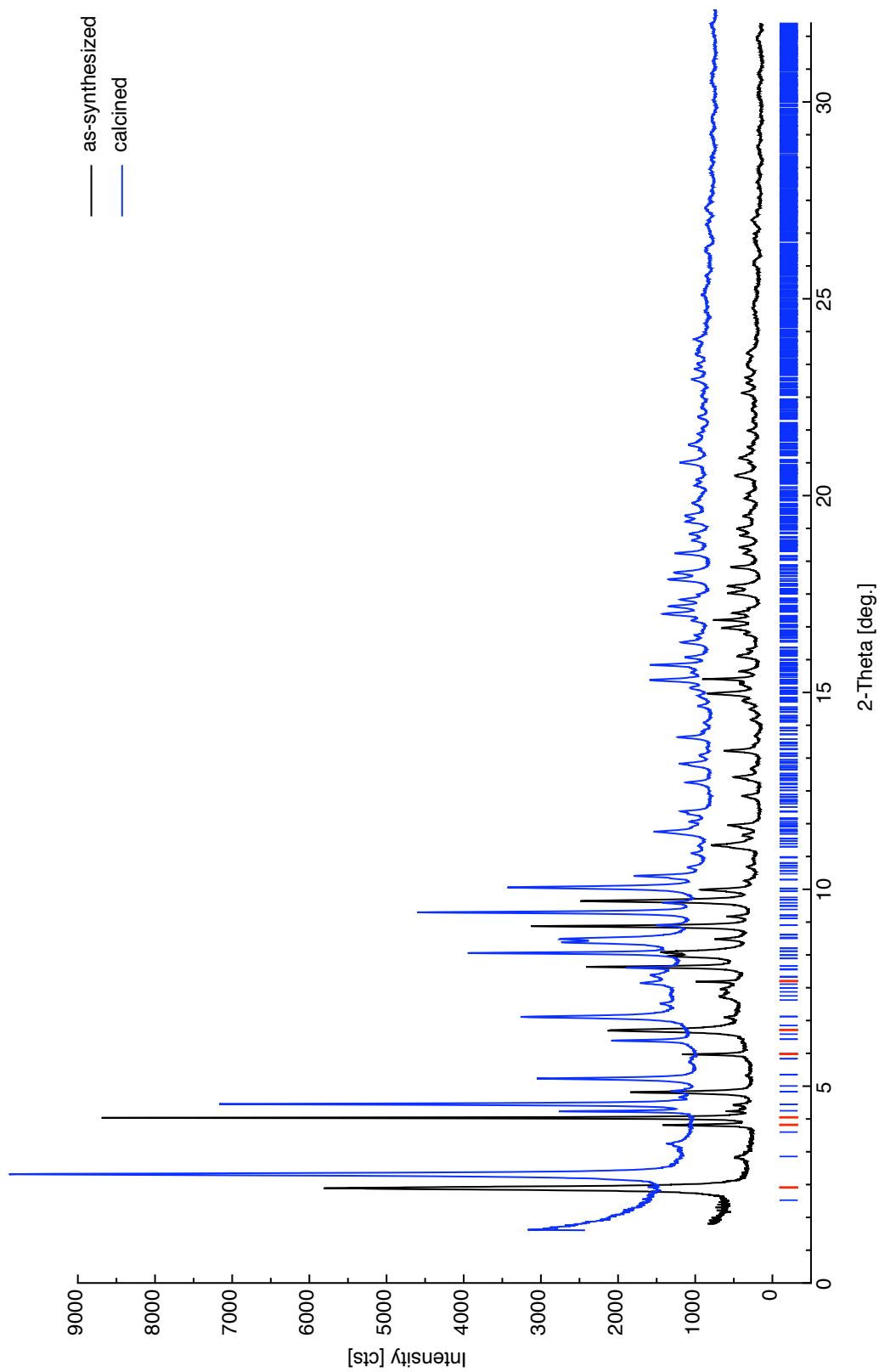
Figure 10.2: High-resolution data collected on an as synthesized (λ=0.50007 Å) and a calcined sample of AM11 on the SNBL (λ=0.5004 Å). Reflections used for the ODF calculation are indicated in red.
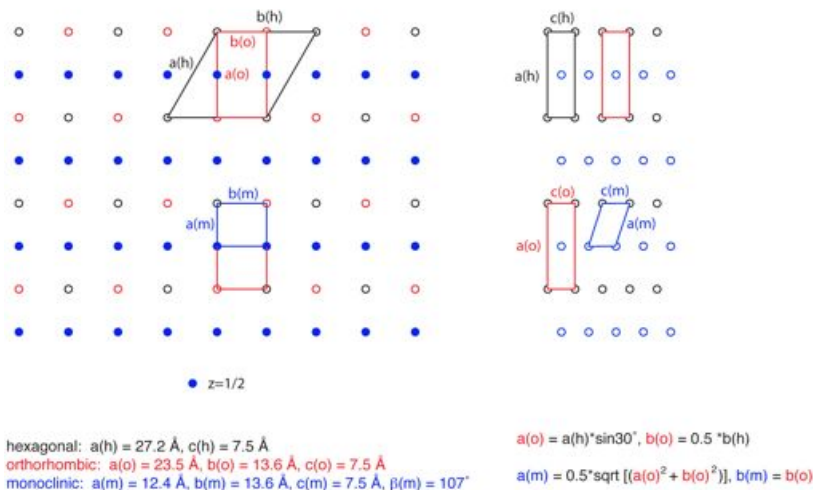
Figure 10.3: The relationships between the hexagonal (black), monoclinic (blue) and the orthorhombic (red) unit cells. The projection perpendicular to the *c*-axis is shown on the left and that perpendicular to the *b*-axis on the right.
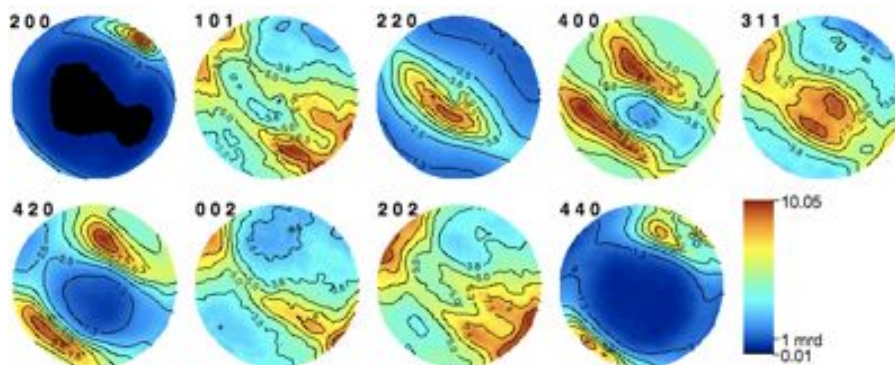

Figure 10.4: Experimental pole figures for AM11 extracted using the hexagonal unit cell (equal area projection)
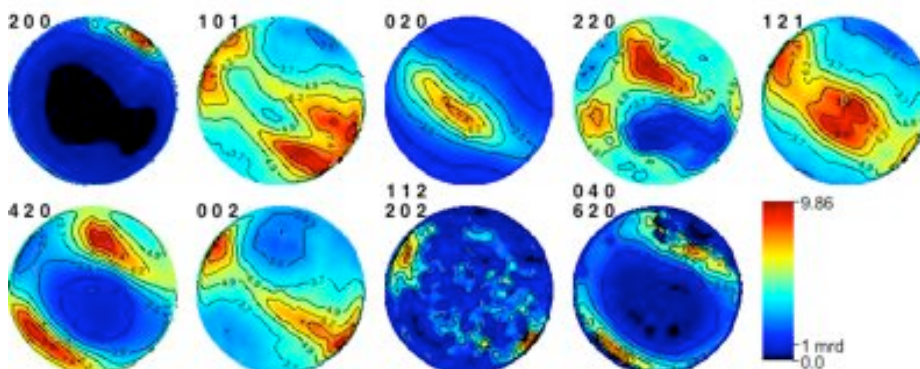

Figure 10.5: Experimental pole figures extracted using the orthorhombic unit cell (equal area projection)

10.3.1 Cluster Analysis

For the texture dataset, the ODF was determined from the first run using the orthorhombic cell with the space group *Pmma*. The 020 reflection was extracted separately, because of it's excessive sharpness in FWHM compared to the other reflections. The reflections used for the ODF calculation were: 200, 101, 020, 121, 420 and 002. The observed and calculated pole figures from the ODF determination are shown in figure 10.6.
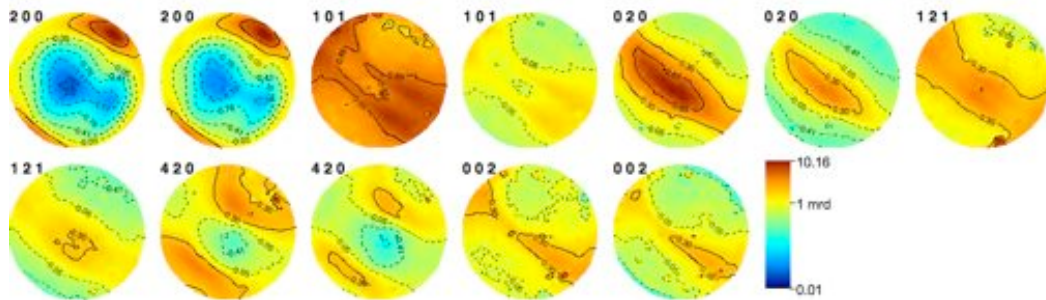

Figure 10.6: Pairs of experimental pole figures extracted using the orthorhombic unit cell (left) and those calculated from the ODF (right), equal area projection and log-scaled

A texture index of 3.7 m.r.d was determined, the Rp-Value was 9.72 %. All the pole figures were calculated from the ODF and converted from the pole figure coverage to the data collection angles. The orientations giving maximum resolution for the overlapping reflection were determined according to the procedure in chapter 5.3.1. The resulting clustering and the 8 orientations, at which data with better statistics were collected, are shown in figure 10.7.
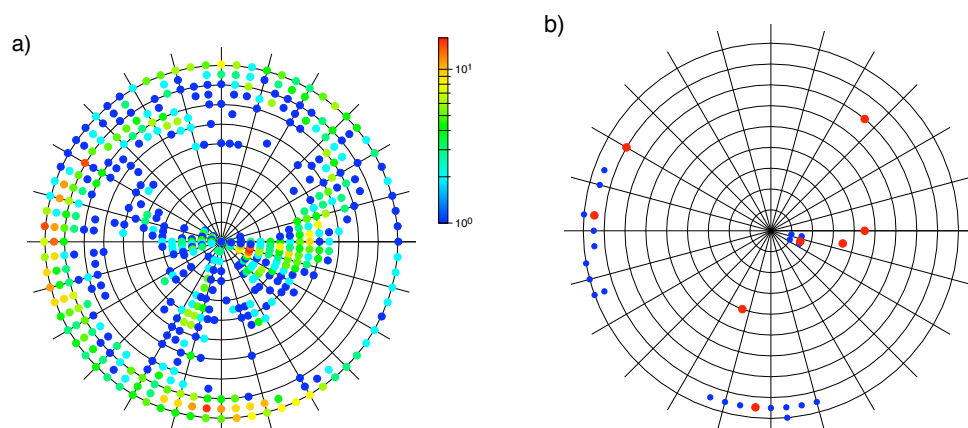
Figure 10.7: (a) Sum of difference pole figure values exceeding 95 % of max. intensity differences for each overlap group (log-scale), (b) data points determined by a cut-off of 8 hits (blue), superimposed the final data collection grid (red)

Five of these patterns, are shown in figure 10.8. They were used for a final joint refinement using *TOPAS*. So far, no sensible solution has been found with either conventional direct methods or charge flipping (*Superflip*).

Figure 10.8: Powder diffraction patterns for AM11 taken at the orientations $(\psi,\ \delta)$: $(340^\circ, 15^\circ)$, $(50^\circ, 70^\circ)$, $(150^\circ, 80^\circ)$, $(0^\circ, 40^\circ)$ and $(350^\circ, 35^\circ)$. Each is the result of merging 600 individual patterns.

10.4 Discussion

The main problem in the joint refinement was the enormous degree of anisotropic line broadening present along the [*h00*]-direction. It could be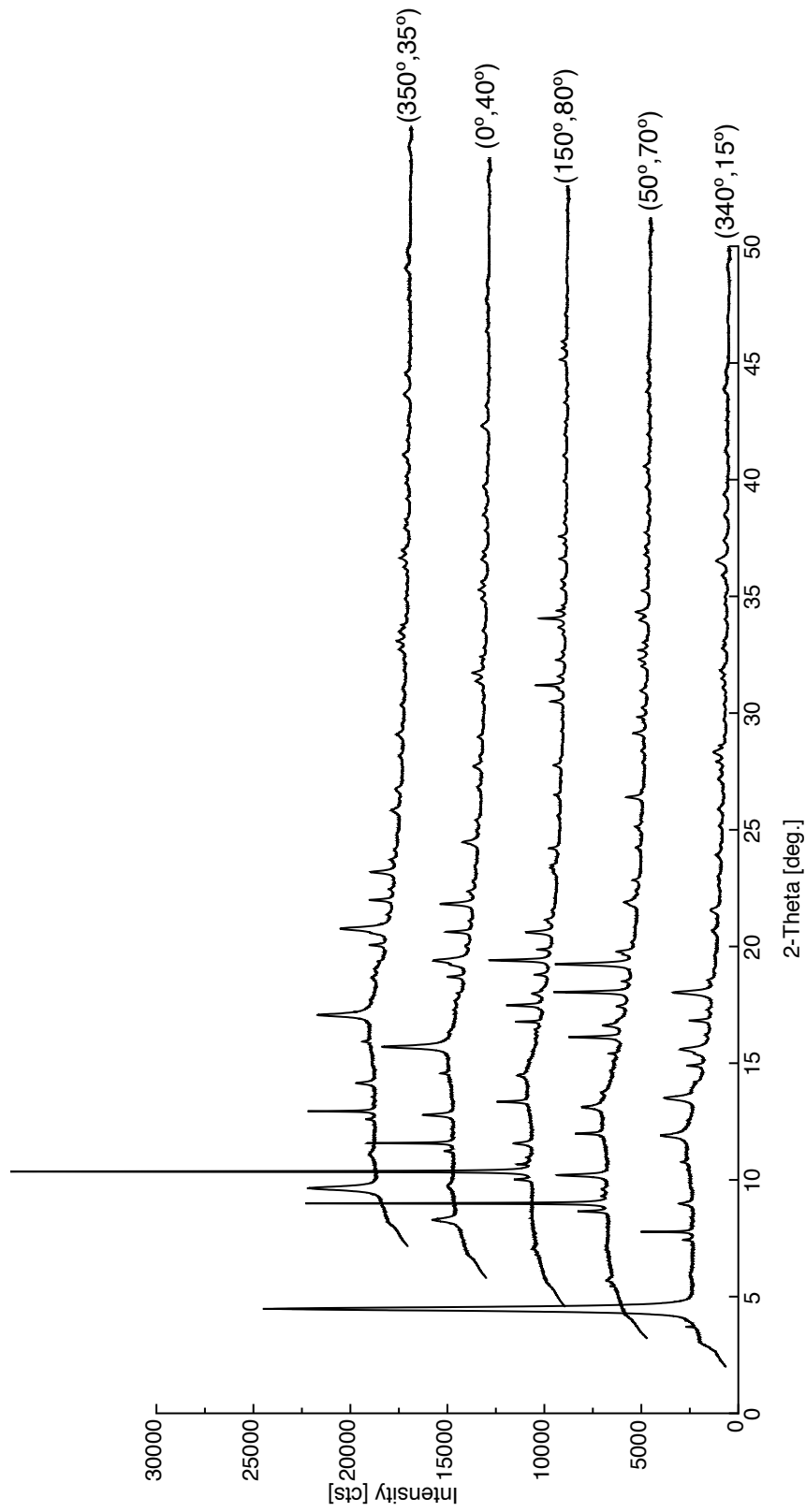 overcome by refining an additional parameter, sharpening the FWHM additionally for the reflections in this direction. Another problem is that the space group is still ambiguous. Additional single-crystal electron diffraction data along the different zone axes [100], [010] and [001], revealed *n*-glide planes perpendicular to [100] and [010], and an *a*-glide perpendicular to [001] (figure 10.9). Ongoing investigations are concentrated on the orthorhombic cell and the space group *Pnna*.
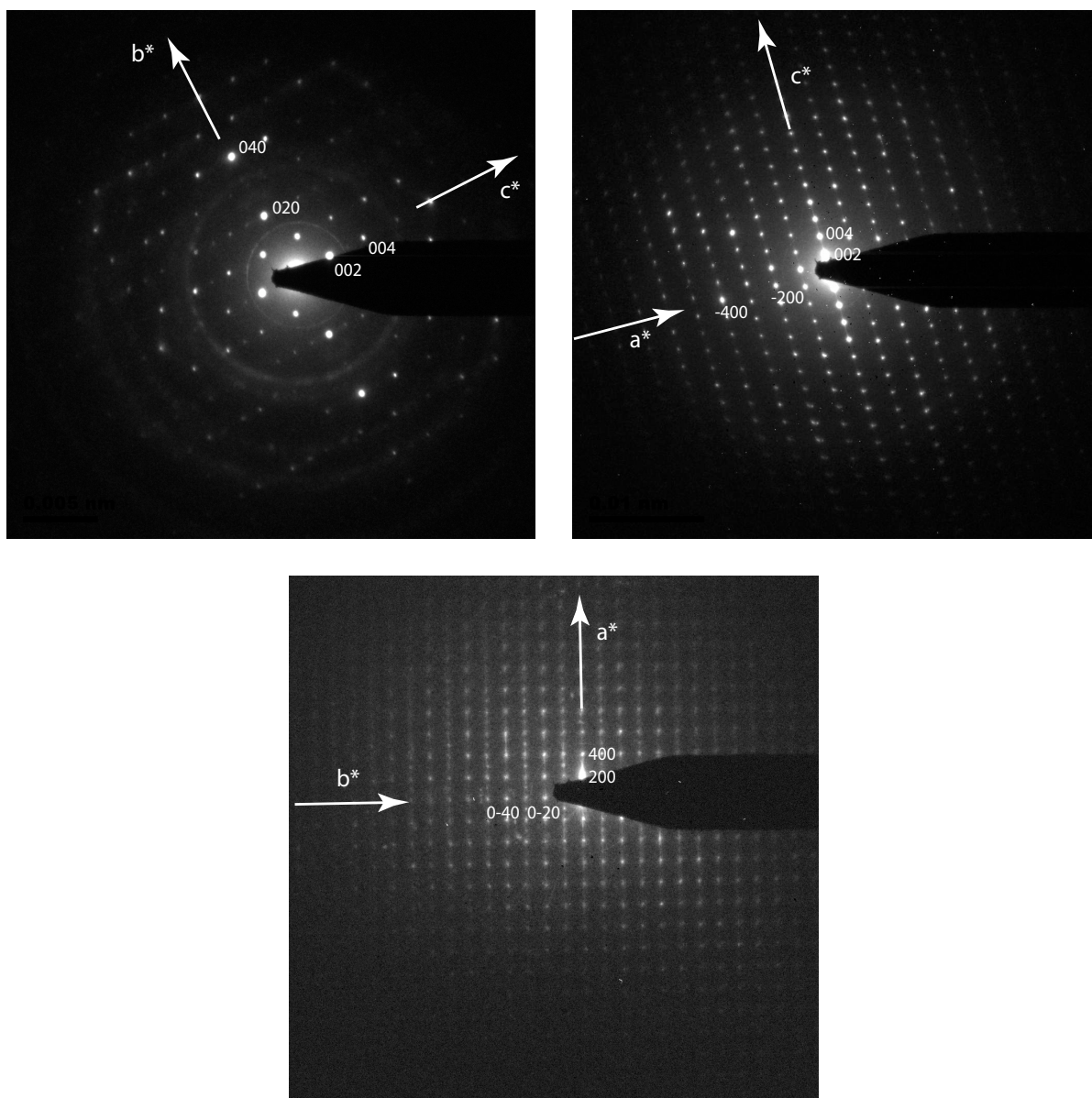

Figure 10.9: Selected area electron diffraction (SAED) patterns along the [100] (top left), along [010] (top right) and along [001] (bottom) zone axes.

11 Conclusions

The collapse of the 3-dimensional information accessible in a single-crystal diffraction experiment, is inherent to any conventional powder diffraction experiment. In contrast, the texture method, which was further developed here, allows some of the 3-dimensionality to be reconstructed.

The main drawbacks of the first implementation of the method in reflection mode were: (1) three days of synchrotron beamtime were required, (2) severe intensity corrections to the data collected at high sample tilt angles had to be applied, and (3) a large homogeneous sample had to be prepared. By collecting data in transmission mode using a 2-dimensional imaging plate detector, these disadvantages could be overcome, but at the cost of poorer resolution. The transfer to transmission geometry was not as straightforward as expected:

- The resolution in 2θ as well as in peakwidth (FWHM) is reduced.

- The experimental rotation and tilt angles have to be converted to pole figure angles to determine the ODF.

- For a reliable extraction and refinement of a set of high-quality reflection intensities, samples with a strong degree of preferred orientation are needed.

To improve the resolution, the experimental setup was modified to take advantage of the features of the 1-dimensional microstrip detector developed at the SLS at the PSI in Villigen. This protoype detector exhibits a resolution in 2θ of 60° and yields data with FWHM's in the range of 0.03°2θ for a typical textured sample (spherical, diameter 0.03 mm). The data analysis software *Expol* was adapted accordingly.

After the intensities for the reflections to be used for the ODF determination have been extracted from all 1368 patterns, the orientation angles (ψ,δ) are converted to the pole figure angles (α,β) using the equations given by (Heidelbach *et al.*, 1999) for the texture analysis. The pole figures for all reflections in the 2θ range are calculated from the ODF and converted back to the experimental angles for the joint refinement.

The sample preparation procedure has been optimized so that textured samples can be produced using a standardized procedure that is not dependent upon the person preparing the sample.

However some problems remain unsolved:

- Si-Microstrip detector: The counting statistics of the measured data are poor, because the count-rate of the prototype detector is limited. The presence of dead and random hot counting channels further reduces the quality of the data.

- Sample preparation: The amount of amorphous matrix material in the sample reduces the signal/background ratio.

- Data analysis: The texture determination is only approximate and comparison of the structure factors obtained from the joint refinement with those calculated from the corresponding structure shows that improvement is needed.

12 Further Developments of the Method

As outlined in the last chapter, the method was transfered from the data collection setup in reflection geometry to a transmission setup, successfully. But, the remaining problems are: intensity differences between the observed and calculated diffraction patterns using the P-values derived from the texture analysis. As a result, differences are found between the refined reflection intensities and those calculated from the structure. This means that the method requires further optimization.

A potential solution to the statistics problem in the data, is the preparation of texture samples containing little or no matrix material. The problem has already been partially solved by collecting high-quality data at orientations yielding the highest intensity contrast for the overlapping reflections. Additional improvement can be expected when the next version of the detector becomes available. This detector does not exhibit any counting failures, and its dynamic range will be about 30 million counts. This will not only reduce the data collection time and improve statistics, but will possibly yield data, that is of sufficient quality for refining the structure in a multi-pattern Rietveld refinement (Von Dreele, 2007).

Finally, to compensate for the uncertainties originating from the texture analysis, the initial set of orientation factors calculated from the ODF, should be refined during the final joint refinement of the single crystal dataset together with the diffraction patterns.

References

Adams B.L., Wright S.I. and Kunze K. (1993), *Met. Trans. A*, **24(4)**, 819-831

Altomare A., Giacovazzo C., Guagliardi A., Moliterni A. G. G., Rizzi R. and Werner P.-E. (2000), *J. Appl. Cryst.*, **33**, 1180-1186

Altomare A., Burla M. C., Camalli B., Carrozzini B., Cascarano G.L., Giacovazzo C., Guagliardi A., Moliterni A.G.G., Polidori G. and Rizzi R. (1999), *J. Appl. Cryst.*, **32**, 339-340

Avanti Polar Lipiuds, Inc., http://avantilipids.com/BicellePreparation.asp

Baerlocher Ch., McCusker L.B. and Palatinus L. (2007), *Z. Kristallogr.*, **222**, 47-53

Baerlocher Ch., Gramm F., Massüger L., McCusker L.B., He Z., Hovmöller S. and Zou S. (2007), *Science*, **315**, 1113-1116

Baerlocher Ch., McCusker L.B., Prokic S. and Wessels T. (2004), *Z. Kristallogr.*, **219**, 803-812

Baerlocher Ch. and Hepp A., XRS-82. X-ray Rietveld System, ETH Zurich, Switzerland, 1982-2003

Barr G., Dong W. and Gilmore Ch. J. (2004), *J. Appl. Cryst.*, **37**, 243-252

Bennett J.M. and Gard J.A. (1967), *Nature*, **214**, 1005-1006

Bricogne G. and Gilmore C.J. (1990), *Acta Cryst.*, **A46**, 284-297

Brunelli M., Wright J.P., Vaughan G.B., Mora A.J. and Fitch A.N. (2003), *Angew. Chem. Int. Ed.*, **42**, 2029-2032

Burla M. C., Caliandro R., Camalli M., Carrozzini B., Cascarano G. L., De Caro L., Giacovazzo C., Polidori G. and Spagna R. (2004), *J. Appl. Cryst.*, **38**, 381-388

Coelho A. A. (2003), *J. Appl. Cryst.*, **36**, 86-95

Dahms M. and Bunge H.J. (1989), *J. Appl. Cryst.*, **22**, 439-447

David W.I.F., Shankland K., Van de Streek J., Pidcock E.,Motherwell W.D.S. and Cole J.C. (2006), *J. Appl. Cryst.*, **39**, 910-915

in, *Structure Determination from Powder Diffraction Data* (Eds. David W.I.F, Shankland K., McCusker L.B. and Baerlocher Ch.), Oxford University Press, England, (2002)

References

Deem M.W. and Newsam J.M. (1989), *Nature*, **342**, 260-262

Eisen M., *Cluster 3.0 Manual* (updated by De Hoon M. in 2002), Stanford University (1999)

Estermann M. and Gramlich (1993), *J. Appl. Cryst.*, **26**, 396-404

Favre-Nicolin V. and Cerny R. (2002), *J. Appl. Cryst.*, **35**, 734-743

Gilmore C.J., Bricogne G. and Bannister C. (1990), *Acta Cryst.*, **A46**, 297-308

Gramm F., Baerlocher Ch., McCusker L.B., Warrender S.J. , Wright P.A. , Han B., Hong S.B., Liu Z., Ohsuna T. and Terasaki O. (2006), *Nature*, **444**, 79-81

Grosse-Kunstleve R. (1999), *Zeolite structure determination from powder diffraction data: Computer-based incorporation of crystal chemical information*, PhD Thesis ETH Zurich, Switzerland

Hülsen G., Broenimann C., Eikenberry E.F. and Wagner A. (2006), *J. Appl. Cryst.*, **39**, 550-557

McCusker L.B., Baerlocher Ch., Grosse-Kunstleve R., Brenner S. and Wessels T. (2001), *Chimia*, **55**, 497-504

Patterson B.D., Abela R., Auderset H., Chen Q., Fauth F., Gozzo F., Ingold G., Kühne H., Lange M., Maden D., Meister P., Pattison P., Schmidt Th., Schmitt B., Schultze-Briese C., Shi M., Stampanoni M. and Willmott P.R. (2004), *Nucl. Instr. and Meth. A*, **540**, 42-67

Hammersley A.P, Svensson S.O., Hanfland M., Fitch A.N. and Häusermann D. (1996), *High Pressure Research*, **14**, 235-248

Hedel R., Bunge H.J. and Reck G. (1997), *Textures Microstruct.*, **29**, 103-126

Hall, S. R., King, G. S. D. & Stewart, J. M. (1995). *Xtal3.4 User's Manual*, University of Western Australia, Perth (1995)

Heidelbach F., Riekel C. and Wenk H.R. (1999), *J. Appl. Cryst.*, **32**, 841-849

Huang T.C., Toraya H., Blanton T.N. and Wu Y. (1993), *J. Appl. Cryst.*, **26**, 180-184

Jorda J.L., Prokic S., McCusker L.B., Baerlocher Ch., Xue C.F. and Dong J. (2005), *C. R. Chimie*, **8**, 331-339

Kariuki B.M., Zin D.M.S., Tremayne M. and Harris K.D.M. (1996), *Chem. Mater.*, **8**, 565-569

Keiderling U., Gilles R. and Wiedemann A. (1999), *J. Appl. Cryst.*, **32**, 456-463

Khavari M. (1990), *Strength-Processing relation of continuous zirconia fiber*, PhD Thesis University of California, Santa Barbara, US

Kocks U.F., Tome C.N. and Wenk H.R., *Texture and anisotropy*, Cambridge University Press, UK (2000)

Louër D. and Boultif A. (2006), *Z. Kristallogr. Suppl.*, **23**, 225-230

Lutterotti L., Personal Communication

Lutterotti L., Matthies S., Wenk H.-R., Schultz A.S. and Richardson J.W.Jr (1997), *J. Appl. Phys.*, **81**, 594-600 or http://www.ing.unitn.it/ maud/

Massüger L., Baerlocher Ch., McCusker L.B. and Zwijnenburg M.A. (2007), *Micropor. Mesopor. Mater.*, **105**, 75-81

Matthies S. and Vinel G. W. (1982), *Physica Status Solidi*, **B112**, K111-K114

Oberhagemann U., Bayat P., Marler B., Gies H. and Rius J. (1996), *Angew. Chem. Int. Ed. Engl.*, **35**, 2869-2872

Oszlányi G. and Sütő A. (2004), *Acta Cryst.*, **A 61**, 147-152

Patterson A.L. (1934), *Phys. Rev.*, **46**, 372-376

Paillaud J.L., Harbuzaru B., Patarin J. and Bats N. (2004), *Nature*, **304**, 990-992

Palatinus L. (2004), *Acta Cryst.*, **A 60**, 604-610

Palatinus L. and Chapuis G. (2006), http://superspace.eplf.ch/superflip

Prokić S. (2004), *Exploiting texture-induced differences in spatially resolved powder diffraction patterns to extract more single-crystal-like reflection intensities*, PhD Thesis ETH Zurich, Switzerland

Rietveld H.M. (1969), *J. Appl. Cryst.*, **2**, 65-71

Rius J. (2004), *Z. Kristallogr.*, **219**, 826-832

Rocha J., Brandão P., Philippou A. and Anderson M.W. (1998), *Chem. Commun.*, **1998**, 2687-2688

Java TreeView written by Saldanha A., Stanford University, USA, http://jtreeview.sourceforge.net/

Sanders Ch.R. and Prestegrad J.H. (1990), *Biophys. J.*, **58**, 447-460

Shankland K., David W.I.F. and Csoka T. (1997), *Z. Kristallogr.*, **212**, 550-552

Shankland K., David W.I.F. and Sivia D.S. (1997), *J. Mater. Chem.*, **7(3)**, 569-572

Schmitt B., Brönnimann Ch., Eikenberry E.F., Hülsen G., Toyokawa H., Horisberger R., Gozzo F., Patterson B., Schulze-Briese C. and Tomizaki T. (2004), *Nucl. Instr. and Meth. A*, **518**, 436-439

Sheldrick G.M. (1997), *SHELXS97*, University of Göttingen, Gremany

Shirley R., *The Crysfire System for Automatic Powder Indexing: User's Manual*, The Lattice Press, 41 Guildford Park Avenue, Gilford, Surrey GU2 7NL, UK (2000)

References

Taupin D. (1973), *J. Appl. Cryst.*, **6**, 380-385

Tjandra N. and Bax A. (1997), *Science*, **278**, 1111-1114

Von Dreele R.B. (1997), *J. Appl. Cryst.*, **30**, 517-525

Von Dreele R.B. (2007), *J. Appl. Cryst.*, **40**, 133-143

Wenk H.R., Matthies S., Donovan J. and Chateigner D. (1998), *J. Appl. Cryst.*, **31**, 262-269

Wenk H.R. in, *Preferred orientation in metals and rocks: An introduction to modern texture analysis* (Ed. Wenk H.R.), Academic Press Inc., UK (1985)

Wenk H.R. and Van Houtte P. (2004), *Rep. Prog. Phys.*, **67**, 1367-1428

Wessels (1999), *Using texture to facilitate structure determination from powder diffraction data*, PhD Thesis ETH Zurich, Switzerland

Wessels T., Baerlocher Ch. and McCusker L.B. (1999), *Science*, **284**, 477-479

Wu J., Leinenweber K., Spence J.C.H. and OKeeffe M. (2006), *Nature Mater.*, **5**, 647-652

Yamaura K., Katoh T., Koezuka K., Iwaseya M. and Lixing D. (2004), *J. Mater. Sci.*, **39**, 1609-1614

Zachariasen W.H. and Ellinger F.H. (19633), *Acta Cryst.*, **16**, 369-375

Acknowledgements

First of all I would like to thank Professor Steurer for being willing to supervise this project and for the freedom granted during its completion.

Many thanks to Lynne McCusker and Christian Baerlocher for their truly inspiring guidance through this thesis, their never-ending support and the readiness for all the fruitful discussions. I would also like to thank all the people at the Laboratory of Crystallography for spending the last 4 years with me. Thank you for the nice working ambience and the help in all the everyday problems.

I'm very grateful to Professor Paul Smith, Kirill Feldmann, Mathias Gössi and Lorenz Brunner from the Polymer Technology Group at ETH, for introducing me into the secrets of polymer processing, the helpful discussions and all the ideas contributed to this project: to Brandon Bürgler for the help with the scanning electron microscopy investigations and to Andre Studart for sharing his knowledge on surfactants. I would also like to thank the students, who contributed to this work with their semester theses: Thomas Schlangenhauf, Daniel Stuber and Thomas Wehrli.

Special thanks to Hans Reifler for many ideas contributed and for finally manufacturing the pressure mold and the fiber spinning setup used for preparing samples.

I would also like to thank my co-PhD student Dan Xie for obtaining and evaluating the SAED patterns of the AM-11 sample.

I'm deeply indebted to Bernd Schmitt, who is developing the microstrip detector and also to Fabia Gozzo for all the support, patience and the numerous hours spent at the beamline with me during my experiments at the SLS. Without them this thesis would not exist. Also many thanks to the people at the SNBL: Hermann Emmerich, Denis Testemale, Phil Pattison, Olga Safonova and Wouter Van Beck for their support in the high-resolution and some of the texture experiments.

I'm very grateful to Luca Lutterotti and Daniel Chateigner for their input and discussions during my stay in Caen. In addition, I would like to thank Luca for the numerous changes in Maud, which made my life much easier, and for finally being willing to serve as an examiner.

Curriculum Vitae

Personal Details

Surname	Lars
First Name	Massüger (né Kocher)
Date of Birth	11. August 1975
Place of Birth	Wettingen (AG), Switzerland
Marital Status	Married, since 11. August 2005

Education

10.2003 - 10.2007	PhD Studies, Laboratory for Crystallography, ETH Zurich
10.1996 - 04. 2003	Material Science Studies, ETH Zurich
08.1991 - 06.1996	Gymnasium in Schiers (GR)

Research Experience

2007	PhD Thesis, Laboratory of Crystallography, ETH Zurich *Experimental extension of the texture method for structure solution of polycrystalline materials*
2003	Diploma Thesis, Institute for Metallurgy and Metals Research, ETH Zurich and Alstom (Schweiz) AG *Temperature estimation by digital image analysis of degraded superalloy microstructures*
2002	Semester Thesis, Institute for Applied Physics, ETH Zurich *Titanium aluminides with controlled lamellar micro-structure*
11.2000 - 07.2001	Intership, Materials Laboratory, Alstom (Schweiz) AG
04.2000-06.2000	Student Research Assistant, Institute for Materials Chemistry and Corrosion, ETH Zurich

Publications

Papers

Mantion A., Massüger L., Rabu P., Palivan C., McCusker L.B. and Taubert A. (2008), *Metal-peptide frameworks (MPFs): "Bioinspired" metal organic frameworks*, J. Am. Chem. Soc., **130**, 8, 2517-2526

Massüger L., Baerlocher Ch., McCusker L.B. and Zwijenburg M. (2007), *Synthesis and structure analysis of the layer silicate DLM-2*, Micropor. Mesopor. Mater., **105**, 75-81

Baerlocher Ch., Gramm F., Massüger L., McCusker L.B., He Z., Hovmöller S. and Zou X. (2007), *Structure of polycrystalline zeolite catalyst IM-5 solved by enhanced charge flipping*, Science, **315**, 1113-1116

Katrych S., Weber Th., Kobas M., Massüger L., Palatinus L., Chapuis G. and Steurer W. (2007), *New stable decagonal quasicrystal in the system Al-Ir-Os*, J. Alloys Compd., **420**, 164-172

Kuelpmann A., Osman M.A., Kocher L. and Suter U.W. (2005), *Influence of platelet aspect ratio and orientation on the storage and loss moduli of HDPE-mica composites*, Polymer, **46**, 523-530

Oral Presentations

Exploiting preferred orientation to resolve the intensities of overlapping reflections, IUCr05, 20th Congress of the International Union of Crystallography, Florence, Italy, 2005

Resolving overlapping reflections using multiple datasets collected on textured powder samples, EPDIC10, European Powder Diffraction Conference, Geneva, Switzerland, 2006

Posters

Using preferred orientation to resolve overlapping reflections, ECM-23, European Crystallographic Meeting, Leuven, Belgium, 2006

Resolving overlapping reflections using multiple datasets collected on textured powder samples, Annual Meeting of the SGK/SSCr, Bern, Switzerland, 2006